NOTICE

The quality of this microform is heavily dependent upon the quality of the original thesis submitted for microfilming. Every effort has been made to ensure the highest quality of reproduction possible.

If pages are missing, contact the university which granted the degree.

Some pages may have indistinct print especially if the original pages were typed with a poor typewriter ribbon or if the university sent us an inferior photocopy.

Reproduction in full or in part of this microform is governed by the Canadian Copyright Act, R.S.C. 1970, c. C-30, and subsequent amendments.

AVIS

La qualité de cette microforme dépend grandement de la qualité de la thèse soumise au microfilmage. Nous avons tout fait pour assurer une qualité supérieure de reproduction.

S'il manque des pages, veuillez communiquer avec l'université qui a conféré le grade.

La qualité d'impression de certaines pages peut laisser à désirer, surtout si les pages originales ont été dactylographiées à l'aide d'un ruban usé ou si l'université nous a fait parvenir une photocopie de qualité inférieure.

La reproduction, même partielle, de cette microforme est soumise à la Loi canadienne sur le droit d'auteur, SRC 1970, c. C-30, et ses amendements subséquents.

Stability Analysis of Initially Weak Converging Cylindrical Shock Waves

Dinh Triet Le

A Thesis

in

The Faculty

of

Engineering

Presented in Partial Fulfillment of the Requirements

for the Degree of Master of Engineering at

Concordia University

Montreal, Quebec, Canada

August 1990

ISBN 0-315-64759-0

ABSTRACT

STABILITY ANALYSIS OF INITIALLY WEAK CONVERGING CYLINDRICAL SHOCK WAVES

Dinh Triet Le

A detailed theoretical and experimental analysis of the stability of initially weak converging cylindrical shocks is presented. The stability was examined by perturbing the converging shocks using cylindrical rods placed in their path and examining their form as they progress. Wave diagrams were constructed based on Whitham's Ray-Shock theory and the Chester-Chisnell-Whitham's Area-Mach number relationship. The results demonstrate that the displacement of the perturbed shock first decreases with shock travel until a critical shock radius is reached, then it increases to large values which makes the perturbed part of the shock surpass the geometric center before collapse. Experimental verification of these results was obtained from the Schlieren photographs taken for shocks of Mach number 1.5, perturbed by rods of diameters 0.4, 0.8, and 1.6 mm, which were placed at a radius of 40 mm. Good agreement is noted for the triple points trajectories and the shock velocities. For the larger rod diameter used, similar shifting in the region of collapse is noted.

ACKNOWLEDGEMENT

The author wishes to express his gratitude to Dr. R.A. Neemeh for his constant encouragement and support throughout the course of this work, for his many helpful suggestions in the improvement of the text, and generous guidances of this work.

Thanks are due to Mr. Domenic Diluca and Miss Laura Neemeh for revising and improvement of the text.

Thanks are due to Mr. Phong. D.H. for his assistance in the experiment.

Thanks are due to Miss Jane Venettacci for typing this thesis.

The present work was supported by the Natural Science and Engineering Research Council of Canada under Grant No. A-4206.

TABLE OF CONTENTS

LIST OF FIGURES

LIST OF TABLES

NOMENCLATURE

A	duct cross-sectional area
a	speed of sound
C	slope of the characteristics in the (α,β) plane
C^+	positive characteristics
C^-	negative characteristics
CD	contact discontinuity
C_p	specific heat at constant pressure
C_v	specific heat at constant volume
d	diameter of cylindrical rod
F,G,H	arbitrary functions (equations 2.15-2.17)
K	Chester function (Fig. 2.1)
M	Mach number
M_o	shock Mach number at radius R_o
MR	Mach reflection
MS	Mach stem
m	characteristic angle
P	pressure of fluid
P_1	pressure of gas driven section
P_4	pressure of gas in driver section
R_s	shock radius
R_o	distance between center of rod and geometric center (40 mm)
ΔR	displacement of the perturbed part of the Shock from the unperturbed one
RR	regular reflection
r	radius of cylindrical rod

S	specific entropy
T	temperature
TP	triple point
t	time
u	velocity of fluid in x direction
v	velocity of fluid in y direction
x	coordinate
y	coordinate
α	Ray-shock coordinate
β	Ray-shock coordinate
γ	ratio of specific heat (C_p/C_v)
θ	angle between the Ray and the x axis
ϕ	angle between the Shock and the y axis
θ_ω	Wall angle
χ	Shock-Shock angle
ω	Riemann Invariant (Equation (2.63))
ξ	Perturbation parameter (Equation (4.4))
μ	parameter defined by Equation (2.20)
ρ	fluid density

Subscripts

o	reference condition
1	condition ahead shock wave
2	condition behind shock wave
s	shock wave
i	incident shock

Chapter 1

INTRODUCTION

Achieving high compression in cylindrical or spherical implosions depends largely on their degree of symmetry before collapse. Theoretically, symmetrical converging shocks are known for their ability to approach infinite strength as their radius tends to zero [1]. Experimentally, any small deviation from perfect symmetry in their shape is found to amplify before collapse [2]. To find out how much deviation can be tolerated from spherical or cylindrical shapes, stability analyses were required.

In 1974, a three element area contraction was used in a conventional shock tube to turn the initially plane annular shock into a cylindrical shock [3]. This area contraction design was chosen because of the low pressure attenuation observed behind the transmitted shock. Stability analysis of initially strong shocks was presented in the 15th symposium on SWST [4]. Both theory and experiments confirmed the previous findings which state that converging shocks are unstable and that the perturbation parameter ξ varies with r^{-n}, where n is an exponent that depends on the size of the perturbation.

In the case of weak shocks, little theoretical work was carried out. The single case analyzed theoretically, was for a small rod placed at a radius of 100

times its diameter. The results show that weak shocks collapse is different from that of strong shocks. Weak shocks are found to collapse very near to the geometric center on the opposite side of the rod, as opposed to that found in the case of the strong shocks. These findings cannot be conclusive since they were obtained from the analysis of a single case ($R_o/d = 100$).

The present study investigates the stability of initially weak (M = 1.5) converging cylindrical shocks which are perturbed by rods of diameter (R_o/d) of 100, 50, and 25. The theoretical analysis was based on wave diagrams constructed using Whitham's Ray-shock Theory and the CCW Area Mach relationship [5,6,7].

The experimental work was carried out to determine the validity of the theoretical results. The work included detailed pressure and shock velocity measurements as well as spark Schlieren photographs of the converging shock. Details will be given in Chapter 2, 3, and 4, followed by concluding remarks.

Chapter 2

THEORETICAL DEVELOPMENT

The theoretical development of the present problem is based on Whitham's Ray Shock Theory and the Chester-Chisnell-Whitham's Area-Mach relationship. In this chapter, a detailed description of the theory used is presented.

2.1 Chester-Chisnell-Whitham's Area-Mach Relationship

The theory of shock propagation in variable area ducts has been analyzed by three different investigators. Each used a different approach but surprisingly, they all obtained the same A-M relationship. A brief discussion of each derivation is presented while that of Chisnell will be analyzed in more detail.

2.1.1 Chester's linearized analysis

Chester's analysis of shock wave propagation in a variable area duct was based on the assumption that the area variations are small, which allows the linearization of the governing equations of the flow behind the shock wave.

Assuming that the duct is uniform for $x < 0$ and for $x > 0$, the cross sectional area of the pipe is a function of x. The one-dimensional gas dynamics equations (Continuity, Momentum and Energy) are:

$$\frac{\partial \rho}{\partial t} + \frac{\partial \rho u}{\partial x} + \rho u \frac{\partial \ln A}{\partial x} = 0 \tag{2.1}$$

$$\frac{\partial u}{\partial t} + \frac{u \partial u}{\partial x} + \frac{1}{\rho} \frac{\partial P}{\partial x} = 0 \tag{2.2}$$

$$\left[\frac{\partial}{\partial t} + u \frac{\partial}{\partial x}\right] S = 0 \tag{2.3}$$

Linearizing the equations above (i.e., $P = P_2 + P'$, $u = u_2 + u'$, ..., etc.), where P_2, ρ_2, u_2 and A_2 are the initial values of pressure, density, velocity, and area of the flow behind the propagating shock and P', ρ', u' are the change in the respective quantities due to area change. The following equations are obtained:

$$\frac{\partial \rho'}{\partial t} + \rho_2 \frac{\partial u'}{\partial x} + u_2 \frac{\partial \rho'}{\partial x} + \frac{\rho_2 u_2}{A_2} \frac{\partial A'}{\partial x} = 0 \tag{2.4}$$

$$\frac{\partial u'}{\partial t} + u_2 \frac{\partial u'}{\partial x} + \frac{1}{\rho_2} \frac{\partial P'}{\partial x} = 0 \tag{2.5}$$

$$\left[\frac{\partial}{\partial t} + u_2 \frac{\partial}{\partial x}\right] S' = 0 \tag{2.6}$$

From the second law of Thermodynamics,

$$P = K\rho^{\gamma} \exp [S/C_v]$$

Linearizing the above equation,

$$\frac{P'}{P_2} = \frac{\gamma\rho'}{\rho_2} + \frac{S'}{C_v} \tag{2.7}$$

Eliminating S' from Equations (2.6) and (2.7),

$$\left[\frac{\partial}{\partial t} + u_2 \frac{\partial}{\partial x}\right]\frac{P'}{P_2} - \gamma\left[\frac{\partial}{\partial t} + u_2 \frac{\partial}{\partial x}\right]\frac{\rho'}{\rho_2} = 0 \tag{2.8}$$

or

$$\left[\frac{\partial P'}{\partial t} + u_2 \frac{\partial P'}{\partial x}\right] - a_2^2\left[\frac{\partial \rho'}{\partial t} + u_2 \frac{\partial \rho'}{\partial x}\right] = 0 \tag{2.9}$$

where $a_2 = \sqrt{\gamma R T}$ is the speed of sound.

Combining Equations (2.4) and (2.9) leads to:

$$\frac{\partial P'}{\partial t} + u_2 \frac{\partial P'}{\partial x} + \rho_2 a_2^2 \frac{\partial u'}{\partial x} + \frac{\rho_2 a_2^2 u_2}{A_2}\frac{dA'}{dx} = 0 \tag{2.10}$$

Multiply Equation (2.10) by η and Equation (2.5) by ζ, then add them and the resulting equation is:

$$\left[\frac{\partial}{\partial t} + \left(u_2 + \frac{\zeta}{\eta \rho_2}\right)\frac{\partial}{\partial x}\right] P' + \frac{\zeta}{\eta}\left[\frac{\partial}{\partial t} + \left(u_2 + \frac{\eta}{\zeta}\rho_2 a_2^2\right)\frac{\partial}{\partial x}\right] u'$$

$$= -\frac{\rho_2 u_2 a_2^2}{A_2}\frac{dA'}{dx} \qquad (2.11)$$

Equation (2.11) can be written in the total differential form if $\zeta/\eta = \pm \rho_2 a_2$,

$$\frac{dP'}{dt} + \rho_2 a_2 \frac{du'}{dt} = -\frac{\rho_2 u_2 a_2^2}{A_2}\frac{dA'}{dx} \qquad (2.12)$$

along the C^+ characteristic where,

$$\frac{dx}{dt} = u_2 + a_2 \qquad \text{and}$$

$$\frac{dP'}{dt} - \rho_2 a_2 \frac{du'}{dt} = -\frac{\rho_2 u_2 a_2^2}{A_2}\frac{dA'}{dx} \qquad (2.13)$$

along the C^- characteristic where,

$$\frac{dx}{dt} = u_2 - a_2 \qquad \text{and}$$

$$\frac{d\rho'}{dt} - \frac{1}{a_2^2}\frac{dP'}{dt} = 0 \qquad (2.14)$$

along the particle path where,

$$\frac{dx}{dt} = u_2$$

The integrated forms of the above 3 equations are as follows:

$$P' + \rho_2 a_2 u' = - \frac{\rho_2 u_2 a_2^2}{(u_2 + a_2)} \frac{A'}{A_2} + F \tag{2.15}$$

$$P' - \rho_2 a_2 u' = - \frac{\rho_2 u_2 a_2^2}{(u_2 - a_2)} \frac{A'}{A_2} + G \tag{2.16}$$

$$\rho' = \frac{P'}{a_2^2} + H \tag{2.17}$$

The functions F, G, and H are to be determined from the boundary conditions. From Chester's theory, the function F represents a re-reflected disturbance travelling downstream, and since there are no mechanisms for the production of such a disturbance from the linear theory, this function must be identically zero. By the substitution of the Rankine-Hugoniot relationships into Equation (2.15), Chester was able to derive the following Area-Mach number relationship:

$$- \frac{A'}{A} = \frac{2M\,M'}{K(M)\,(M^2 - 1)} \tag{2.18}$$

where

$$K(M) = 2\left[\left(1 + \frac{2}{\gamma+1}\left(\frac{1-\mu^2}{\mu}\right)\right)\left(2\mu + 1 + \frac{1}{M^2}\right)\right]^{-1} \tag{2.19}$$

and

$$\mu^2 = \frac{(\gamma - 1)\, M^2 + 2}{2\gamma M^2 - (\gamma - 1)} \tag{2.20}$$

The function K(M) was first obtained by Chester [6,8] and was referred to as the Chester's function. It is a function with a small total variation as shown in Fig. (2.1). For $\gamma = 1.4$, the value of K(M) varies from the value of 0.5 for weak shocks to the asymptotic value of 0.394 for strong shocks.

2.1.2 Chisnell's derivation

Chisnell [7] derived the A-M function in a totally different manner. In his analysis, he considered the interaction of a shock propagating in a uniform duct of area A, with a small area change dA. The various waves resulting from the interaction are shown in Fig. (2.2). Regions (1) and (2) are separated by the incident shock while regions (5) and (6) are divided by the transmitted shock. A reflected disturbance separates regions (3) and (4). If the area change is positive, the reflected wave is an expansion wave, but a compression wave results when the area change is negative. A contact discontinuity divides the flow into two parts and separates them into regions (4) and (5) that originate from either side of the transition section of the duct. Here, the flow was assumed to be supersonic so that the reflected disturbance was swept downstream of the transition region. Note that, similar results were obtained with the subsonic flow as well, where the reflected wave moves upstream of the transition region. Also note that regions (1) and (2), (5) and (6) are related by the Rankine-Hugoniot relationships, while across the

contact discontinuity we have $P_4 = P_5$ and $u_4 = u_5$. After a sufficiently long period of time following the passage of the shock, steady flow conditions can be assumed between regions (2) and (3). For steady isentropic flow in a duct with area variation, we have:

$$\frac{dP}{\rho} + udu = 0 \tag{2.21}$$

The conservation of mass gives:

$$\rho u A = \text{const} \tag{2.22}$$

then

$$\frac{dA}{A} = \frac{dP\,(1 - M^2)}{M^2 \gamma P}$$

or

$$\boxed{\frac{dP}{P} = -\frac{\gamma M^2}{(M^2 - 1)} \frac{dA}{A}} \tag{2.23}$$

Integrating the above equation:

$$\int_{P_2}^{P_3} \frac{dP}{P} = \int_{A}^{A+dA} -\frac{\gamma M_2^2}{(M_2^2 - 1)} \frac{dA}{A}$$

$$\ln \frac{P_3}{P_2} = -\frac{\gamma M_2^2}{M_2^2 - 1} \ln\left(\frac{A + dA}{A}\right) = K \ln\left(\frac{A + dA}{A}\right)$$

where

$$K = -\frac{\gamma M_2^2}{M_2^2 - 1}$$

$$\ln \frac{P_3}{P_2} = \ln\left(1 + \frac{dA}{A}\right)^K \tag{2.24}$$

For a small area change,

$$\frac{P_3}{P_2} = \left(1 + \frac{dA}{A}\right)^K \simeq 1 + K \frac{dA}{A}$$

$$\boxed{\frac{P_3}{P_2} = 1 - \frac{\gamma M_2^2}{M_2^2 - 1} \frac{dA}{A}} \tag{2.25}$$

Using the isentropic relation p/ρ^γ = const., Equation (2.24) becomes

$$\ln\left(\frac{P_3}{P_2}\right) = \ln\left(1 + \frac{dA}{A}\right)^{K/\gamma}$$

or

$$\boxed{\frac{P_3}{P_2} = 1 - \frac{M_2^2}{M_2^2 - 1} \frac{dA}{A}} \tag{2.26}$$

From the continuity equation,

$$\frac{du}{u} = -\frac{dA}{A} - \frac{d\rho}{\rho}$$

$$\ln \frac{u_3}{u_2} = -\ln \frac{A_3}{A_2} - \ln \frac{\rho_3}{\rho_3} = -\ln \frac{A_3 \rho_3}{A_2 \rho_2} = \ln \frac{A_2 \rho_2}{A_3 \rho_3}$$

then

$$\frac{u_3}{u_2} = \frac{1}{\left(1 - \frac{M_2^2}{M_2^2 - 1} \frac{dA}{A}\right)\left(1 + \frac{dA}{A}\right)}$$

Expand the R.H.S. and neglect the term $\left(\frac{dA}{A}\right)^2$,

$$\frac{u_3}{u_2} = \left(1 + \left(\frac{M_2^2}{M_2^2 - 1} - 1\right)\frac{dA}{A}\right)$$

or

$$\boxed{\frac{u_3}{u_2} = 1 + \frac{1}{M_2^2 - 1} \frac{dA}{A}} \qquad (2.27)$$

In Chisnell's original analysis, the pressure ratio $Z = P_2/P_1$ is chosen to be the strength parameter rather than the shock Mach number, M_s. Hence, the Rankine-Hugoniot relations for the propagating shock are:

$$Z = \frac{P_2}{P_1} \tag{2.28}$$

$$\rho_2 = \rho_1 \frac{(\gamma + 1) Z + (\gamma - 1)}{(\gamma - 1) Z + (\gamma + 1)} \tag{2.29}$$

$$u_2 = (Z - 1) \left(\frac{2 P_1}{\rho_1 \{(\gamma - 1) + Z(\gamma + 1)\}} \right)^{1/2} \tag{2.30}$$

$$M_2 = (Z - 1) \left(\frac{2}{\gamma Z \{(\gamma + 1) + (\gamma - 1)Z\}} \right)^{1/2} \tag{2.31}$$

For the transmitted shock, it is assumed that the strength may be written as Z+Z'. Therefore, the density, velocity and Mach number in region (5) (i.e. ρ_5, u_5, M_5, ...) can be obtained from the same relationships given above. If we replace the subscript 2 by 5 and Z by Z+Z', regions (1) and (6) are identical if there is no flow initially in the duct. Since,

$$\frac{P_5}{P_6} = \frac{P_4}{P_1} = Z + Z' = Z\left(1 + \frac{Z'}{Z}\right) \tag{2.32}$$

and

$$\frac{P_3}{P_2} = 1 - \frac{\gamma M_2^2}{M_2^2 - 1} \frac{dA}{A} \tag{2.33}$$

and

$$\frac{P_3}{P_1} = \frac{P_2}{P_1}\left(1 - \frac{\gamma M_2^2}{M_2^2 - 1}\frac{dA}{A}\right) = Z\left(1 - \frac{\gamma M_2^2}{M_2^2 - 1}\frac{dA}{A}\right)$$

therefore we get

$$\frac{P_4}{P_3} = \frac{Z(1 + Z'/Z)}{Z\left(1 - \frac{\gamma M_2^2}{M_2^2 - 1}\frac{dA}{A}\right)} = \left(1 + \frac{Z'}{Z}\right)\left(1 + \frac{\gamma M_2^2}{M_2^2 - 1}\frac{dA}{A} + \ldots\right)$$

Obtaining only the first order terms of the primed quantities, we get

$$\frac{P_4}{P_3} = 1 + \frac{Z'}{Z} + \frac{\gamma M_2^2}{M_2^2 - 1}\frac{dA}{A} \tag{2.34}$$

Similar manipulation gives,

$$\frac{u_4}{u_3} = 1 + \frac{Z'}{Z - 1} - \frac{(\gamma + 1)\,Z'}{2\,[(\gamma + 1)\,Z + (\gamma - 1)]} - \frac{1}{(M_2^2 - 1)}\frac{dA}{A} \tag{2.35}$$

Across the reflected wave separating regions (3) and (4), we have the acoustic relation $P' = -\rho a u'$, or

$$\frac{P_4 - P_3}{P_3} = \frac{-\rho_3 a_3}{P_3}\left(\frac{u_4 - u_3}{u_3}\right)u_3$$

$$\left[\frac{P_4}{P_3} - 1 = -\gamma M_3\left(\frac{u_4}{u_3} - 1\right)\right] \tag{2.36}$$

Substituting the expression for P_4/P_3 and u_4/u_3 into Equation (2.36), we get

$$\frac{Z'}{Z} + \frac{\gamma M_2^2}{M_2^2 - 1}\frac{dA}{A} =$$

$$-\gamma M_3\left(\frac{Z'}{Z' - 1} - \frac{(\gamma + 1)\,Z'}{2\{(\gamma + 1)\,Z - (\gamma - 1)\}} - \frac{1}{M_2^2 - 1}\frac{dA}{A}\right)$$

Since M_2 and M_3 differ by a term of the order of A'/A, as $A'/A \to 0$, we may replace M_3 by M_2 and write,

$$M_3 = M_2 = (Z - 1)\left(\frac{2}{Z\{(\gamma + 1) + (\gamma - 1)Z\}}\right)^{1/2} \tag{2.37}$$

Letting $A' \to 0$, we get

$$-\frac{1}{A}\frac{dA}{dZ} = \frac{1}{\gamma Z} + \frac{1}{Z - 1} - \frac{\gamma + 1}{2\{(\gamma + 1)\,Z + (\gamma - 1)\}}$$

$$+\left(\frac{2}{\gamma Z\{(\gamma - 1)\,Z + (\gamma + 1)\}}\right)^{1/2}$$

$$*\left(1 - \frac{(\gamma + 1)\,(Z - 1)}{2\{(\gamma + 1)\,Z + (\gamma - 1)\}} + \frac{(\gamma - 1)\,Z + (\gamma + 1)}{2(Z - 1)}\right) \tag{2.38}$$

If we replace Z by the Rankine-Hugoniot relation,

$$Z = \frac{2\gamma M_s^2 - (\gamma - 1)}{\gamma + 1} \tag{2.39}$$

Equation (2.38) can be reduced to the form given previously by Chester where the shock Mach No., M_s, is used instead of A as the parameter. The above equation for A(Z) or Z(A) can be integrated analytically. Chisnell gave the following result:

$$Af\,(Z) = \text{constant} \tag{2.40}$$

$$f(Z) = Z^{1/\gamma}\,(Z-1)\left[Z+\frac{\gamma-1}{\gamma+1}\right]^{-1/2}\left[\frac{1+\left(1+\dfrac{\gamma+1}{(\gamma-1)Z}\right)^{-1/2}}{1-\left(1+\dfrac{\gamma+1}{(\gamma-1)Z}\right)^{-1/2}}\right]\sqrt{\frac{\gamma}{2(\gamma-1)}}$$

$$\times\left[\frac{\left(1+\dfrac{\gamma+1}{(\gamma-1)\,Z}\right)^{-1/2}-\left(\dfrac{\gamma-1}{2\gamma}\right)^{1/2}}{\left(1+\dfrac{\gamma+1}{(\gamma-1)\,Z}\right)^{-1/2}+\left(\dfrac{\gamma-1}{2\gamma}\right)^{1/2}}\right]$$

$$\times\,\mathrm{EXP}\left[\left(\frac{2}{\gamma-1}\right)^{1/2}\mathrm{TAN}^{-1}\left\{\frac{2}{(\gamma-1)}\left(\frac{\gamma Z}{Z+\dfrac{\gamma+1}{\gamma-1}}\right)^{1/2}\right\}\right] \tag{2.41}$$

Given the initial shock strength Z_o, and the duct area A_o, the constant in the above equation can be evaluated.

Chisnell's derivation is simple. The key assumption is to consider steady flow across the area change. This can be achieved after a considerable time period following the passage of the shock. Applying the results to a duct whose cross sectional area changes continuously, we see that Chisnell's

analysis ignores the influence of the wave interactions behind the shock on the shock motion itself. This can be illustrated by the multiple, sudden area change, as shown in Fig. (2.3). Here, the reflected wave from the second area change interacts with the first area change to form a re-reflected wave which eventually overtakes the shock and influences its motion. For a continuous area change, re-reflected waves are generated continuously and their cumulative effect can influence the motion of the shock. For a small area change, the reflected waves are weak. Their interaction with an area change can only produce re-reflected waves of second order in magnitude. In the linearized theory, re-reflected waves play no part in the results because they are of second order effects, thus making the shock strength dependent only on the local area change, and not on the upstream conditions.

2.1.3 Whitham's approach

G.B. Whitham simplified the derivation of shock propagation in a non-uniform tube by using the characteristic rule [30]. According to Whitham, the C^+ characteristic equation which is obtained from the basic gas dynamic Equations (2.1) - (2.3), can be written as:

$$\frac{dP}{dx} + \rho a \frac{du}{dx} + \frac{\rho u a}{u + a} \frac{1}{A} \frac{dA}{dx} = 0 \tag{2.42}$$

The shock conditions are:

$$P = \rho_o a_o \left(\frac{2}{\gamma + 1} M^2 - \frac{\gamma - 1}{(\gamma + 1)\gamma} \right) \tag{2.43}$$

$$u = a_o \frac{2}{\gamma + 1}\left(M - \frac{1}{M}\right) \tag{2.44}$$

$$\rho = \rho_o \frac{(\gamma + 1) M^2}{[2 + (\gamma - 1) M^2]} \tag{2.45}$$

Substituting the shock conditions into Equation (2.42), we get

$$\frac{M}{M^2 - 1} \lambda(M) \frac{dM}{dx} + \frac{1}{A} \frac{dA}{dx} = 0 \tag{2.46}$$

where

$$\lambda(M) = \left(1 + \frac{2}{\gamma + 1}\left(\frac{1 - \mu^2}{\mu}\right)\right)\left(2\mu + 1 + \frac{1}{M^2}\right) \tag{2.47}$$

with $$\mu^2 = \frac{(\gamma - 1) M^2 + 2}{2\gamma M^2 - (\gamma - 1)}$$

These are the same results obtained by Chisnell and Chester in spite of the various different ways in which the Area-Mach relationship has been derived. Although this relationship was obtained by making various assumptions, the true reason why it works so well for finite area changes and for arbitrary shock strength is still open for discussion.

2.1.4 Application of the CCW theory

For symmetrical converging shocks, the CCW theory was found to give

excellent results in comparison with the self similar solution of Butler [32] and Guderley [1]. According to the CCW Area-Mach relation:

$$\frac{dA}{A} = -\frac{2M \quad dM}{K(M)\,(M^2 - 1)} \tag{2.48}$$

For cylindrical and spherical shocks,

$$\frac{dA}{A} = j\frac{dR_s}{R_s} \tag{2.49}$$

where

j = 1, for cylindrical shocks

j = 2, for spherical shocks

For strong shocks $M_s^2 \gg 1$, therefore Equation (2.49) can be written as:

$$j\frac{dR_s}{R_s} = \frac{-2}{K(M_s)}\frac{dM_s}{M_s} \tag{2.50}$$

When $M_s \rightarrow \infty$, the function $K(M_s)$ approaches asymptotically a constant value $K(\infty)$. For $\gamma = 1.4$, $K(\infty) = 0.394$. By integrating Equation (2.50), the following relationship was obtained:

$$M_s \propto R_s^{-j\frac{K(\infty)}{2}}$$

or

$$M_s \propto R_s^{-.197} \qquad \textit{for cylindrical shocks}$$

and

$$M_s \propto R_s^{-.394} \qquad \textit{for spherical shocks}$$

which are practically the same results obtained using the self similar solution.

2.2 Whitham's Ray Shock Theory

Whitham [5] introduced a theory, called the Ray-Shock theory to handle the problems of curved shock wave dynamics. An orthogonal curvilinear coordinate system (α,β) was chosen, and this is shown in Figure 2.4. One coordinate represents the shock fronts at successive instant of time and the other, orthogonal to the shock front, is called a ray. The shock at time t is denoted by $\alpha = a_o t$, where a_o is the speed of sound ahead of the shock wave. The distance between the shock fronts at α and $\alpha+d\alpha$ is $R_s dt$, where R_s is the speed of the shock and dt is the time taken from the shock to travel from α to $\alpha+d\alpha$.

Coordinate β represents the Ray. The distance between the rays β and $\beta+d\beta$ is $A(\alpha,\beta)d\beta$ where A is the cross sectional area of the ray tube. To establish the geometrical relationship between A and M, a curvilinear quadrilateral PQRS, shown in Fig. 2.5, with vertices (α,β), $(\alpha+\delta\alpha,\beta)$, $(\alpha,\beta+\delta\beta)$, and $(\alpha+\delta\alpha,\beta+\delta\beta)$ respectively, was introduced. In the figure:

θ_1 is the angle between the ray and the x axis at P,

θ_2 is the angle between the successive ray and the x axis at S,

ϕ_1 is the angle between the shock and the y axis at R,

ϕ_2 is the angle between the successive shock and the y axis at Q.

The change in direction of the ray from P to S is $\delta\theta = \theta_1 - \theta_2$.

$$\delta\theta = \frac{QR\text{-}PS}{PQ} = \frac{\left(A + \frac{\partial A}{\partial \alpha}\delta\alpha\right)\delta\beta - A\delta\beta}{M\delta\alpha}$$

then

$$\frac{\partial \theta}{\partial \beta} - \frac{1}{M}\frac{\partial A}{\partial \alpha} = 0 \qquad (2.51)$$

Similarly,

$$-\delta\phi = \frac{\left(M + \frac{\partial M}{\partial \beta}\delta\beta\right)\delta\alpha - M\delta\alpha}{A\delta\beta}$$

$$-\frac{\partial \phi}{\partial \alpha} = \frac{1}{A}\frac{\partial M}{\partial \beta} \qquad (2.52)$$

Since the rays and shock fronts are orthogonal, therefore $\theta = \phi$.

$$\frac{\partial \theta}{\partial \alpha} + \frac{1}{A} \frac{\partial M}{\partial \beta} = 0 \tag{2.53}$$

Multiply Equation (2.51) by η and Equation (2.53) by ζ, then add them,

$$\left(\frac{\partial}{\partial \alpha} + \frac{\eta}{\zeta} \frac{\partial}{\partial \beta}\right)\theta - \left(\frac{\eta}{\zeta} \frac{A'}{M}\right)\left[\frac{\partial}{\partial \alpha} + \left(-\frac{M}{A'} \frac{\zeta}{\eta} \frac{\partial}{\partial \beta}\right)\right] M = 0 \tag{2.54}$$

The terms in the left hand side of Equation (2.54) are total differential if

$$\frac{\eta}{\zeta} = \frac{\zeta}{\eta}\left(-\frac{M}{A' A}\right)$$

or

$$\frac{\eta}{\zeta} = \pm\sqrt{\left(-\frac{M}{A' A}\right)} = \pm C \tag{2.55}$$

where C is a function of M. Equations (2.54) and (2.55) can be written as:

$$D^{+}\theta + \frac{1}{AC} D^{+} M = 0 \tag{2.56}$$

and

$$D^{-}\theta + \frac{1}{AC} D^{-} M = 0 \tag{2.57}$$

where

$$D^+ = \frac{\partial}{\partial \alpha} + C\frac{\partial}{\partial \beta}, \qquad D^- = \frac{\partial}{\partial \alpha} - C\frac{\partial}{\partial \beta}$$

The operators D^+ and D^- represent the derivatives along the two families of curves C_1 and C_2, corresponding to $\left(\frac{d\beta}{d\alpha}\right)_{C_1} = C$, and $\left(\frac{d\beta}{d\alpha}\right)_{C_2} = -C$, respectively.

Equations (2.56) and (2.57) can be integrated as follows:

$\theta + \int \frac{dM}{AC}$ = Constant along the C^+ characteristic where,

$$\frac{d\beta}{d\alpha} = C \tag{2.58}$$

$\theta - \int \frac{dM}{AC}$ = Constant along the C^- characteristic where,

$$\frac{d\beta}{d\alpha} = -C \tag{2.59}$$

or

$$\theta \pm \omega = \text{Constant along } C^{\pm} \tag{2.60}$$

where ω is the Riemann invariant which is defined as:

$$\omega = \int \frac{dM}{AC}$$

The A(M) relation is derived from Equation (2.46), which may also be written as:

$$\frac{1}{A}\frac{dA}{dM} = -\frac{M}{M^2-1}\lambda(M) \tag{2.61}$$

Hence,

$$AC = \left\{\frac{M^2-1}{\lambda(M)}\right\}^{\frac{1}{2}} \tag{2.62}$$

then

$$\omega = \int_1^M \frac{dM}{AC} = \int_1^M \left\{\frac{\lambda(M)}{M^2-1}\right\}^{1/2} dM \tag{2.63}$$

The shapes and strength of shock waves were determined by means of the wave diagrams constructed based on the above mentioned theory. For simplicity, the curvilinear coordinate system (α,β) was transformed to the Cartesian coordinate system (x,y). This was carried out as follows:

From Fig. 2.6, by geometrical manipulation:

$dx = Md\alpha \cos\theta - Ad\beta \sin\theta$

$dy = Md\alpha \sin\theta + Ad\beta \cos\theta$

but

$$x = x(\alpha,\beta) \text{ and } y = y(\alpha,\beta)$$

then

$$dx = \frac{\partial x}{\partial \alpha} d\alpha + \frac{\partial x}{\partial \beta} d\beta$$

$$dy = \frac{\partial y}{\partial \alpha} d\alpha + \frac{\partial y}{\partial \beta} d\beta$$

Comparing the coefficient of $d\alpha$ and $d\beta$, the following equation is obtained:

$$\frac{dy}{dx} = \frac{\sin\theta \pm \frac{AC}{M}\cos\theta}{\cos\theta \pm \frac{AC}{M}\sin\theta} \tag{2.64}$$

$$\frac{dy}{dx} = \tan(\theta \pm m) \tag{2.65}$$

where

$$\tan m = \frac{AC}{M} \tag{2.66}$$

The angle 'm' is the angle between the characteristics and the ray direction. Hence, the slopes of the characteristics are:

$$C^+ \qquad \frac{dy}{dx} = \tan(\theta + m) \tag{2.67}$$

$$C^- \qquad \frac{dy}{dx} = \tan(\theta - m) \tag{2.68}$$

The values of 'm' can be determined by substituting Equation (2.64) into Equation (2.68) so that

$$\tan(m) = \left(\frac{(M^2 - 1)\,\lambda(M)}{2\,M^2}\right)^{1/2} \tag{2.69}$$

but according to Skew [35], the values of 'm' calculated for weak shocks do not agree with experiments. He has suggested the use of the following equation when M is less than 3:

$$\tan(m) = \frac{(M^2 - 1)\,[2 + (\lambda - 1)\,M^2]}{(\gamma + 1)\,M^4} \tag{2.70}$$

Equation (2.48) is integrated to give:

$$A = k \cdot e^{\int_1^M \frac{M\lambda(M)}{(M^2-1)}} \cdot dM \tag{2.71}$$

Equations (2.63) and (2.70) together with Equation (2.71) are used to obtain the values of ω, m and A for a given shock Mach number and the results are

tabulated in Table 1. These values can be used to draw the characteristic lines in the continuous portion of the wave diagram.

2.3 Discontinuities

The two well known shock wave reflections on a concave surface are illustrated in Figure 2.7a for regular reflection and Figure 2.7b for Mach reflection. Depending on the wall angle θ_ω and the incident shock Mach number M_o, the Mach reflection will take place. In Figure 2.7b, the point of contact of the incident and the reflected shock moves away from the wall leaving a Mach stem connecting the triple point to the wall. χ is the angle of the triple point locus from the wall, and θ_ω is the wall angle. The relationship for these parameters can be obtained by the application of the Ray-shock theory.

Consider a wedge of finite angle which causes the Mach reflection of an incident shock, as shown in Figure 2.8. Let α and $\alpha+\Delta\alpha$ be the two successive positions of the shock wave of Mach number M_o and also let R and S be the corresponding triple points. By geometrical manipulation, the ratio of Ray tube area at successive positions of the shock can be given as:

$$\frac{A}{A_o} = \frac{\sin(\chi - \theta_\omega)}{\sin \chi} \tag{2.72}$$

The velocity of the triple point 'C_T' in the α,β plane can be obtained as follows:

$$(RS)^2 = (M\,\Delta\alpha)^2 + (A\,\Delta\beta)^2 = (M_o\,\Delta\alpha)^2 + (A_o\,\Delta\beta)^2$$

or

$$(C_T)^2 = \left(\frac{\Delta\beta}{\Delta\alpha}\right)^2 = \frac{M_o^2 - M^2}{A^2 - A_o^2} \tag{2.73}$$

where M_o and M represent the incident shock and Mach stem respectively. From Fig. 2.8:

$$\text{Tan}\,(\chi - \theta_\omega) = \frac{A \cdot \Delta\beta}{M \cdot \Delta\alpha} = \frac{A \cdot C_T}{M}$$

$$= \frac{A}{M}\left(\frac{M^2 - M_o^2}{A_o^2 - A^2}\right)^{1/2} \tag{2.74}$$

$$\text{Tan}\,(\chi) = \frac{A_o}{A} \cdot \frac{M}{M_o} \tan\,(\chi - \theta_\omega) \tag{2.75}$$

The corresponding change in θ_ω can be obtained by noting that

$$\cot\,(\theta_\omega) = \tan\,(TRS + SR\theta)$$

$$\cot\,(\theta_\omega) = \frac{\frac{AC_T}{M} + \frac{M_o}{A_o}\,\frac{1}{C_T}}{1 - \frac{A}{A_o}\,\frac{M_o}{M}}$$

substituting the value of C from Equation (2.55) and rearranging it, we get:

$$\tan(\theta_\omega) = \frac{[(M^2 - M_o^2)(A_o^2 - A^2)]^{1/2}}{AM + A_oM_o} \tag{2.76}$$

Since the Mach stem and the incident shock wave remain contingious during the movement of the triple point locus, the velocity of both sections must be identical and this yields the following equation:

$$\frac{M}{M_o} = \frac{\cos(\chi - \theta_\omega)}{\cos(\chi)} \tag{2.77}$$

The Mach stem and the shock-shock angle can be obtained by solving Equations (2.77), (2.76), and (2.40) simultaneously.

The Ray-shock theory assumes that the stem is always straight and normal to the wall, whereas the stem in the experiment was observed to be curved, as shown in Fig. 2.9. Especially for the case of weak shock waves, the curvature appears at larger angles of θ_ω. Therefore, the results taken from the Ray-shock theory represent the mean value. B.E. Milton [17] has considered the effect of a curved Mach stem, and has given his experimental results of the case which slightly deviates (2-3%) from the Ray-shock theory, this is illustrated in Figures 2.10 and 2.11.

It is inherent that the Ray-shock theory does not exactly predict the Mach shock angle and the characteristic angle m in the case of weak incident shock

waves. In the present work, the values of χ and m were taken from the experimental results, illustrated in Fig. 2.12, of Shirouzu and Glass [25] and Skew's Equation (2.70), respectively.

2.4 Transition Process from Regular Reflection to Mach Reflection of A Shock Wave Over a Circular Cylinder

When a planar shock wave encounters a circular cylinder, it initially reflects as a regular reflection, RR, as shown in Fig. 2.13a. As the incident shock, IS, propagates downstream, the incident angle, θ_ω, varies and reaches the critical value θ_{crit}, where transition from regular to Mack reflection takes place. A schematic drawing of such a Mach reflection is shown in Fig. 2.13b. In the figure, the point T where the incident shock IS, the regular reflection RR, and the Mach stem MS intersect is called the triple point. The Mach stem, MS, which is generated from the Mach reflection, detaches from the curved wall and the triple point. A contact discontinuity which divides the flow into two parts is shown by the dotted line.

Itoh and Itaya [22] constructed the theory and verified through experiments, the transition process for both convexed and concaved curved wall boundaries. The theory predicts fairly well the transition from RR to MR in a convexed curved wall, whereas, in the case of a concaved curved wall, the theory is not too applicable. This theory applies the Ray shock theory and the geometry relation of the shock. The transition process from

Regular Reflection to Mach reflection is shown in Fig. 2.14. From its geometry, we get:

$$L = M_o\, a_o\, dt$$

$$S = M_1\, a_o\, dt$$

$$L' = S \sin(\alpha_{crit})$$

where a_o is the sonic velocity at the undisturbed region ahead of the transmitted shock, dt is the infinitesimal time, and M_o and M_1 are the Mach numbers of the incident shock wave and the Mach stem, respectively. As the shock wave propagates downstream:

$$L' = L + K$$

which is

$$M_1/M_o \sin(\theta_{crit}) = \mathrm{Tan}(\theta_{crit}) \qquad (2.78)$$

where $\theta_{crit} = \pi/2 - \alpha_{crit}$.

As $dt \rightarrow 0$, M_1 is estimated fairly well by the Ray Shock theory when the wedge wall boundary case is applied. The relation between the wall angle, θ_ω, and the strength of the Mach stem is given by:

$$\theta_\omega = \int_{M_o}^{M_1} \frac{\sqrt{2}\, dM}{\{(M^2 - 1)\, K(M)\}^{1/2}} \qquad (2.79)$$

where K(M) is known as the Chester function. K(M) = 0.5 when $M \rightarrow 1$ and when $M \rightarrow \infty$, K(M) = 0.3941. Supposing K(M) is equal to a constant n, the integration of Equation (2.79) is:

$$\frac{M_1}{M_o} = \frac{1}{2 M_o}\left[\left\{\left(\sqrt{M_o^2 - 1} + M_o\right)\exp\left(\sqrt{\frac{\pi}{2}}\,\theta_\omega\right)\right\} + \left\{\left(\sqrt{M_o^2 - 1} + M_o\right)\exp\left(\sqrt{\frac{\pi}{2}}\,\theta_\omega\right)\right\}^{-1}\right] \tag{2.80}$$

When $M_o \rightarrow 1$, Equation (2.80) becomes:

$$\frac{M_1}{M_o} = \cosh\left(\frac{1}{2}\,\theta_\omega\right) \tag{2.81}$$

Expanding Equation (2.81) by using the power series, the equation for weak shock waves has been acquired:

$$\frac{M_1}{M_o} = 1 + \theta_\omega^2 \tag{2.82}$$

When $M_o \rightarrow \infty$,

$$\frac{M_1}{M_o} = \exp\left(\sqrt{\frac{\pi}{2}}\,\theta_\omega\right) \tag{2.83}$$

Combining Equation (2.80) with Equation (2.78), we get

$$\frac{1}{2M_o}\left[\left\{\left(\sqrt{M_o^2-1}+M_o\right)\exp\left(\sqrt{\frac{\pi}{2}}\theta_\omega\right)\right\}+\right.$$

$$\left.\left\{\left(\sqrt{M_o^2-1}+M_o\right)\exp\left(\sqrt{\frac{\pi}{2}}\theta_\omega\right)\right\}^{-1}\right]\mathrm{SIN}\,(\theta_\omega)=\mathrm{TAN}\,(\theta_\omega) \qquad (2.84)$$

The results obtained from the equation above are plotted in Fig. 2.15. For a given Mach number of the incident shock wave, the position where the transition process take places will be found. Similarly, Bendor and Takayama's theory [37] also lacks the ability to account for the dependence of the transition angle on the radius of curvature of the cylindrical rod.

2.5 Construction of Wave Diagrams

A great variety of unsteady flow problems can be solved by means of the wave diagrams which are constructed based on Whitham's Ray-shock theory. In the present work, the wave diagrams provide the shape of the shock front as it progresses downstream and also near the region of collapse, the trajectories of triple points and the examination of the stability of converging shocks. External perturbations were created by placing cylindrical rods of various diameters in the shock path and the effects were observed during the propagation of the shock.

When a cylindrical converging shock encounters a circular rod placed in its path, it initially reflects as a regular reflection 'RR'. The step by step process of the interaction is illustrated schematically in Figure 2.16. Fig. 2.16a describes the incoming converging cylindrical shock wave just upstream of

the rod. In Fig. 2.16b, a regular reflection takes place due to the small angle of incidence. As the shock wave propagates along the surface of the rod, the angle of incidence increases and eventually approaches the critical value where the transition from regular to Mach reflection 'MR' takes place. Also, a pair of Mach stems (MS_1) and contact discontinuity (CD_1) form, as shown in Fig. 2.16c. The two Mach stems, MS_1, on both sides of the rod propagates along the rod surface and collides downstream of the rod (see Fig. 2.16d). Regular reflections followed by the second Mach reflections take place between the first Mach stems, MS_1, as shown in Figs. 2.16e and 2.16f.

The interaction between the rod and a cylindrical shock wave described above gives the general image of the flow perturbed by an external factor, and the wave diagram is constructed as follows:

1. The two nondimensional coordinates are set up by taking the ratio R_o/d for both vertical and horizontal axes. If more nondimensional units are used, the wave diagrams will be more accurate.

2. The CCW theory is then employed to find the shock Mach number as the radius of cylindrical shape is varied. These Mach numbers describe the speed of the shock in unperturbed regions and it is determined either by Equation (2.71) or Table (2.1). From the Mach number of the unperturbed region, Shock Mach numbers in the perturbed regions are determined by Equation (2.77).

3. After the critical angle is determined from Fig. 2.15, the positions of the Mach stem and the point of contact discontinuity are known. An arbitrary point is chosen to draw the shock-shock trajectory. An iteration procedure is required to determine the exact slope of the shock-shock angle. In such cases, by assuming a value for $\delta\theta$, then from Figs. 2.11 and 2.12, the Mach number downstream the shock-shock in the perturbed region and the shock-shock angle can be determined. Once M and χ are known, the values of ω and θ in the perturbed region can be found from Table 2.1. The slope of the shock-shock trajectory must pass through the calculated chosen point. If it does not pass through the calculated point, a new value of $\Delta\theta$ should be assumed. The characteristic lines in perturbed regions are drawn due to one of the three cases presented below:

a) *Crossing the C^+ and C^- characteristics*

Generally, the conditions of the gas at 1 and 2 are known, as shown in Figure 2.17a, and they intersect at point 3 which is unknown. The C^+ through point 2 and the C^- through point 1 both intersect at point 3. (The characteristics are shown in dotted line but they can be approximated by straight lines of the many grids of the wave diagrams). To locate the point 3, one has to use the characteristic rule as follows:

$$C^+ = \theta + \omega = \text{const} \qquad \text{for points along } C^+ \text{ characteristics}$$

or

$$C_2^+ = \theta_2 + \omega_2 = \theta_3 + \omega_3$$

$C^- = \theta - \omega = \text{const}$ for points along C^- characteristics

or

$$C_1^- = \theta_1 - \omega_1 = \theta_3 - \omega_3$$

solving for θ and ω,

$$\theta_3 = \frac{1}{2}(C_2^+ + C_1^-)$$

$$\omega_3 = \frac{1}{2}(C_2^+ - C_1^-)$$

The C^+ and C^- characteristics can be drawn by taking the average of the slope of each point, i.e.

$$(\theta + m)_{2\text{-}3} = 1/2\,[(\theta + m)_2 + (\theta + m)_3]$$

and

$$(\theta - m)_{1\text{-}3} = 1/2\,[(\theta - m)_1 + (\theta - m)_3]$$

b) *The intersection between the characteristic lines and the plane of symmetry*

For the points on the plane of symmetry, Fig. 2.17b, the Ray angle θ is equal to zero. Since

$$C^+ + C^- = 2\theta$$

then

$$C^+ = C^-$$

Therefore, points on the plane of symmetry are located according to the procedure discussed above.

c) *The characteristic and the shock-shock*

Once ω, m, and θ are known, the C^+ and C^- characteristic, downstream of the shock-shock can be found. The values of C^+ passing through points 3 and 10, as shown in Fig. 2.18, must be the same, i.e. $(\theta + \omega)_{10}$ equals to $(\theta + \omega)_3$, whose value is interpolated by assuming linear relation between neighboring characteristics.

Chapter 3

EXPERIMENTAL SET UP AND PROCEDURE

The present investigation was carried out using the 15.24-cm nominal size, commercial steel, shock tube located in the SHOCK WAVE DYNAMICS LABORATORY. All experiments were conducted by using air as the fluid. The cylindrical shock waves in the implosion chamber were perturbed by placing rods of various diameters in their path. Spark Schlieren photographs of the converging shocks were taken to study their stability as they approached the center of collapse.

The apparatus used to produce converging cylindrical shock waves consists of the following main components:

a) The axisymmetric shock tube;

b) The Schlieren system;

c) The mechanical plunger.

A schematic of the shock tube is shown in figure (3.1) together with the Spark Schlieren-Delay system used for photographing the converging shocks. Details are given in the next section.

3.1 Experimental Apparatus

3.1.1 The axisymmetric shock tube

The axisymmetric shock tube consists of a driver section 2.0-meter long, and a driven section 3.81-meter long. The two sections were separated by mylar diaphragms of various thicknesses. Air was used as the fluid in both the driver and driven sections. To prevent air leakage, O-rings were installed in the raised face of the flanges connecting the driver to the driven sections. After setting the required pressure, the mylar diaphragm was split open by a mechanical plunger located in the driver section and operated pneumatically by compressed air. This produced a circular plane shock which was later divided into a circular and annular parts, by an aluminum tube 4-inches in diameter, placed concentric with the outer one. The inner aluminum tube was supported by 4 fins, as shown in Fig. 3.2. The annular part of the shock was turned 90 degrees using the conical three elements area contraction, illustrated in Fig. 3.3, that was found to offer the lowest pressure attenuations behind the transmitted shock. At the downstream end of the shock tube and upstream of the area contraction, two transducers were installed; one for triggering the oscilloscope beam and the Schlieren-delay system, and the other for pressures and shock velocity measurements.

Induced rupture of the diaphragms by mechanical or electrical means is often preferable over to natural bursting by pressure alone in order to gain precise control of the bursting pressure. The most common method of rupturing the diaphragm is to use a mechanical piercer with a sharpened

plunger. A plane shock of Mach number 1.21 was obtained using a mylar diaphragm 0.08-mm thick and loading the driver section with air at a pressure of 27 psig, then firing the shock by piercing the diaphragm with the mechanical plunger which was activated by compressed air at high pressures. This plunger is put concentric with the shock tube and is controlled by a switch located on the control panel, as illustrated in Fig. 3.4.

3.1.2 The Schlieren system

In the present work, the Schlieren method was employed to photograph the converging shock. The Schlieren system consists of a 5 KV-spark source, a double headed spherical mirror, a plane mirror, a knife edge and a camera, as illustrated in Fig. 3.5. The light generated from the source becomes parallel following its reflection from the double headed spherical mirror located at the focal length distance from the source. At the test section, all incoming rays are reflected by the flat mirror placed inside. The spherical mirror, once again, receives and transmits all the light rays from the test section to a second small plane mirror which finally directs the light rays to an open shutter camera. The Spark source was triggered by a transducer placed just upstream of the conical area contraction. All sets of photographs were taken by a Polaroid camera (Mp-3) and type 41 ASA Polaroid film.

3.2 Experimental Procedure

Before joining the two sections of the shock tube, they were first checked and cleaned from any mylar fragments which could have remained from the

previous firing. A 0.08-mm thick mylar sheet was used to separate the driver and driven chambers. The pressure in the driven section was kept at atmospheric conditions, while that in the driver section was raised to the desired pressure of 185.4 KPa. After the mylar diaphragm was ruptured by the plunger, a plane shock wave was formed.

The Mach number of the shock can be determined by either the shock tube equation or from the experimental data.

From the shock tube equation:

$$M_s - \frac{1}{M_s} = \left(\frac{a_4}{a_1}\right)\left(\frac{\gamma_1 + 1}{\gamma_4 - 1}\right)\left[1 - \left(\frac{2\gamma_1 M_s + (\gamma_1 - 1)}{\gamma_1 + 1}\left(\frac{P_1}{P_4}\right)\right)^{\frac{\gamma_4 - 1}{2\gamma_4}}\right] \qquad (3.1)$$

where $\gamma_1 = \gamma_4 = 1.4$ for air, and $a_1 = a_4$.

M_s can be determined for any given pressures P_1 and P_4. From the experiment, the strength of the shock was calculated by means of two transducers mounted on the driven section; one for triggering the oscilloscope beam and the other for measuring the pressure. Since the distance between the two transducers, Δx, and the time of propagation, Δt, are known, the shock velocity, V_s, can therefore by calculated as follows:

$$V_s = \frac{\Delta x}{\Delta t} \qquad (3.2)$$

The shock Mach number, M_s, was calculated when the room temperature, T_r, was recorded.

$$M_s = \frac{V_s}{a_o} = \frac{V_s}{\sqrt{\gamma R T_r}} \tag{3.3}$$

The pressure across the shock was determined by taking the transducer contents multiplied by the voltage, which was recorded on the oscilloscope.

The experiments on weak shock waves were done after the three transducers had been calibrated many times. Their constants are tabulated with their manufactured numbers.

SN 1178	SN 1175	SN 1239
32 mv/psia	26 mv/psia	20 mv/psia

In the cylindrical chamber, the shock Mach number varies with shock travel. The local values of the shock Mach number were determined by means of three transducers placed at radii 24.13, 13.97 and 3.81-mm from the geometric center.

From the oscilloscope trace, the voltage rise due to the passage of the shock, ΔV, was measured and then divided by the appropriate transducer constant to yield the pressure difference across the shock. Knowing that the pressure ahead of the shock is atmospheric, the pressure ratio across the shock

was therefore determined from the normal shock tables. The local values of the converging shock Mach number were then calculated.

A plane shock of Mach number 1.21 was obtained with the driver and driven pressures set at 27 and 0 psig, respectively. This produced a converging shock Mach number of 1.5 in the cylindrical chamber at a radius of 40-mm from the geometric center. At smaller radii, two other transducers were placed for local shock Mach number measurements with and without external perturbations. The Schlieren photographs of the shock waves were obtained with the same set up conditions stated previously. The cylindrical shocks were perturbed by rods of diameters 0.4, 0.8, and 1.6-mm placed at a radius of 40-mm from the geometric center. More details on the experiments and their results are given in the following chapter.

Chapter 4

RESULTS AND DISCUSSION

The stability of converging cylindrical shock waves was studied by placing cylindrical rods in the converging shock paths. Wave diagrams constructed using Whitham's Ray-shock theory and the CCW Area Mach relationship were used to theoretically determine the flow field generated by the impingement of the cylindrical shock on the rod, as well as the variation in its shape as it propagates towards the center of collapse. For weak shocks, the Ray-shock theory does not accurately predict the values of the characteristics or the shock-shock angles. Accordingly, the results of Shirouzu and Glass [23], and Skews [39], were used instead to determine the shock-shock angles. In addition, the Mach number of the incident shock was chosen to be 1.5 because Mach reflection is not well defined for small Mach numbers. The trajectories of the inner and outer shock-shocks were theoretically obtained from the wave diagrams and experimentally obtained from the Schlieren photographs. The details are presented in the following sections.

4.1 Shock Velocity Measurements of Perturbed and Unperturbed Shocks

The Ray-shock theory used in the present work depends largely on the CCW Area-Mach number relationship. Therefore, experimental verification of this relationship was necessary for obtaining reliable results. Various

pressure transducers were placed at different locations along the converging shock path to determine the pressure increase across the shock by measuring the corresponding voltage rise in the oscilloscope traces. The local values of the shock Mach number were then calculated from the well known shock relationship,

$$M = \sqrt{1 + \frac{\gamma + 1}{2\gamma} \frac{\Delta P}{P}} \tag{4.1}$$

where

ΔP is the pressure difference across the shock in the annular section

P is the absolute value of the pressure ahead of the shock.

Two series of tests were carried out. The first series were for unperturbed shocks at the three different radii, r/R_o = 0.6, 0.35 and 0.095, where R_o is the radius where the initial value of the shock Mach number is 1.5. The results are presented in Fig. 4.1. Excellent agreement is noted between the CCW theory and experiment. This could be due to the type of area contraction used (the three-elements-area-contraction) which was previously found to prevail transmitted shocks with minimum pressure attenuation.

The second series of tests were for converging shocks perturbed by rods of diameters 1.6- and 0.4-mm. The rods were placed at a radius of 40-mm from the geometric center. The transducers were set along the radial line connected to the center line of the rod. The results are shown in Figs. 4.2 and

4.3. From the figures, the Mach numbers of perturbed shocks are found to be superior to those of the unperturbed ones. For the latter, reasonable agreement between the theory and experiment is noted. Details will be given later.

4.2 Spark Schlieren Photography of the Converging Cylindrical Shock Perturbed by Different Rods

Two sets of Spark Schlieren photographs (Fig. 4.4) were taken for converging cylindrical shocks of Mach number 1.5 perturbed by rods of diameters 0.8- and 1.6-mm, placed in their path at a radius, R_o, of 40-mm.

The first set of photographs taken for a rod diameter of 1.6-mm and for $R_s/R_o < 0.31$, is presented in Fig. 4.4a. As noted in photograph (A), the shock is near perfect symmetry. When the shock progresses, the perturbed part is found to propagate faster than the unperturbed one and the shock collapses in a region close to the geometric center, on the opposite side of the rod (photograph C). From these photographs, it was possible to obtain the inner and outer shock-shock trajectories. The shock-shocks are found to merge into one before the final state of collapse.

For comparison purposes, the second set were taken with a small rod having a diameter of 0.8-mm, shown in Fig. 4.4b. In this series, the effect of the rod is not as noticeable as in the first case. The two shock-shocks are visible but are much weaker and the shock is seen to collapse very near the

geometric center. To understand and to analyze these pictures in more detail, wave diagrams were constructed for the three rod diameters (R_o/d) of 25, 50, and 100. Details are given below.

4.3 Wave Diagrams for a Converging Cylindrical Shock Perturbed by Different Cylindrical Rods

The complete wave diagram for the largest rod used ($R_o/d = 25$) is shown in Fig. 4.5. As previously demonstrated, two pairs of discontinuity are present in the shock front, representing the inner and outer triple points of the Mach reflection. In the figure, the inner shock-shock forms at a distance of about 1.2 rod diameter, downstream of the rod surface, and sweeps faster than the outer shock-shock until they merge at a radius R_s/R_o of 0.006. The perturbed part of the shock is also found to travel faster than the unperturbed one. This results in the shifting of the region of collapse beyond the geometric center and on the opposite side of the rod. The calculated values of the perturbed portion of the shock Mach number are plotted in Fig. 4.2 together with those obtained experimentally. From the wave diagram, it was possible to obtain both the outer and inner shock-shock angles. These values together with those extracted from the Spark-Schlieren photos were plotted in Figures 4.6 and 4.7. Good agreement between theory and experiments is noted indicating the validity of the present results.

The wave diagram for $R_o/d = 50$ is presented in Fig. 4.8. In this case, the inner shock-shock begins at a distance of one rod diameter. In this case, the

center of collapse is observed to shift beyond the geometric center and on the opposite side of the rod. Good agreement between the theoretical and experimental results of the outer shock-shock angle (Fig. 4.10) and the inner shock-shock angle (Fig. 4.11) is also noted.

For $R_o/d = 100$, the wave diagram is shown in Fig. 4.11. The inner shock-shock trajectory was found at the shortest distance, 0.55 of rod diameter behind the cylinder. As compared with the two previous cases, the inner trajectory develops with the lowest values of flow deflection angle, presented in Fig. 4.12, and merges with the outer trajectory at a radius of $R_s/R_o = 0.096$ as opposed to 0.012 and 0.064 obtained with the R_o/d of 25 and 50, respectively. It shows that the inner shock-shock is found to sweep at a faster pace than the two previous cases and collapses with the outer shock-shock.

The shock fronts were drawn using the Ray-Shock theory. The slopes of the shock fronts, which are inclined with the vertical axis, increases as they are propagating downstream. The shock fronts perturbed by the smaller rod is less distorted than the shock fronts perturbed by the larger rod.

From the wave diagrams, it was possible to obtain the inner and outer shock-shock trajectories. The trajectories, obtained theoretically and experimentally for three cases studied, are presented in Figs. 4.13, 4.14, and 4.15. For the smaller diameter rod, observed in Fig. 4.14, it is clear that the theory is in good agreement with the experimental results, while some discrepancies were found with the inner shock-shock of the bigger diameter

rod, as shown in Fig. 4.13. The experimental values are found to be larger than those obtained theoretically. This could be partially due to the difficulty in defining an exact value of χ in the case of weak shock waves.

When $d/R_o \rightarrow 0$, both inner and outer shock-shocks become one and of very small strength, and therefore propagates along the shock front with the speed of sound behind the converging shock, i.e.

$$\dot{\theta} = a(R_s)/R_s \tag{4.2}$$

where

R_s is the instantaneous shock radius

$a(R_s)$ is the instantaneous speed of sound behind the shock front

$\dot{\theta}$ is the angular velocity of the triple point.

By integration, Equation (4.2) yields:

$$\theta = \pm \int_{R_o}^{R_s} \frac{a(R_s)}{R_s} dt$$

but $dR_s = -R_s \cdot dt$, then

$$\theta = \pm \int_{R_o}^{R_s} -\frac{a(R_s)}{R_s \cdot R_s} dR_s = \pm \int_{R_o}^{R_s} \frac{a}{a_o} \frac{1}{M} \frac{dR_s}{R_s} \tag{4.3}$$

Using both the Rankine Hugoniot relations and the CCW Area-Mach relationship, this equation was integrated and the results are plotted in Fig. 4.16. As d/R_o decreases, the shock-shock trajectories tend to spread out toward the limiting case. The locations where the two shock-shock merge are shown in Fig. 4.17 and from the figure using extrapolation, the rod diameter d/R_o, where all shock-shocks merge together at one point (θ = 180 degrees), is found to be equal to 0.057. For rods of larger diameters, the two shocks do not intersect during shock convergence.

4.4 Perturbation Growth and Stability of Initially Weak Converging Cylindrical Shock Waves

The perturbation factor ξ is defined as the ratio between the shock displacement from the perfect circular shape, ΔR, and the instantaneous radius of the unperturbed portion of the cylindrical shock, R_s, i.e.

$$\xi = \frac{\Delta R}{R_s} \tag{4.4}$$

The values of the shock displacement, ΔR, were determined theoretically from the three wave diagrams presented in Figs. 4.18, 4.19, and 4.20. In the figures, the absolute value of the initial displacement is found to be proportional to the size of the perturbations used. For R_o/d of 25, the value of ΔR is practically equal to zero at R_s/R_o = 0.31, which corresponds to photo "A" in Fig. 4.4a. Beyond this limit and with the velocity of the unperturbed part exceeding that of the perturbed one, ΔR is found to increase again up to a

finite value at the region of collapse. From the wave diagram, the displacement is about 0.3 of the rod diameter which is close to that observed in photograph "C" of Fig. 4.4a.

For rods of smaller diameter, the theoretical values of ΔR were found to decrease until a critical radius R_s/R_o of 0.5 was reached, then increased to larger values with shock travel. This, however, was not observed experimentally. The discrepancy could be due to the error in calculating the strength of the Mach stem for the lower values of $\Delta\theta$ (see Fig. 4.12). The combination of these small values and weak shocks made the results unreliable as far as the shock shifting was concerned. From the above results, it is clear that with small but finite perturbation, converging cylindrical shocks are unstable due to the absolute value of the shock displacement, ΔR, and not to its relative value to shock radius. At large radii, the decrease in the value of ΔR is not monotonic but oscillates about a mean value which decreases initially with shock travel. Such a statement is in agreement with the theoretical analysis of reference 36 which has proven that ΔR varies in a similar fashion with shock travel.

Chapter 5

CONCLUDING REMARKS

The stability of converging cylindrical shock waves of Mach number 1.5, perturbed by cylindrical rods placed in their paths, was studied both theoretically and experimentally. From this study, the following conclusions are drawn:

(i) Weak converging cylindrical shocks have shown some sign of stability when perturbed by smaller rods ($R_o/d \geq 50$). With larger perturbation, especially when $R_o/d = 25$, partial stability is noted up to a critical radius $R_s/R_o = 0.31$, where the perturbation parameter decreases to zero. Beyond that critical radius, it then increases to larger values before collapse.

(ii) Weak shocks perturbed by small rods tend to collapse in a region close to the geometric center, on the opposite side of the rod. This could be due to the fact that the triple points tend to sweep faster for weak shocks than for strong ones.

(iii) The Ray-shock theory is found to accurately predict the triple points trajectories in all the cases studied. Best agreement between the theory and experiments was observed for the small rod diameter used ($R_o/d = 50$). For a larger diameter rod, the discrepancies

between the two were noted due to the error incorporated in the calculation of the Mach number of Mach stem. In order to minimize these discrepancies, a better theoretical prediction of the latter is required.

REFERENCES

1. Gurdeley, G., "Powerful Spherical and Cylindrical Compression Shocks in the Neighbourhood of the Center of the Sphere and of the Cylindrical Axis", Luftfahrtforschung, Vol. 19, 1942, p. 302.

2. Neemeh, R.A. et al., "Experiments on the Stability of Converging Cylindrical Shock Waves", AIAA Journal, Vol. 19, March 1981, p. 257.

3. Wu, J.H.T., Neemeh, R.A. and Ostrowski, P.P., "Experimental Studies of the Production of Converging Cylindrical Shock Waves (SYN)", AIAA Journal, Vol. 18, No. 1, pp. 47-49.

4. Neemeh, R.A. and Ahmad, Z., "Stability and Collapsing Mechanism of Strong and Weak Converging Cylindrical Shock Waves Subjected to External Perturbation", 15th Int. Symp. on SWST, Berkeley, California, August 1985, p. 47.

5. Whitham, G.B., "A New Approach to Problems of Shocks Dynamics Part I Two-Dimensional Problems", J. Fluid Mech., 1957, Vol. 5, pp. 145-171.

6. Chester, W., "The Quasi-Cylindrical Shock Tube", Phi. Mag., 1954, Vol. 45, pp. 1239-1301.

7. Chisnell, R.F., "The Motion of a Shock Wave in a Channel, with Applications to Cylindrical and Spherical Shock Waves", J. Fluid Mech., 1958, Vol. 4, pp. 268-298.

8. Chester, W., "The Propagation of Shock Waves in a Channel of Non-Uniform Width", Quart. J. Mech. and Appl. Math., 1953, Vol. VI, Part 4, pp. 440-452.

9. Chester, W., "The Propagation of Shock Waves along Ducts of Varying Cross Section", Advances in Appl. Mech., 1960, Vol. 6, pp. 119-152.

10. Wu, J.H.T., Yu, T.S., Neemeh, R.A., and Ostrowski, P.P., "Stability of Cylindrical Converging Shock Perturbed by a Bleed Aperature", Proceeding of the 12th Symposium on Shock Tubes and Waves, Jerusalem, 1979, p. 324.

11. Perry, R.W. and Kantrowitz, A., "The Production and Stability of Converging Shock Waves", Journal of Applied Physics, Vol. 22, No. 7, July 1951, p. 878.

12. Lapworth, M.G., "An Experimental Investigation of a Plane Shock Waves", Journal of Fluid Mechanics, Vol. 6, pp. 469-480.6. Freeman, N.C., "On the Stability of Plane Shock Waves", Journal of Fluid Mechanics, Vol. 31, 1968, p. 529.

13. Freeman, N.C., "A Theory of the Stability of Plane Shock Waves", Proc. Royal Society, London, 2281, 1954, p. 341.

14. Lee, J.H., Knystautas, R., "Experiments on the Stability of Converging Cylindrical Detonation", Combustion and Flame Journal, Vol. 16, 1971, pp. 61-73.

15. Payne, R.B., "A Numerical Method for a Converging Cylindrical Shock", Journal of Fluid Mechanics, Vol. 2, 1957, p. 185.

16. Whitham, G.B., "On the Propagation of Shock Waves through Regions of Non-Uniform Area or Flow", J. Fluid Mech., 1958, Vol. 4, pp. 337-360.

17. Milton, B.E., "Shock Wave Motion and Focusing in Area Construction", Ph.D., Thesis, University of New South Wales, Australia, 1971.

18. Neemeh, R.A., "Experimental Studies of Converging Cylindrical Shock Waves Produced by Area Contractions", Ph.D. Thesis, Mc Gill University, 1976.

19. Whitham, G.B., "A New Approach to Problems of Shock Dynamics Part 2 Three Dimensional Problems", J. Fluid Mech., 1957, Vol. 2, pp. 369-386.

20. Bryson, A.E. and Gross, R.W.F., "Diffraction of Strong Shocks by Cones, Cylinders and Spheres", J. Fluid Mech., 1961, Vol. 10, pp. 1-16.

21. Yang, Y.J., Yen Liu and Harvard Lomax, "Computation of Shock Wave Reflection by Circular Cylinders", AIAA Journal, Vol. 25, No. 5, May 1987, pp. 683-689.

22. Itoh, S. and Itaya, M., "On the Transition between Regular and Mach Reflection", Proceedings of the 10th International Symposium on Shock Tube, Jerusalem, 1979, pp. 314.

23. Henderson, L.F. and Lozzi, A., "Experiments on Transition of Mach Reflection", Journal of Fluid Mechanics, Vol. 68, 1975, pp. 139-155.

24. Ben-Dor, G. and Glass, I.I., "Domains and Boundaries of Nonstationary Oblique Shock-Wave Reflections in Perfect and Imperfect Monatomic and Diatomic Gases", Proceeding of the International Symposium on Shock Tube.

25. Glass, I.I. and Shirouzu, M., "An Assessment of Recent Results on Pseudo-Stationary Oblique Shock Wave Reflections", UTIAS Report No. 264, 1982.

26. Bleakney, W. and Taub, A.M., "Interaction of Shock Waves", Rev. Mod. Phys., Vol. 21, 1949, p. 584.

27. Gurdeley, G., "Non-Stationary Gas Flow in Thin Pipes of Variable Cross Section", N.A.C.A., TM1196, 1948.

28. Rudinger, G., "Passage of Shock Waves through Ducts of Variable Cross Section", Physics of Fluids, 1960, Vol. 3, pp. 449-455.

29. Takayama, K., Kleine, H., and Gronig, G., "An Experimental Investigation of the Stability of Converging Cylindrical Shock Waves in Air", Exp. Fluid 5, pp. 315, 1987.

30. Whithan, G.B., "Linear and Nonlinear Waves", Wiley, New York, 1974.

31. Rudinger, G., "Wave Diagram for Nonsteady Flow in Ducts", D. Van Nostrand Company, Inc., Toronto, 1955.

32. Butler, D.S., "The Stability of Converging Spherical and Cylindrical Shock Waves, Armament Research and Development Establishment, Report No. (B) 18/56, 1956.

33. Henderson, L.F. and Lozzi, A., "Experiments of Reflections of Plane Shoch Waves at Cylindrical Surfaces", Journal of Fluid Mechanics, Vol. 68, 1975, p. 363.

34. Shapiro, A.H., "The Dynamics and Thermodynamics of Compressible Fluid Flow", The Ronal Press Co., New York, Vol. 1 and Vol. 2, 1954.

35. Skews, B.W., "The Shape of a Diffracting Shock Wave", Journal of Fluid Mechanics, 1967, Vol. 29, pp. 297-305 and pp. 705-719.

36. Gardner, J. and Book, D., "Stability of Imploding Shocks in the CCW Approximations", J. Fluid Mechanics, Vol. 114, 1982, pp. 41-58.

37. Bendor, G. and Takayama, K., "Analytical Prediction of the Transition from Mach to Regular Reflection Over Cylinder Concave Wedges", J. Fluid Mech., 1985, Vol. 158, pp. 365-380.

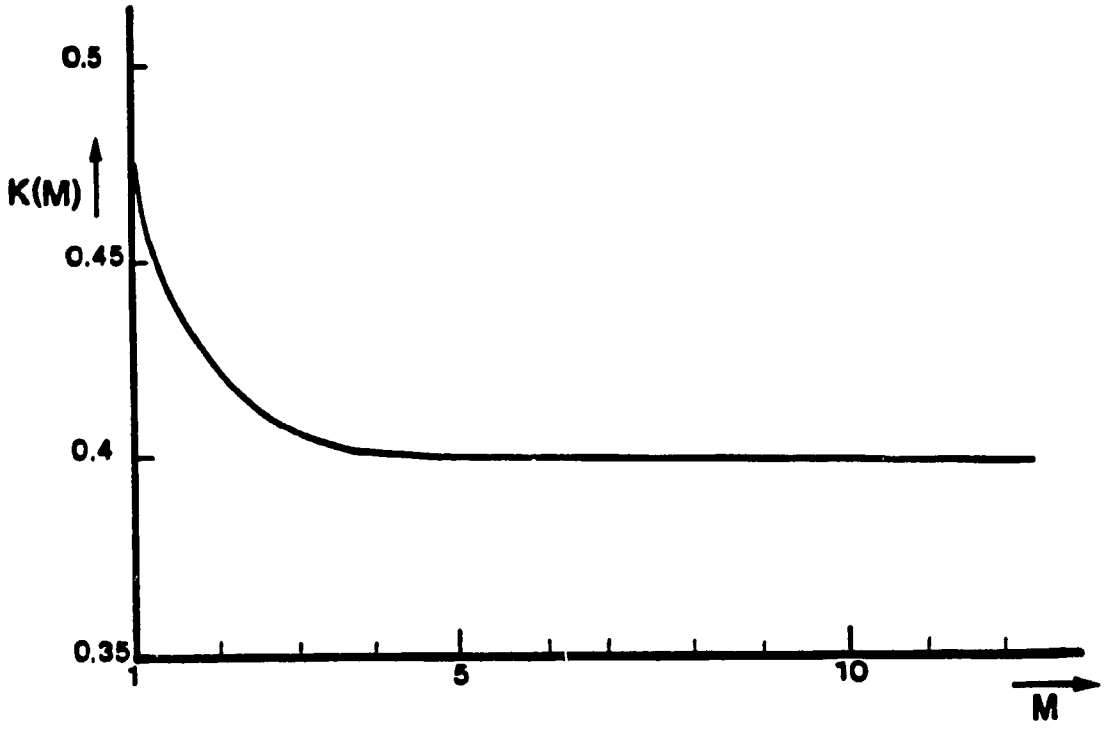

Fig. 2.1 The Graph of Chester's Function

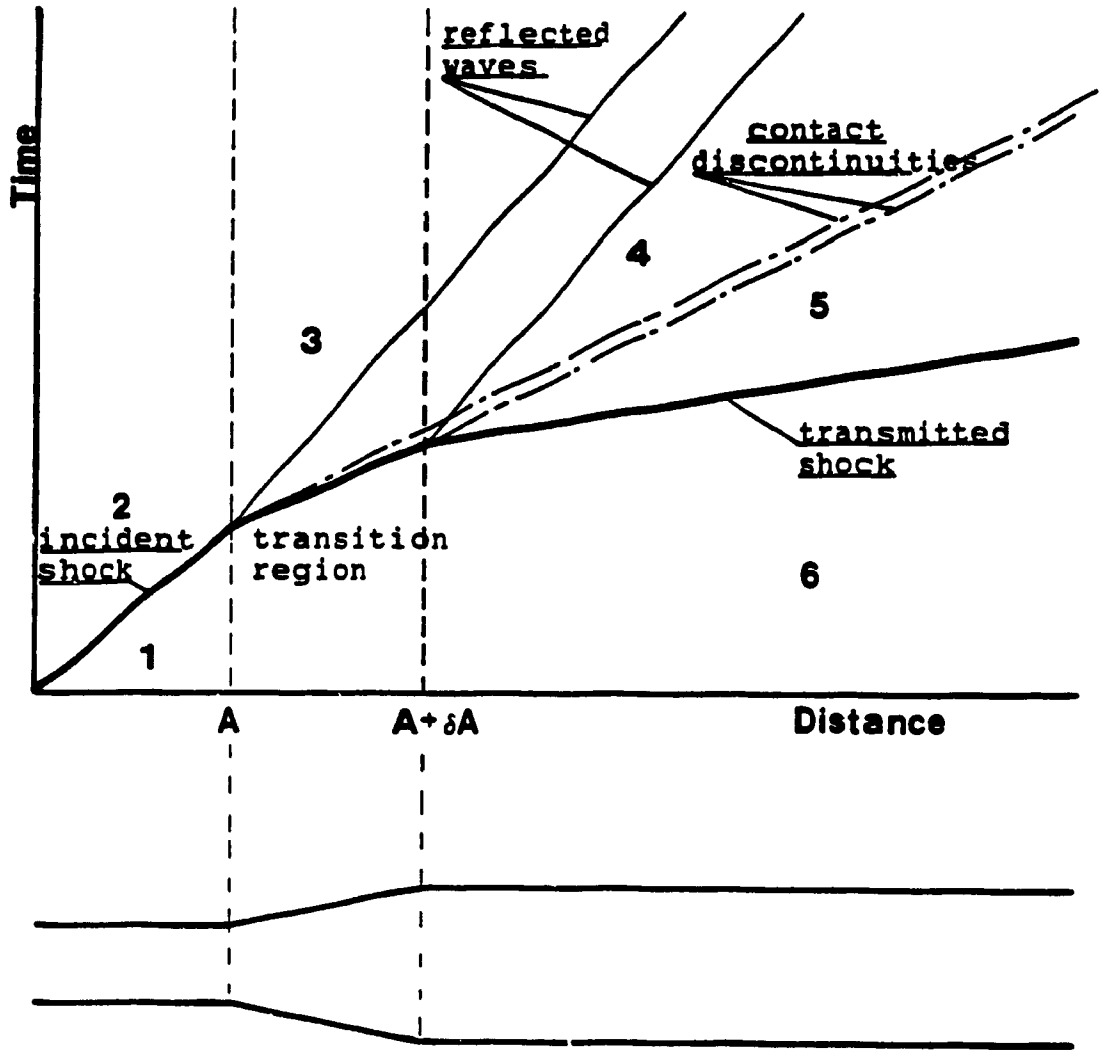

Fig. 2.2 Propagation of Shock Wave in Small Area Change of Duct

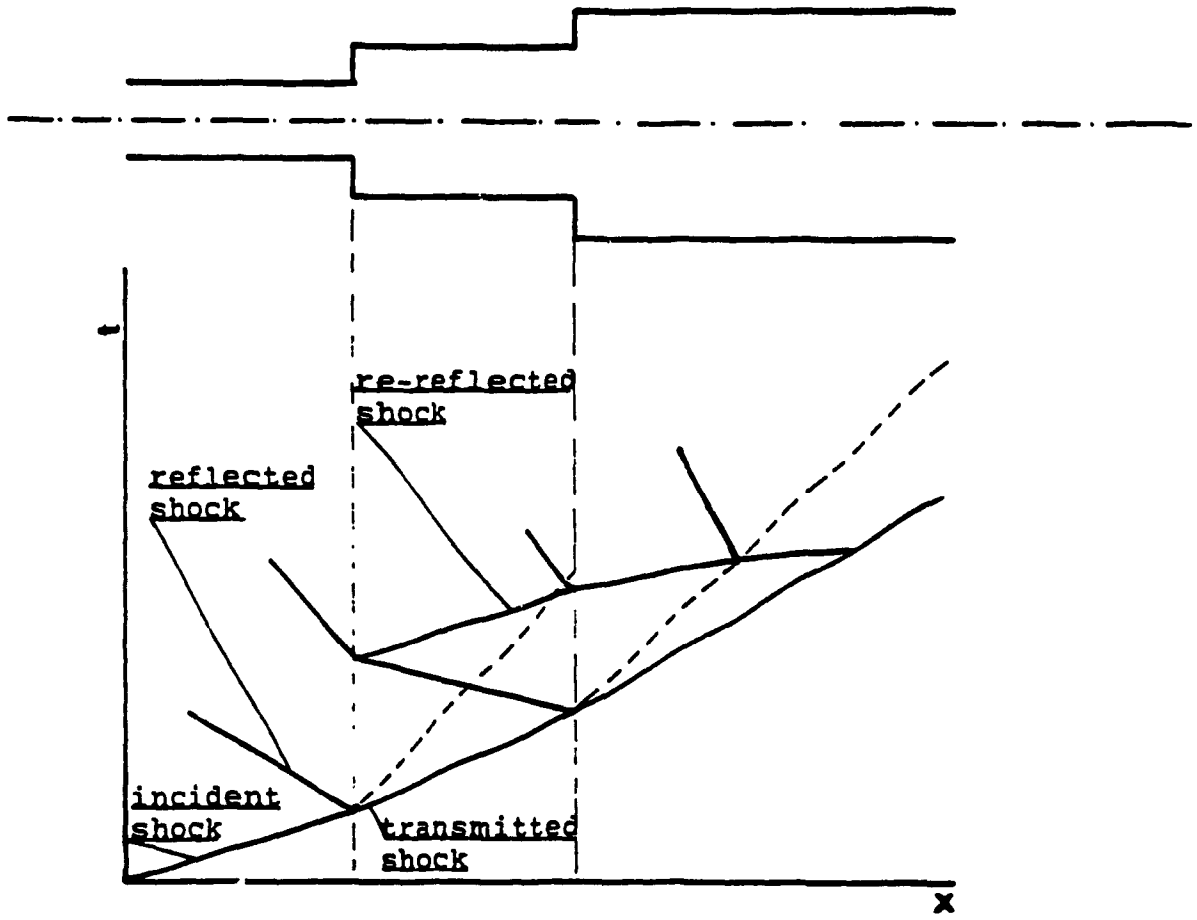

Fig. 2.3 Transmission of Shock Wave in Small Area Change of Duct

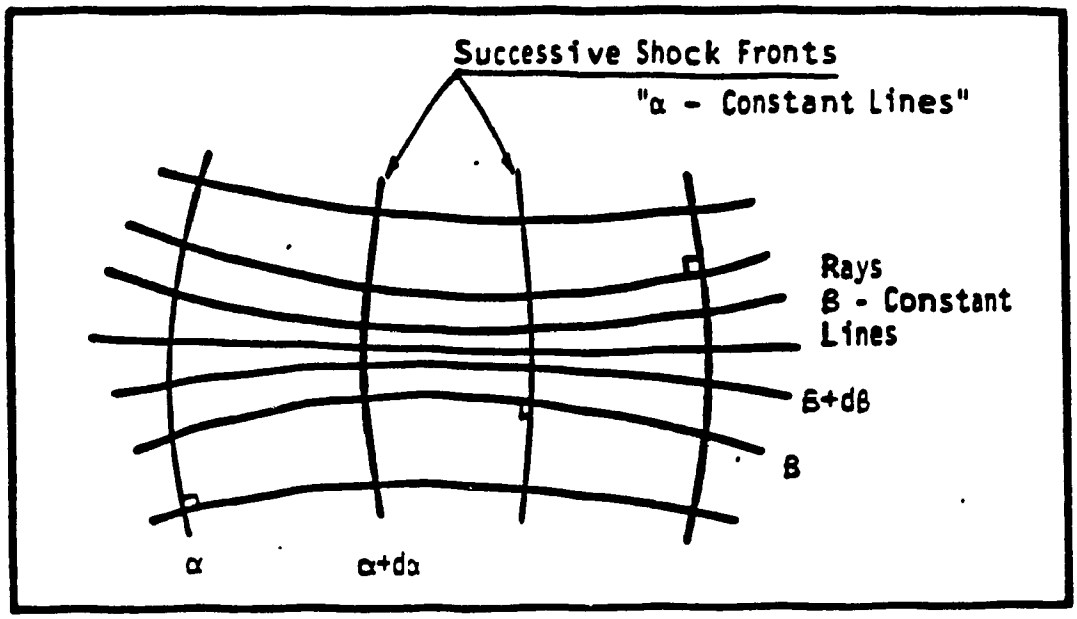

Fig. 2.4 Orthogonal Ray-Shock Grid

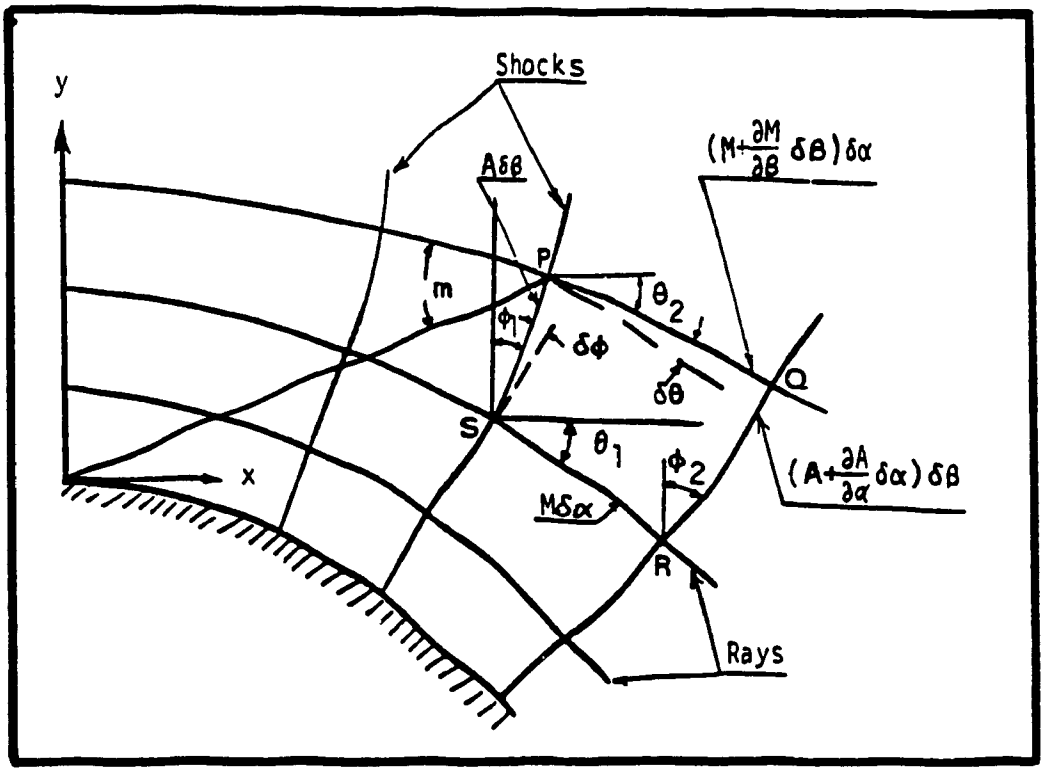

Fig. 2.5 Geometry of Ray-Shock Coordinates

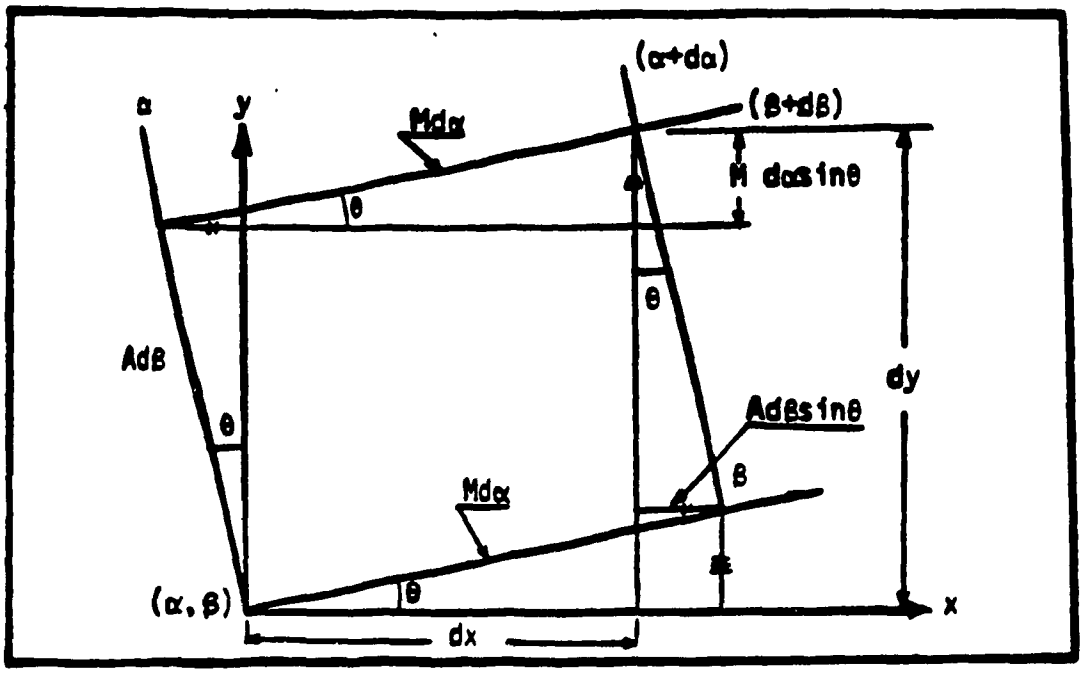

Fig. 2.6 Transformation Between Curvilinear and Cartesian Coordinates

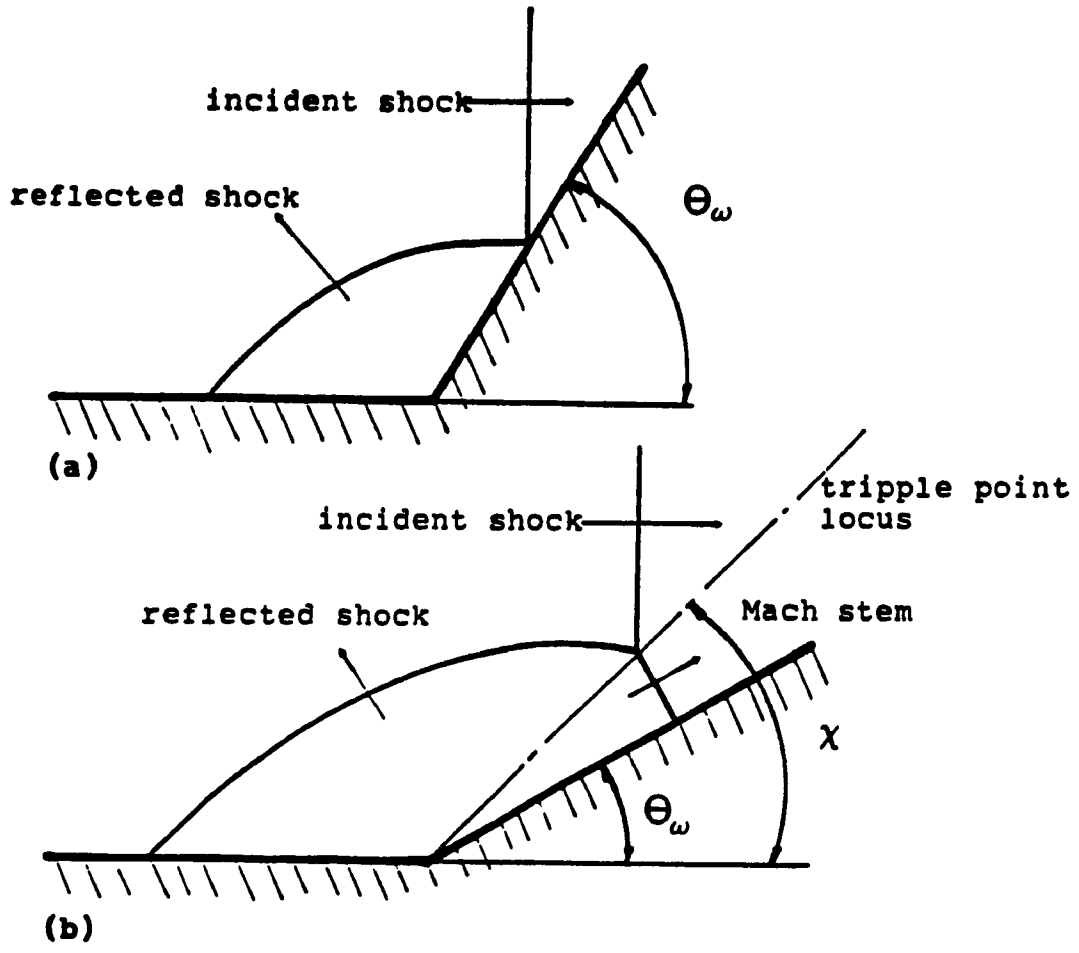

Fig. 2.7 Reflection at Concave Surface

(a) Regular Reflection

(b) Mach Reflection

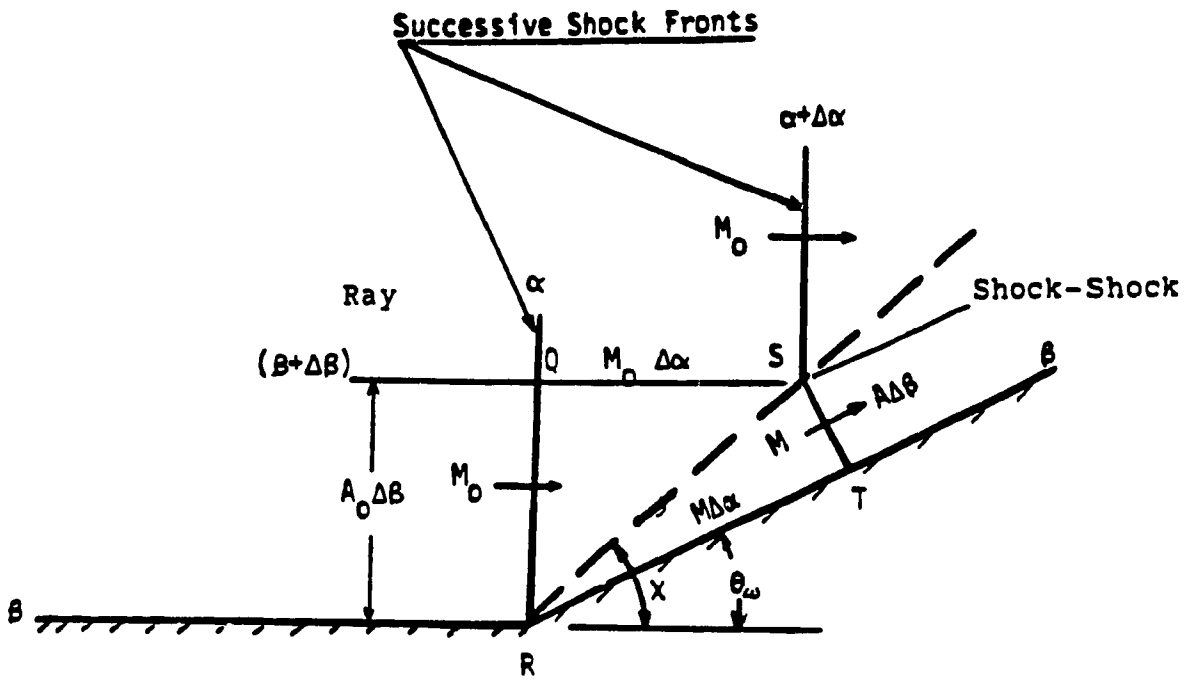

Fig. 2.8 Ray-Shock Grid at a Discontinuity

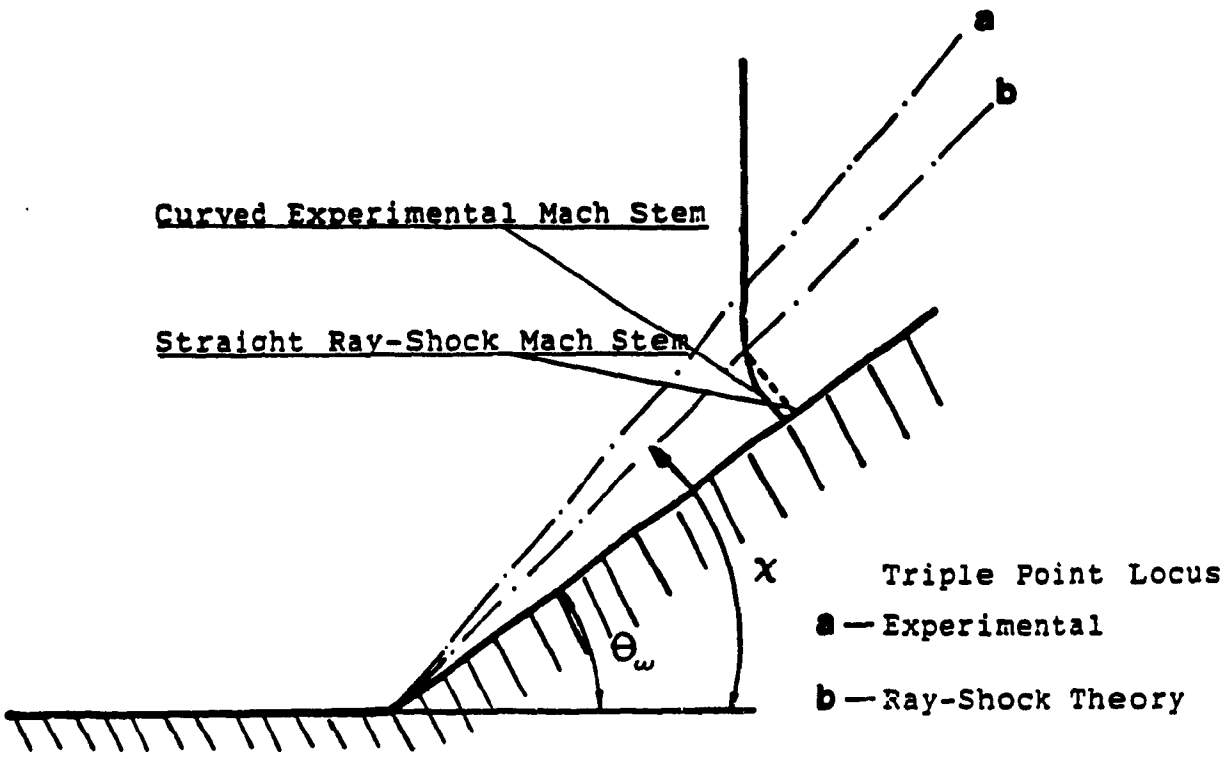

Fig. 2.9 Mach Stem Details for Weak Shocks

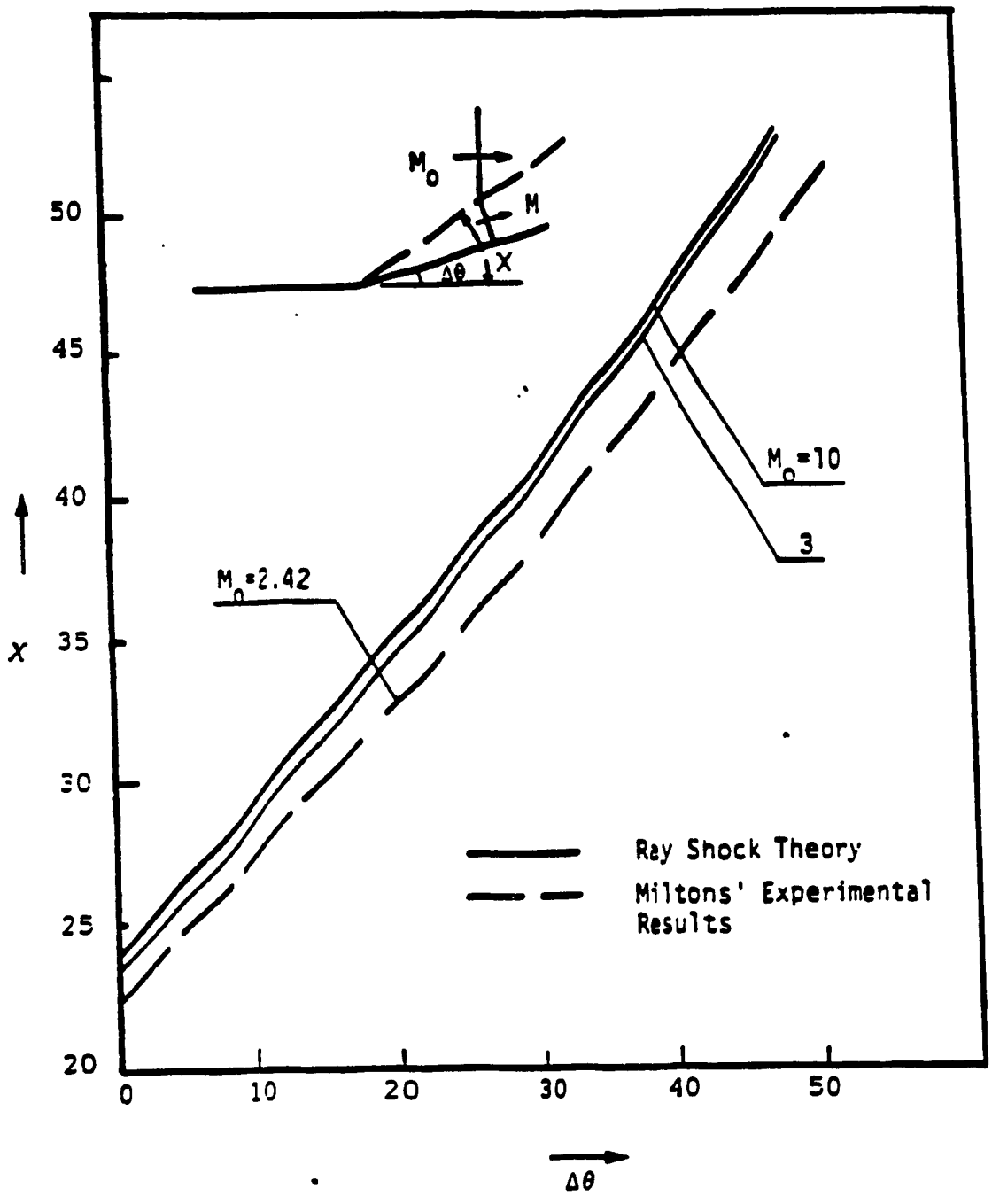

Fig. 2.10 Triple-Point Locus Angles Versus Deflection Angles

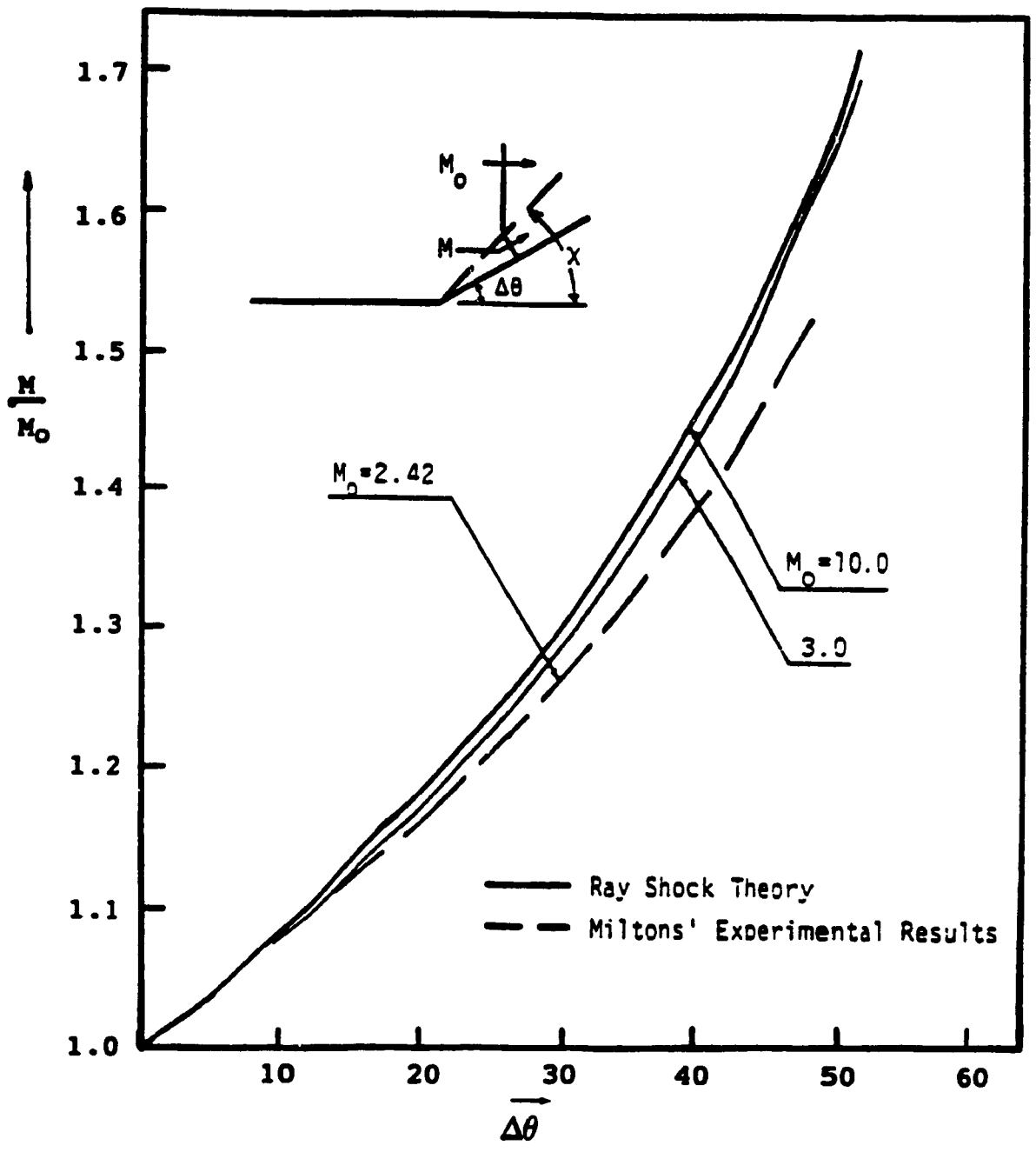

Fig. 2.11 Mach Number Ratio Across Shock-Shock Versus Deflection Angle

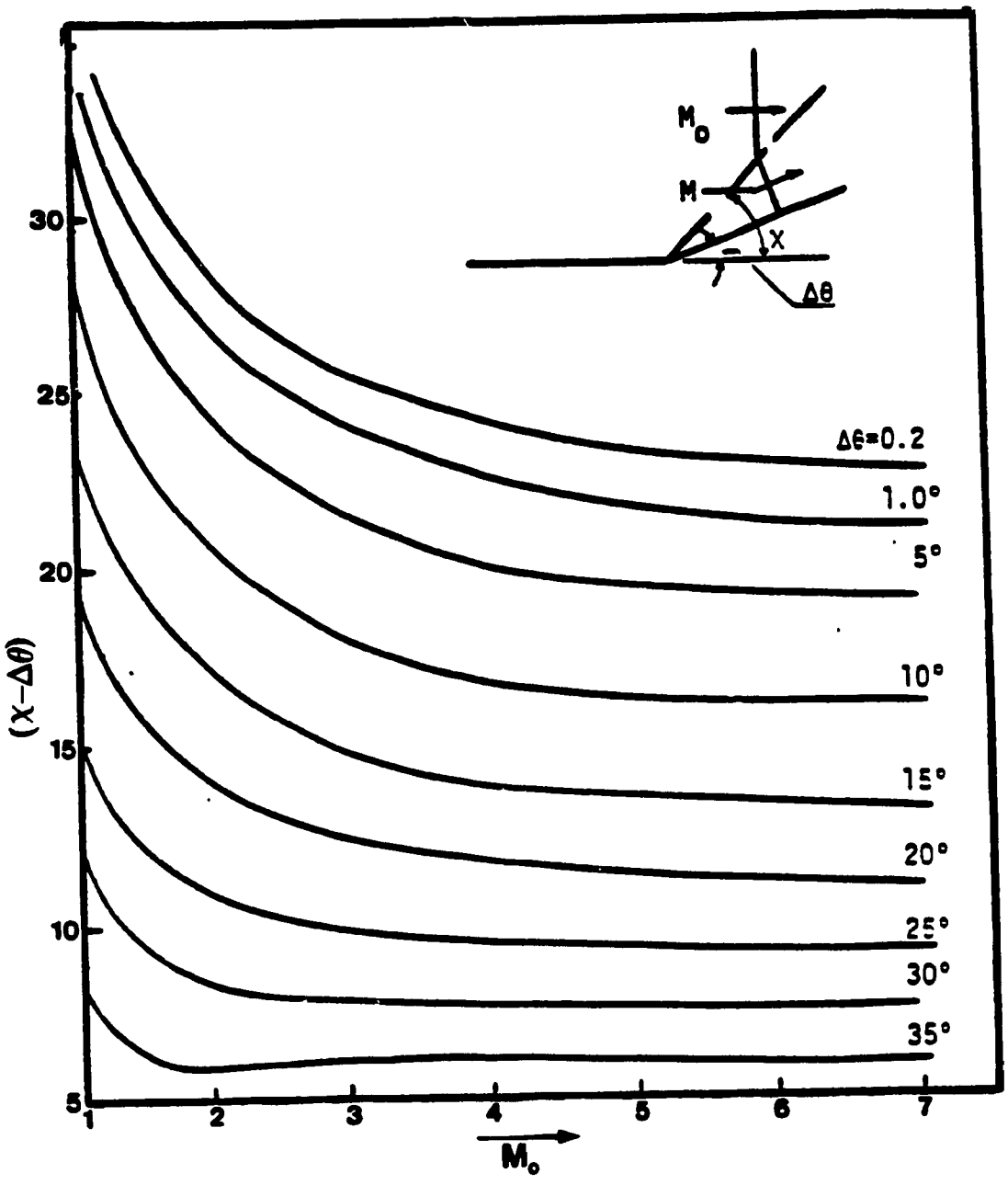

Fig. 2.12 Triple Point Trajectory Angle Versus Incident Shock Mach Number

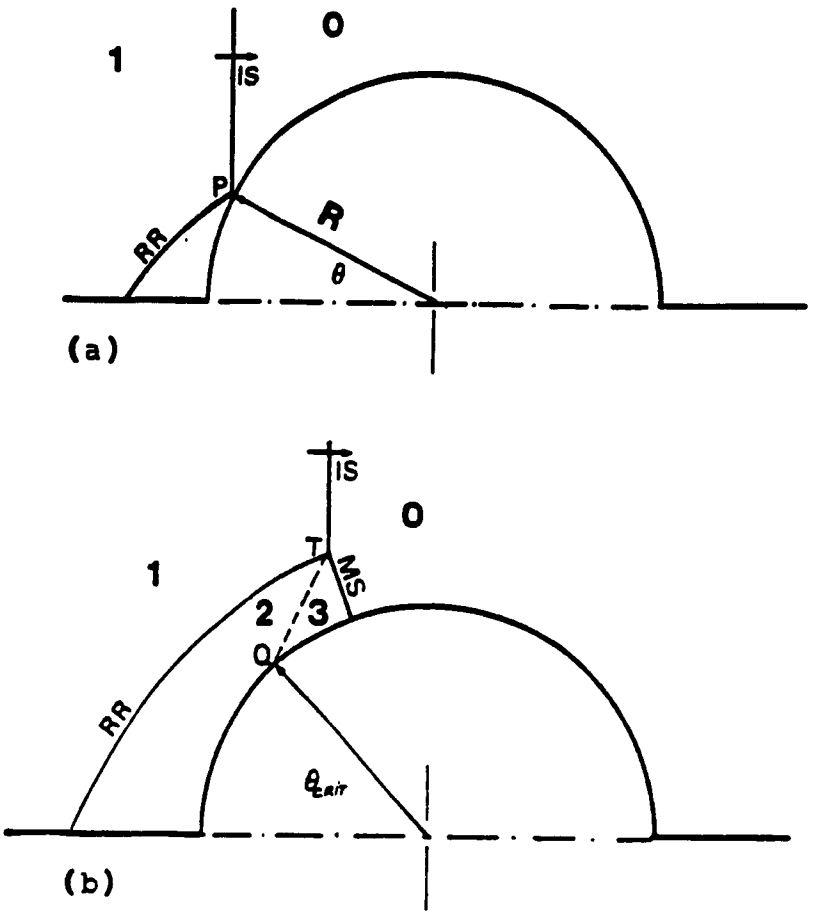

Fig. 2.13 Schematic Illustration of
(a) A Regular Reflection Over an Upper Half Cylindrical Rod
(b) A Mach Reflection Over an Upper Half Cylindrical Rod

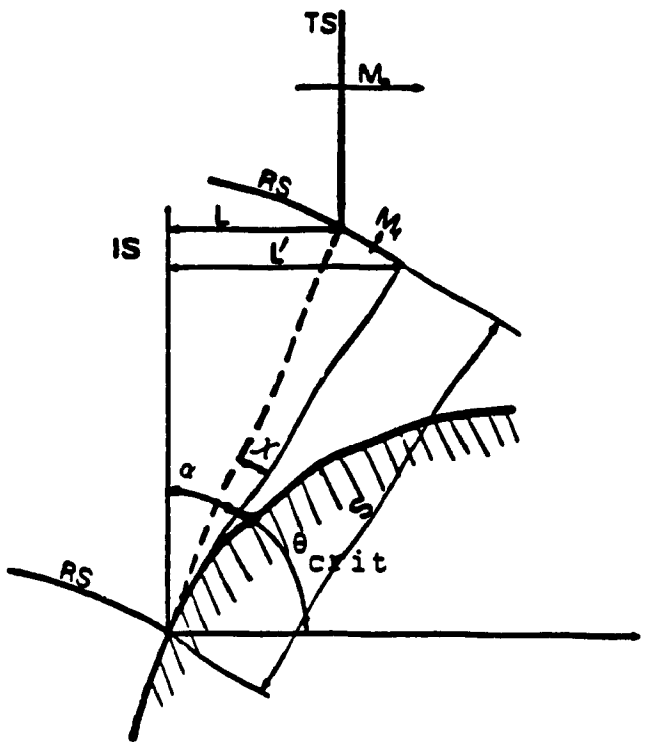

Fig. 2.14 Shock Wave System in the Vicinity of a Transition Point

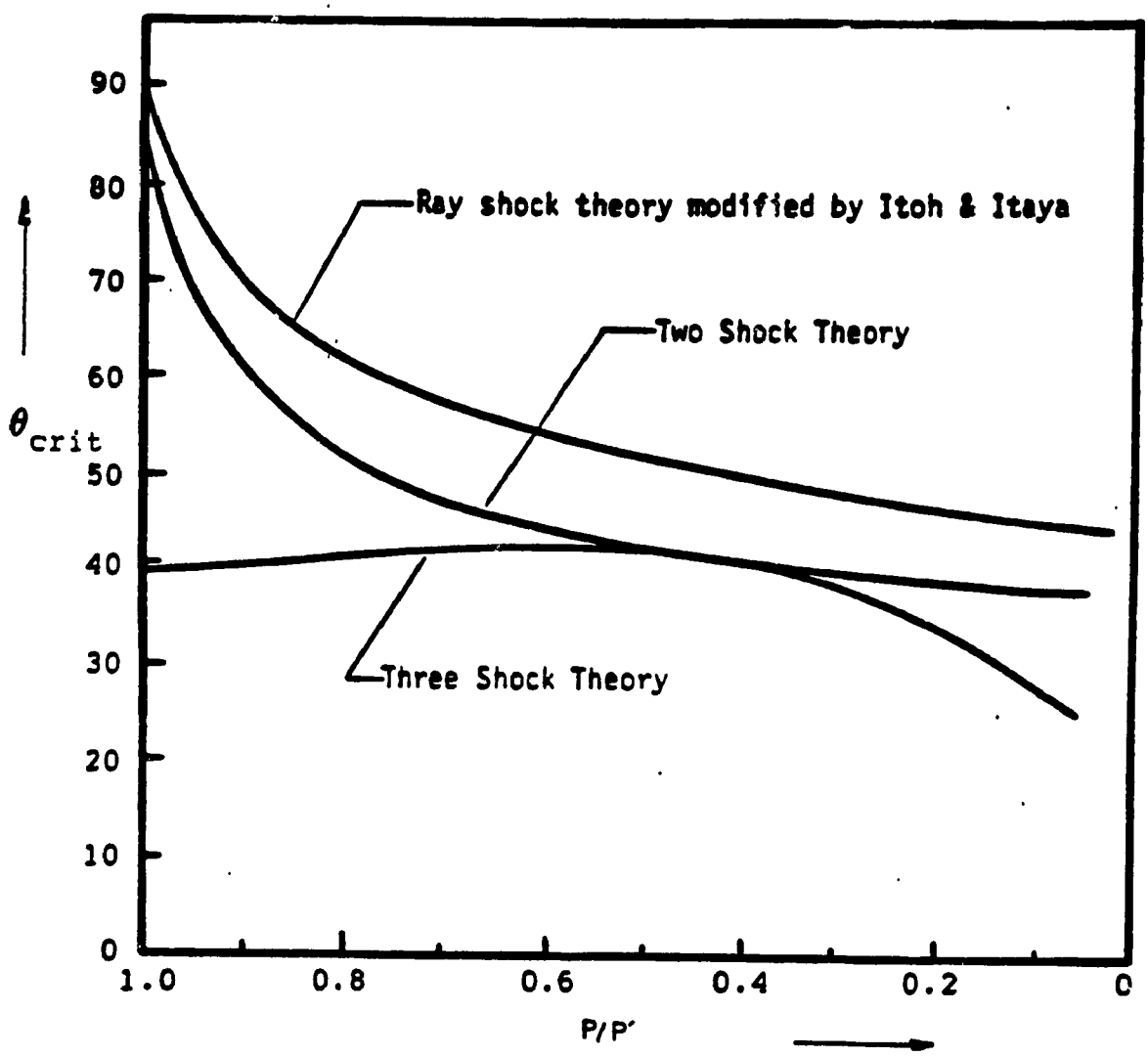

Fig. 2.15 Critical Angle Versus Pressure Ratio Across the Incident Shock

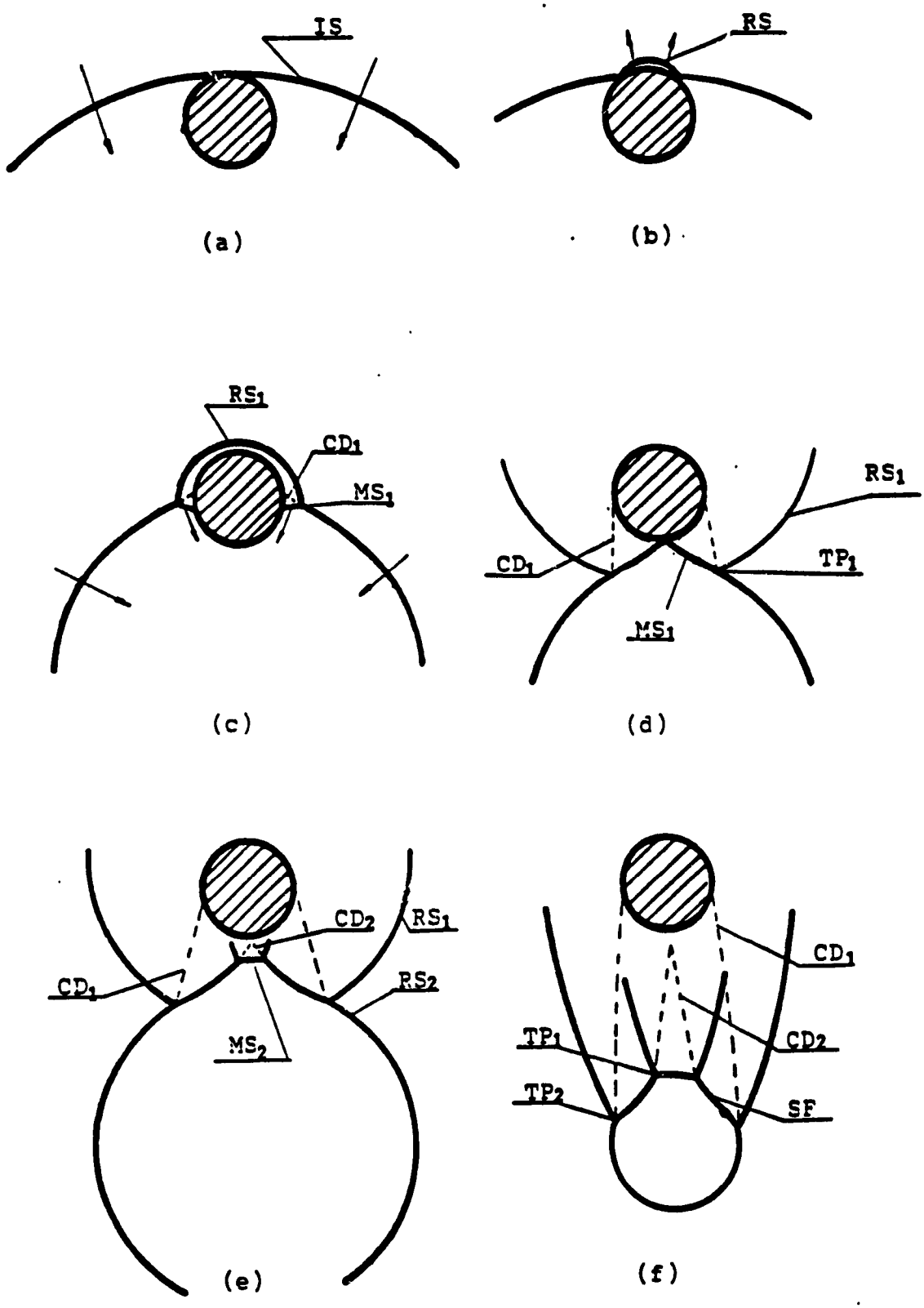

Fig. 2.16 Schematic Illustration for the Interaction of a Converging Cylindrical Shock with a Rod

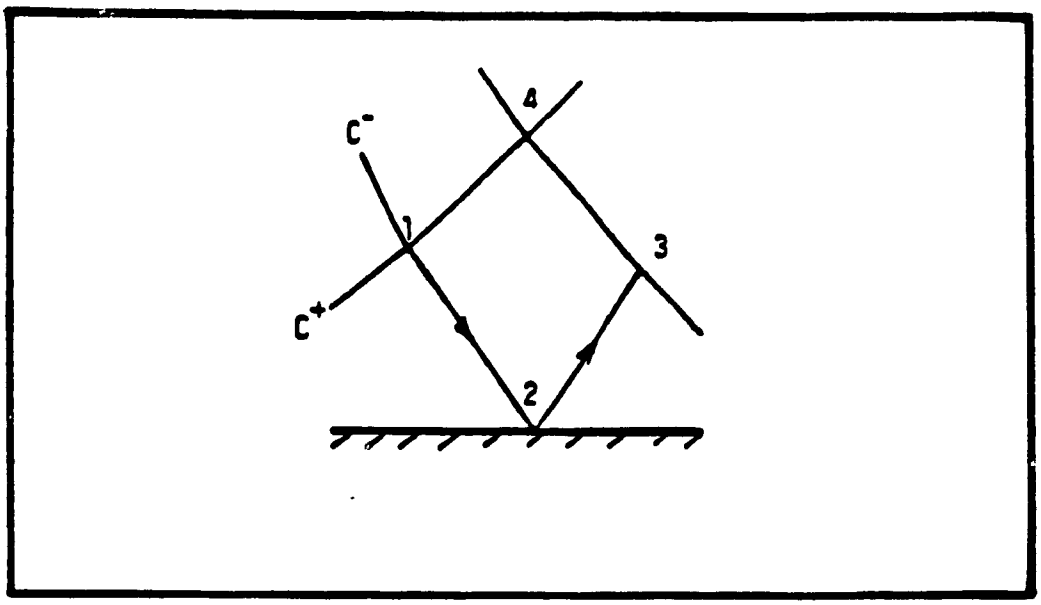

a) Interaction of Two Characteristics

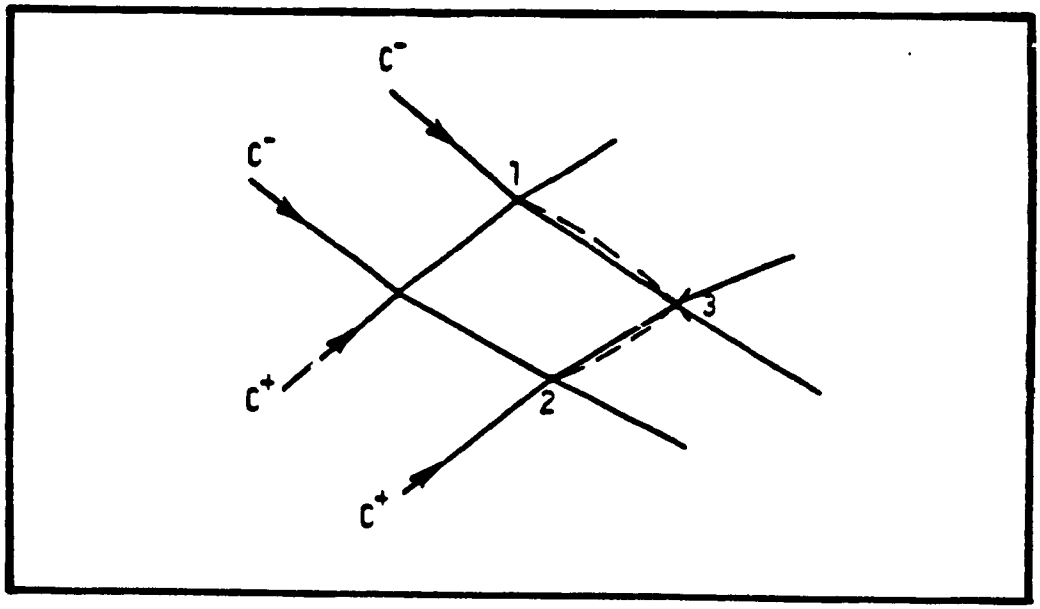

b) Interaction of Characteristics with Plane of Symmetry

Fig. 2.17 Interaction of Characteristics

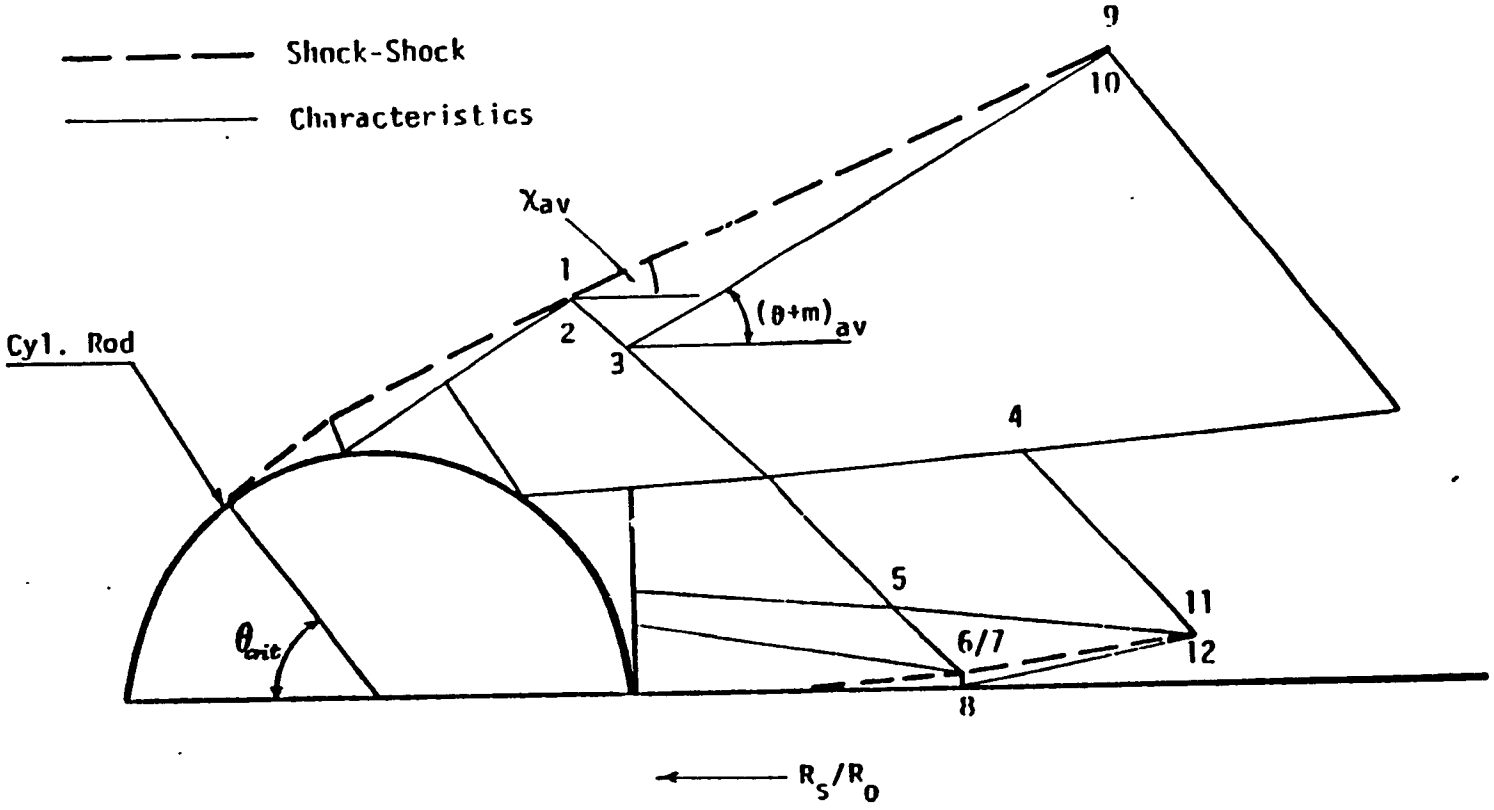

Fig. 2,18 Interaction of Shock-Shock with Characteristics

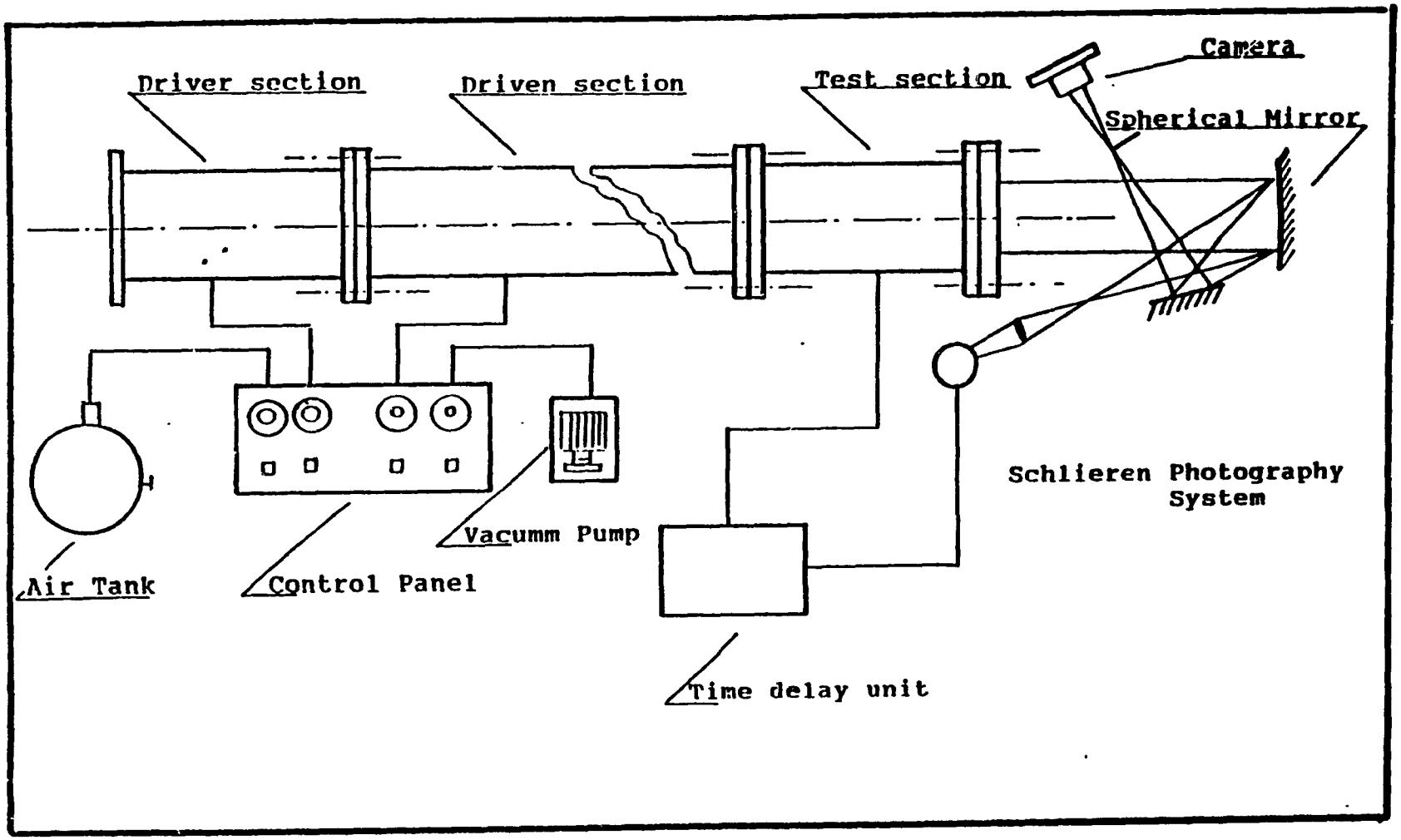

Fig. 3.1 A Schematic of the Shock Tube together with the Schlieren Photography System

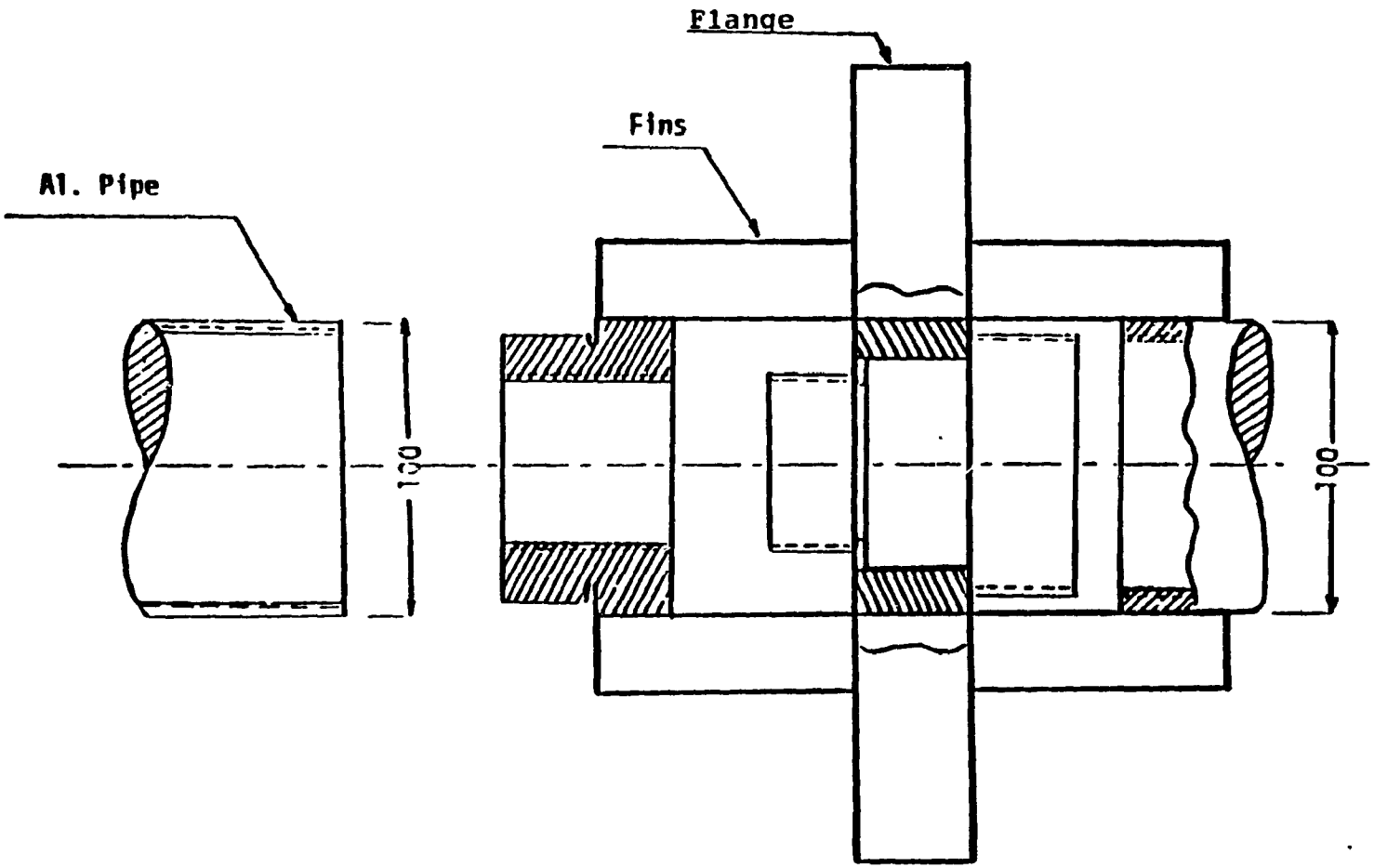

Fig. 3.2 Sectional View of the Device Supporting the Inner Tube

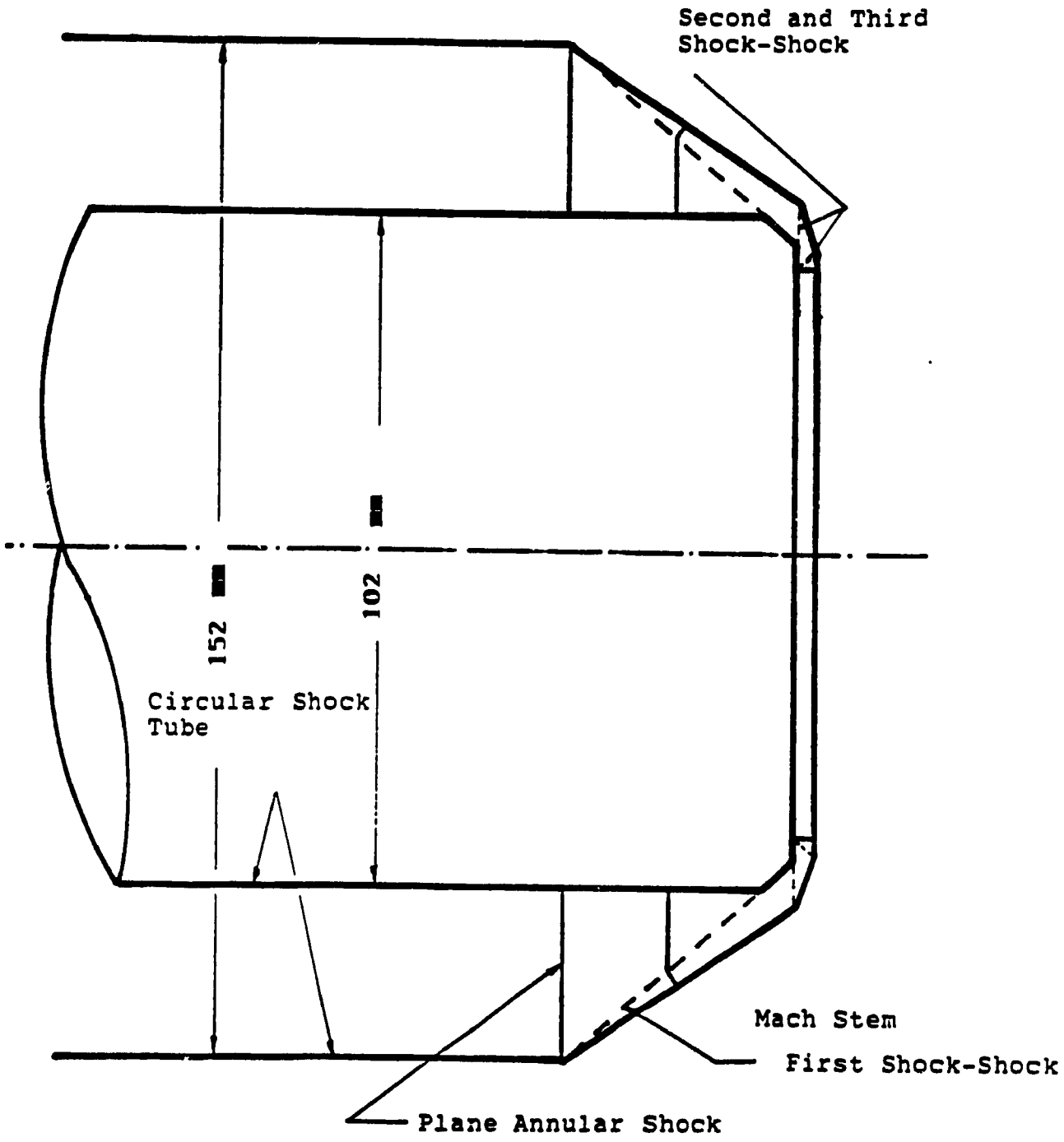

Fig. 3.3 Converging Cylindrical Shock Formed By The Three-Increment Area Contraction Axisymmetric Shock Tube

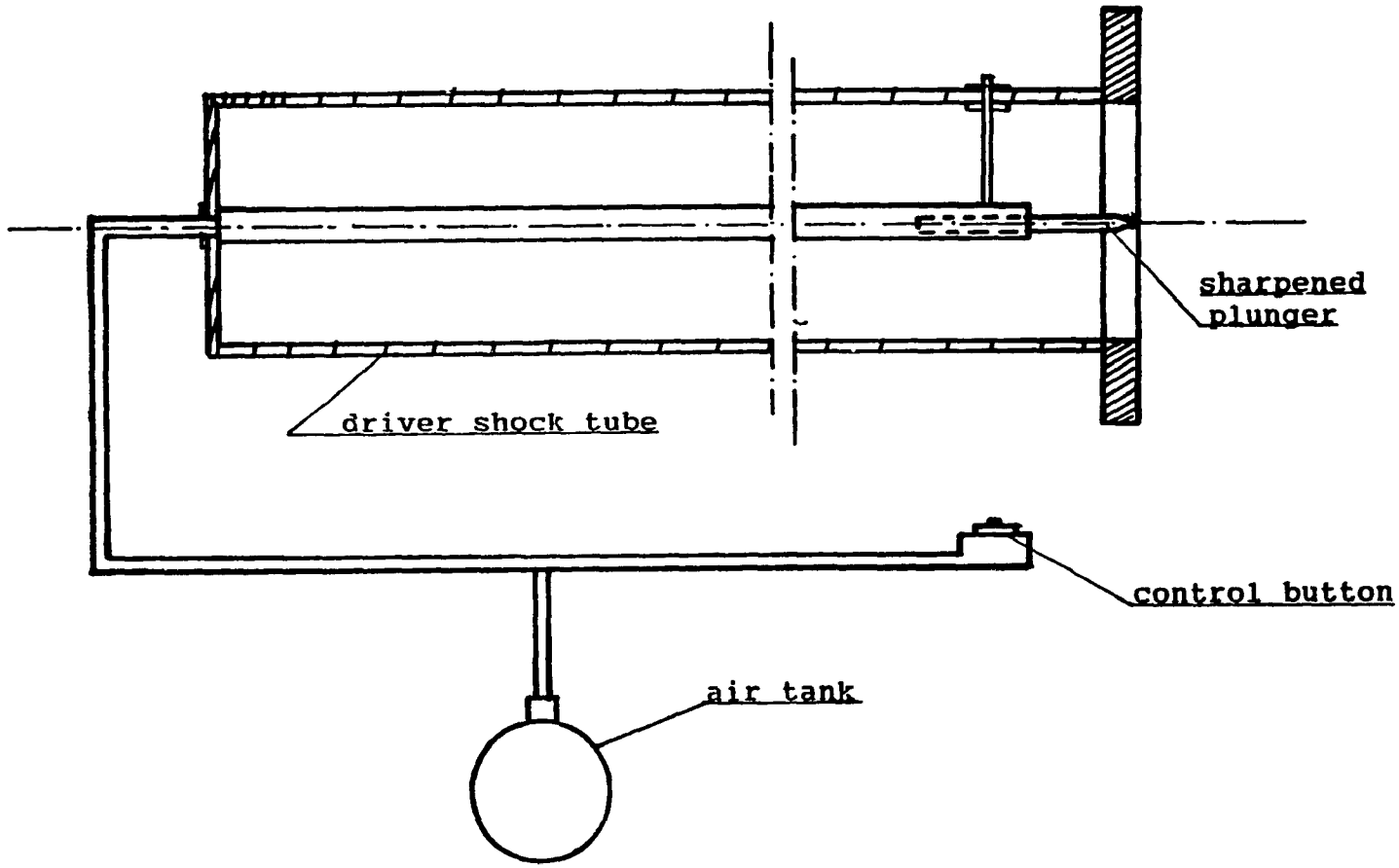

Fig. 3.4 Schematic Diagram of Mechanical Plunger

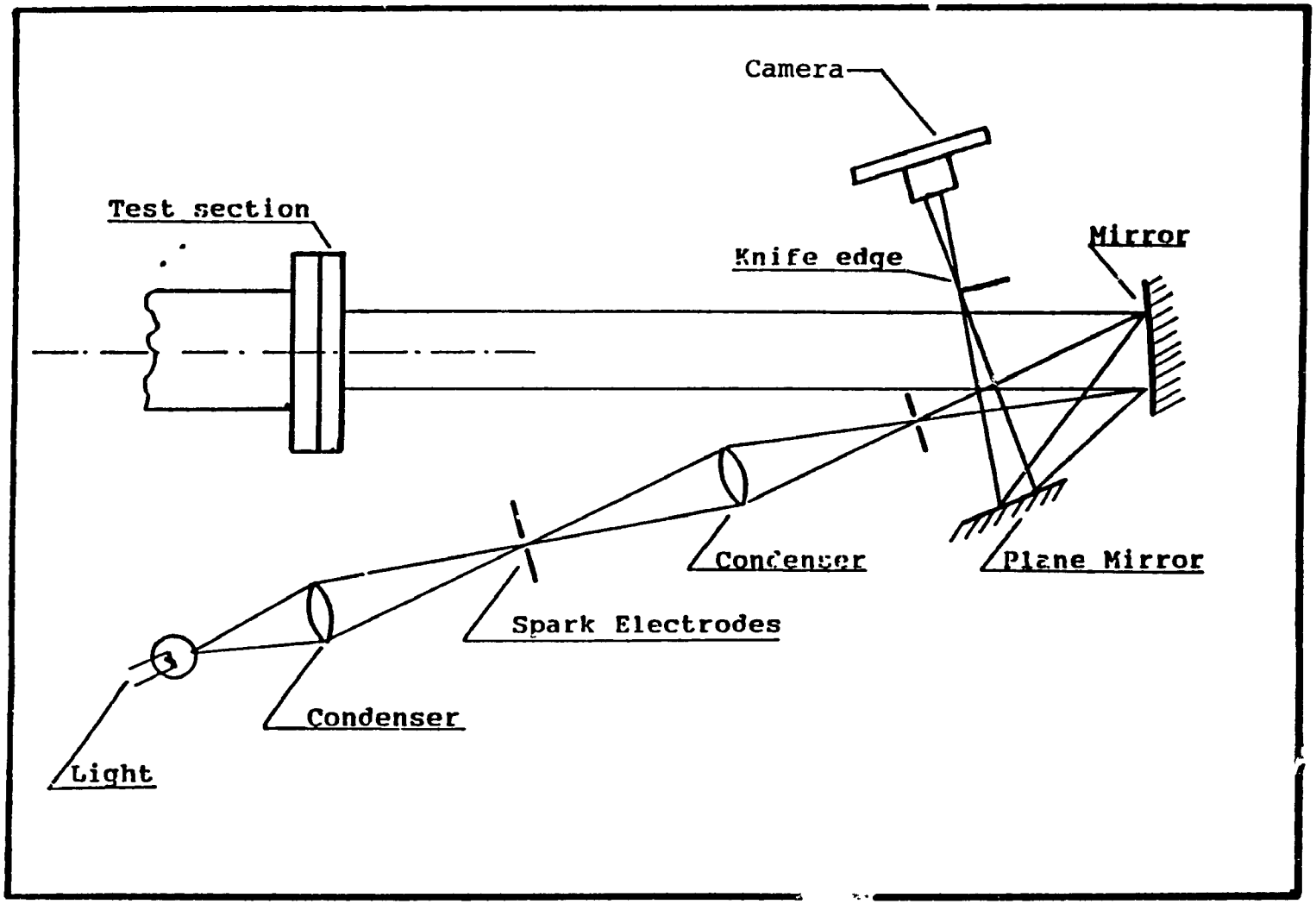

Fig. 3.5 Schematic View of Schlieren Photogra, System

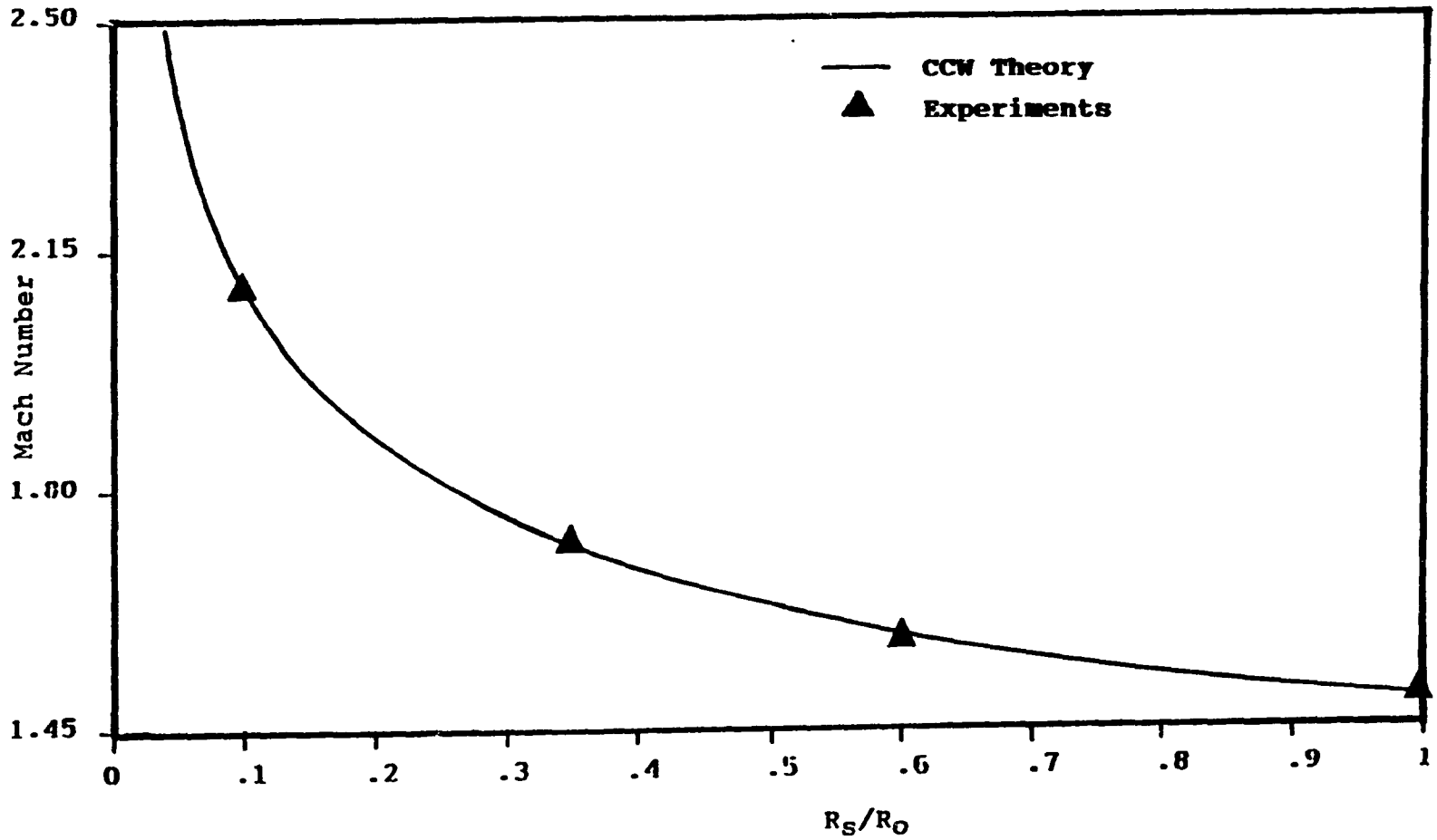

Fig. 4.1 Shock Mach Number Versus Radius of Converging Cylindrical Shock (M_O=1.5)

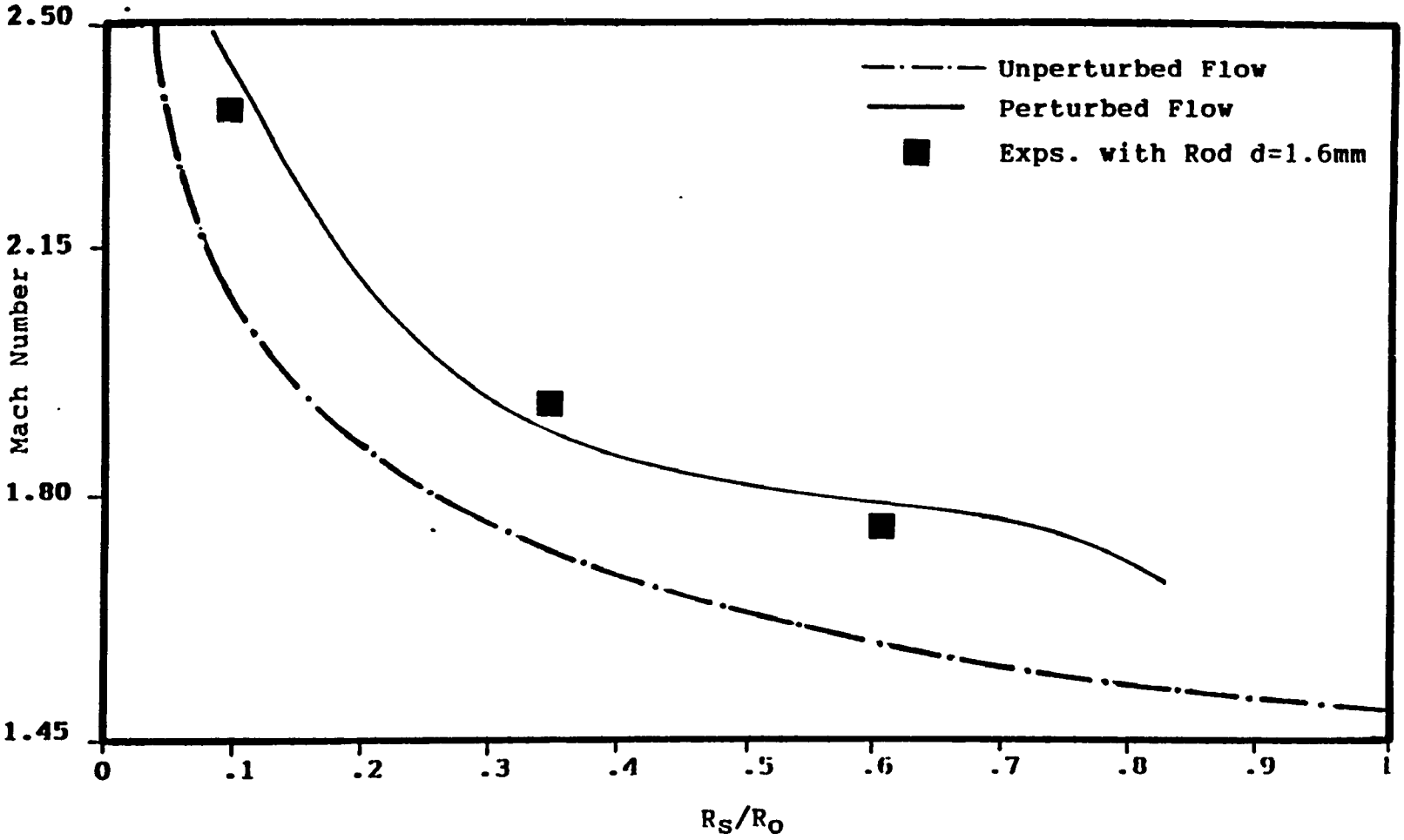

Fig. 4.2 Comparison Between Experimental and Theoretical Shock Mach Number of Perturbed Shock, $R_O/d=25$, d=1.6mm

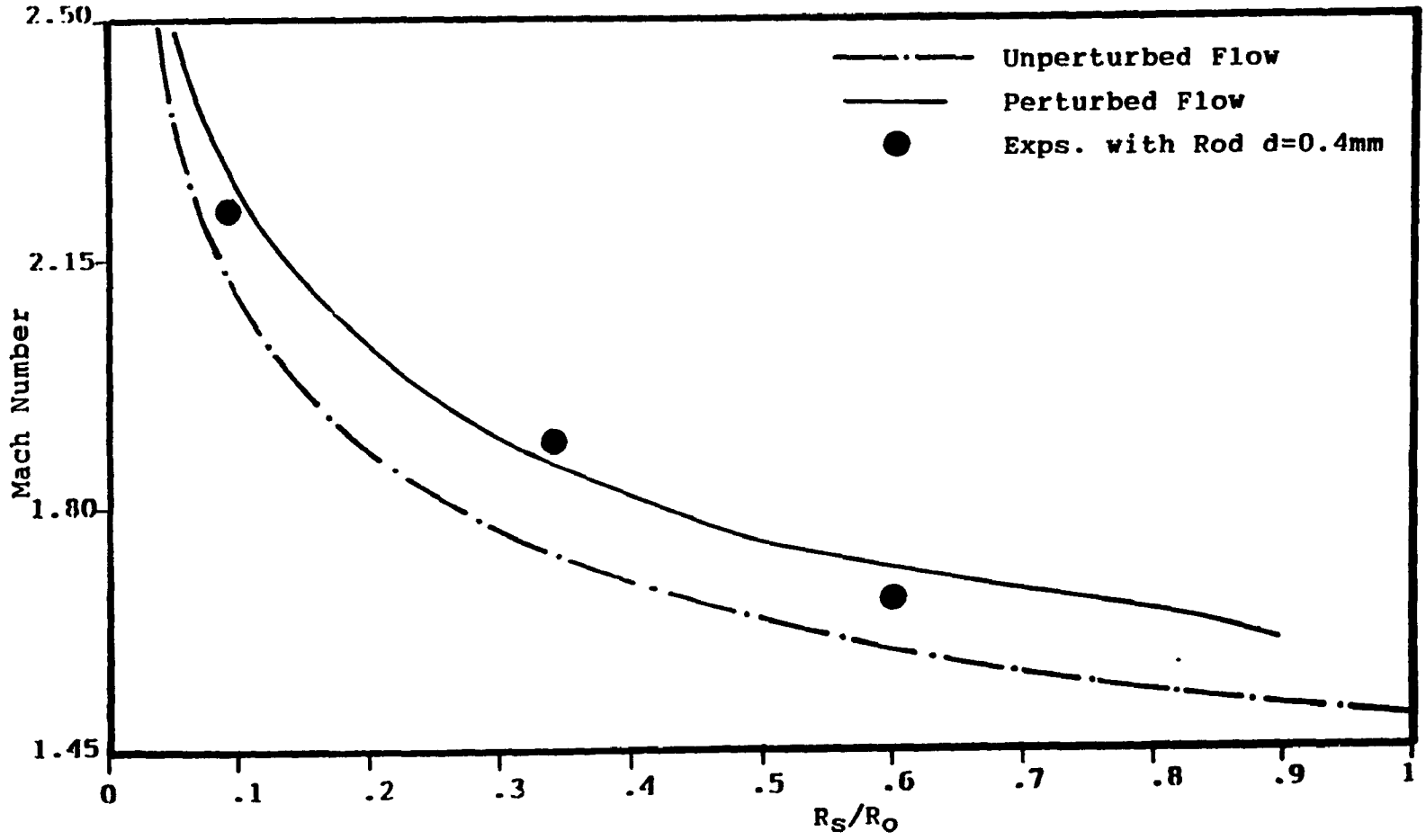

Fig. 4.3 Comparison Between Experimental and Theoretical Shock Mach Number of Perturbed Shock, $R_O/d=100$, d=0.4mm

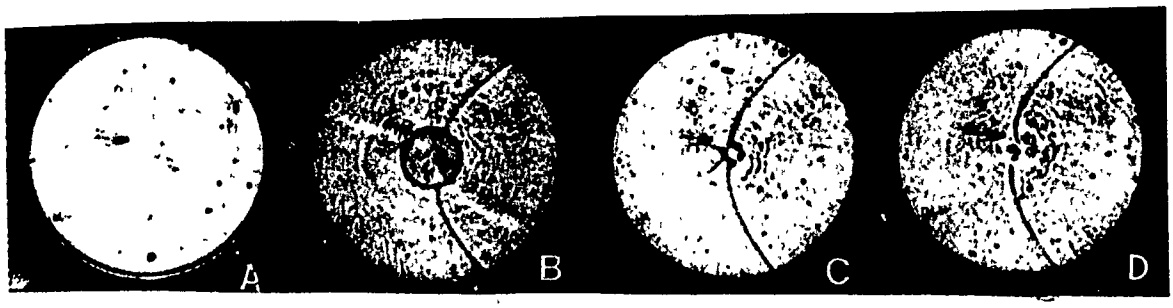

(a) With Rod Diameter 1.6 mm

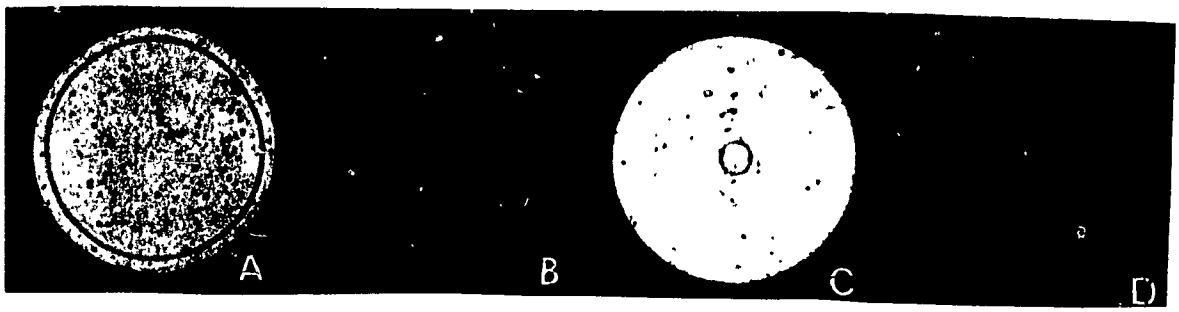

(b) With Rod Diameter 0.8 mm

Fig. 4.4 Spark-Schlieren Photographs Illustrating the Propagation of Converging Cylindrical Shock Wave Perturbed by Different Size of Rods

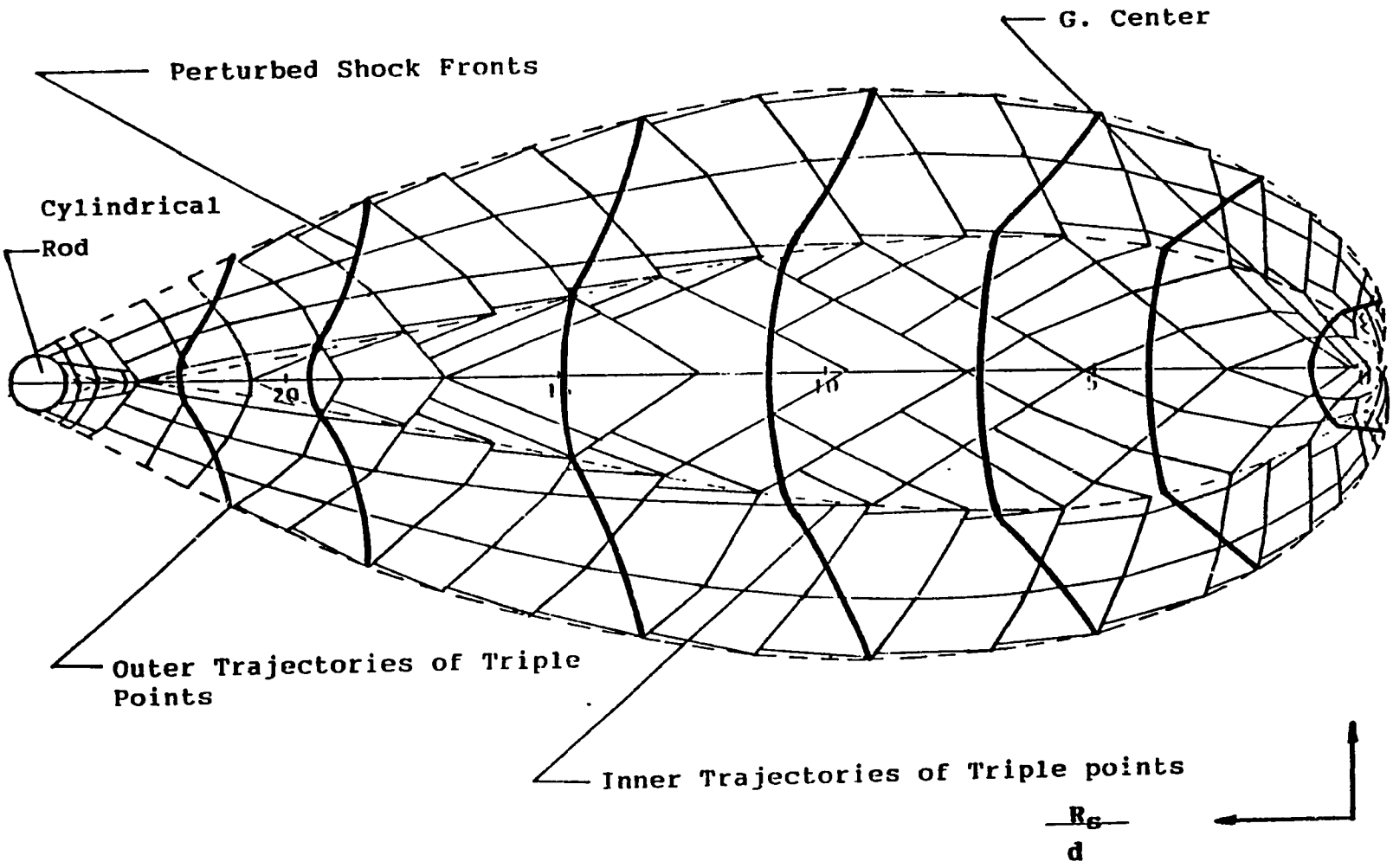

Fig. 4.5 Wave Diagram Illustrating the Successive Positions of Shock Fronts of a Weak Shock Perturbed by a Cylindrical Rod of Diameter 1.6 mm.

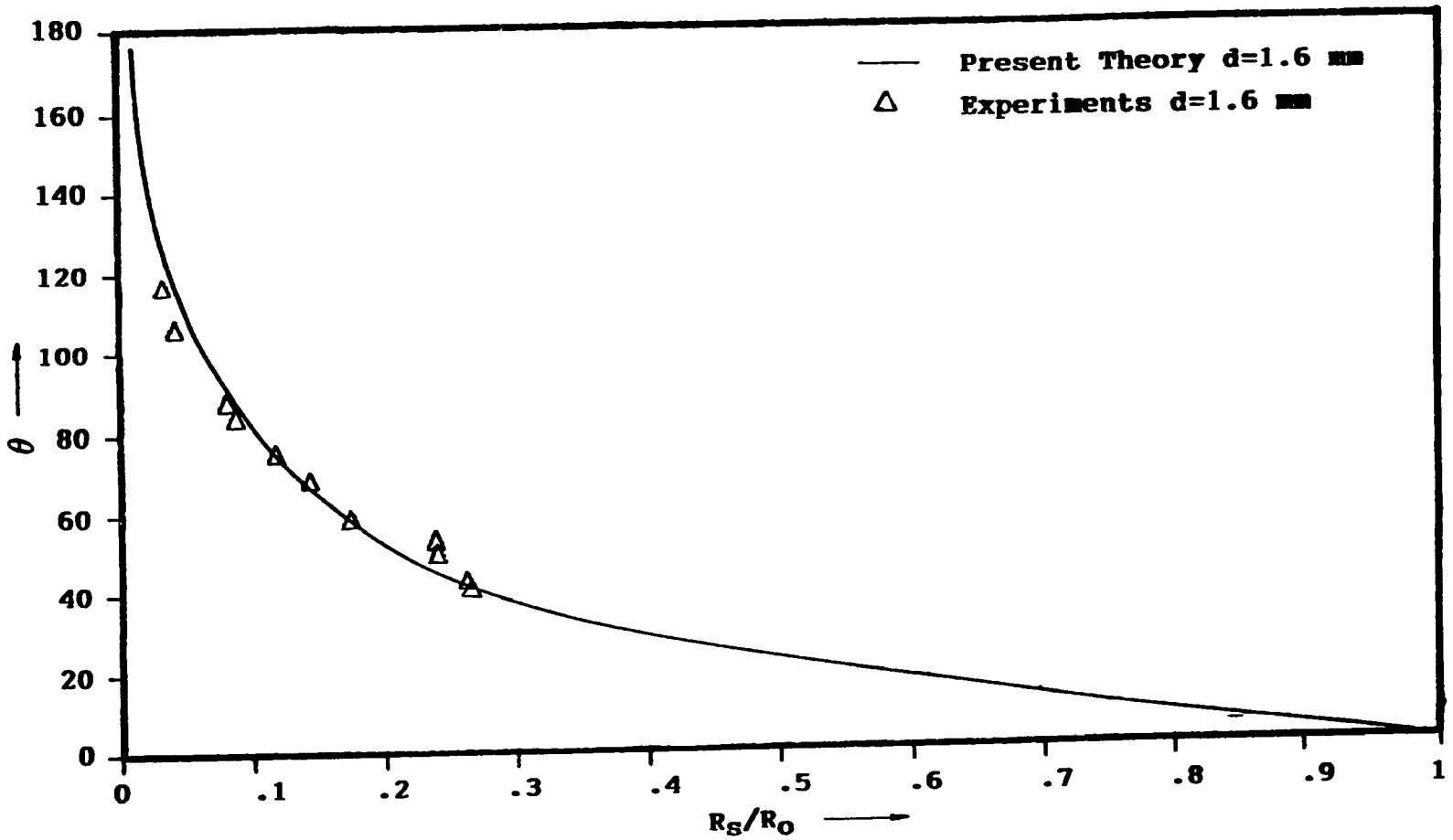

Fig. 4.6 Outer Shock-Shock Angle Versus Shock Radius, Rod Diameter = 1.6 mm

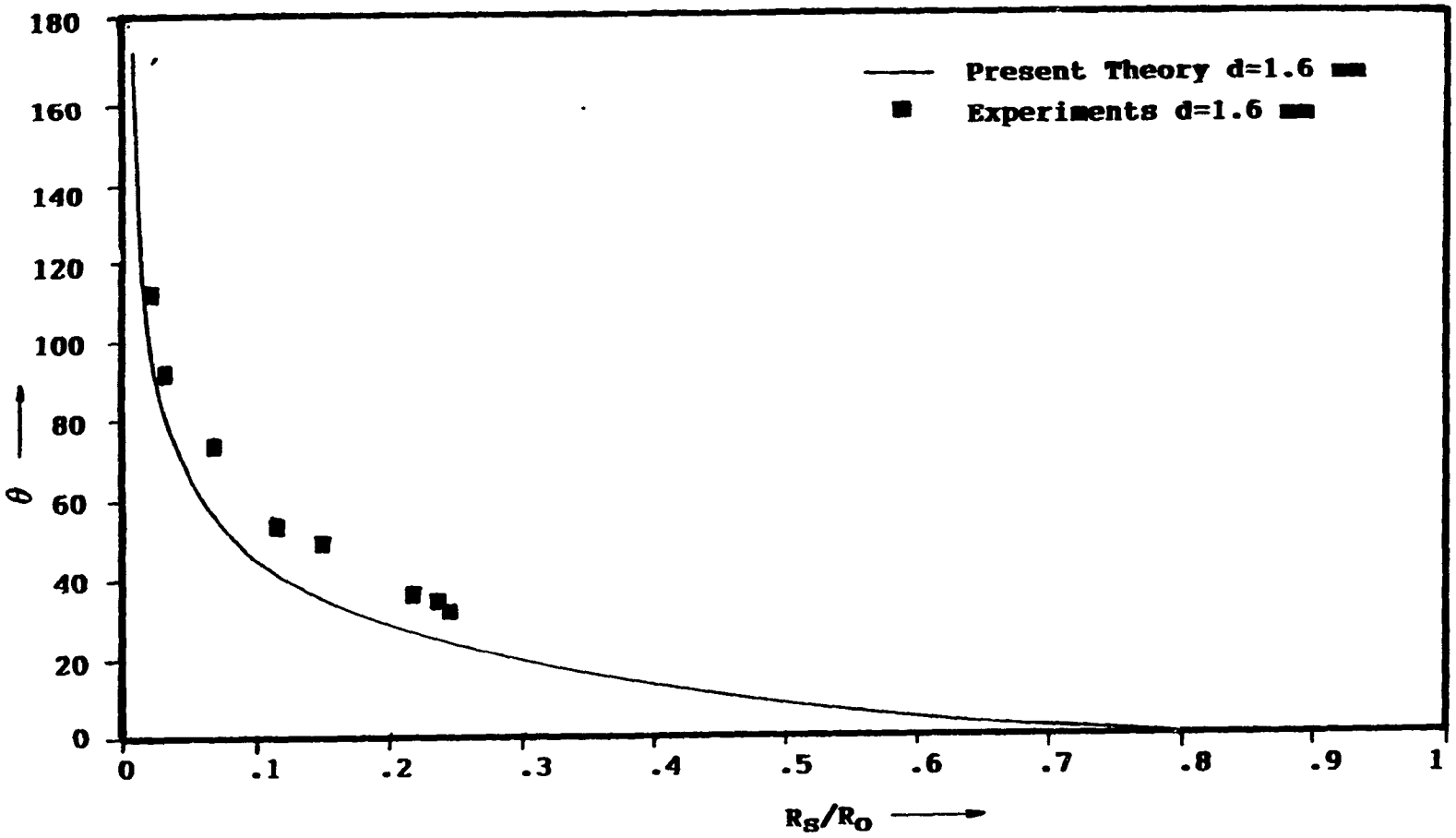

Fig. 4.7 Inner Shock-Shock Angle Versus Shock Radius, Rod Diameter = 1.6 mm

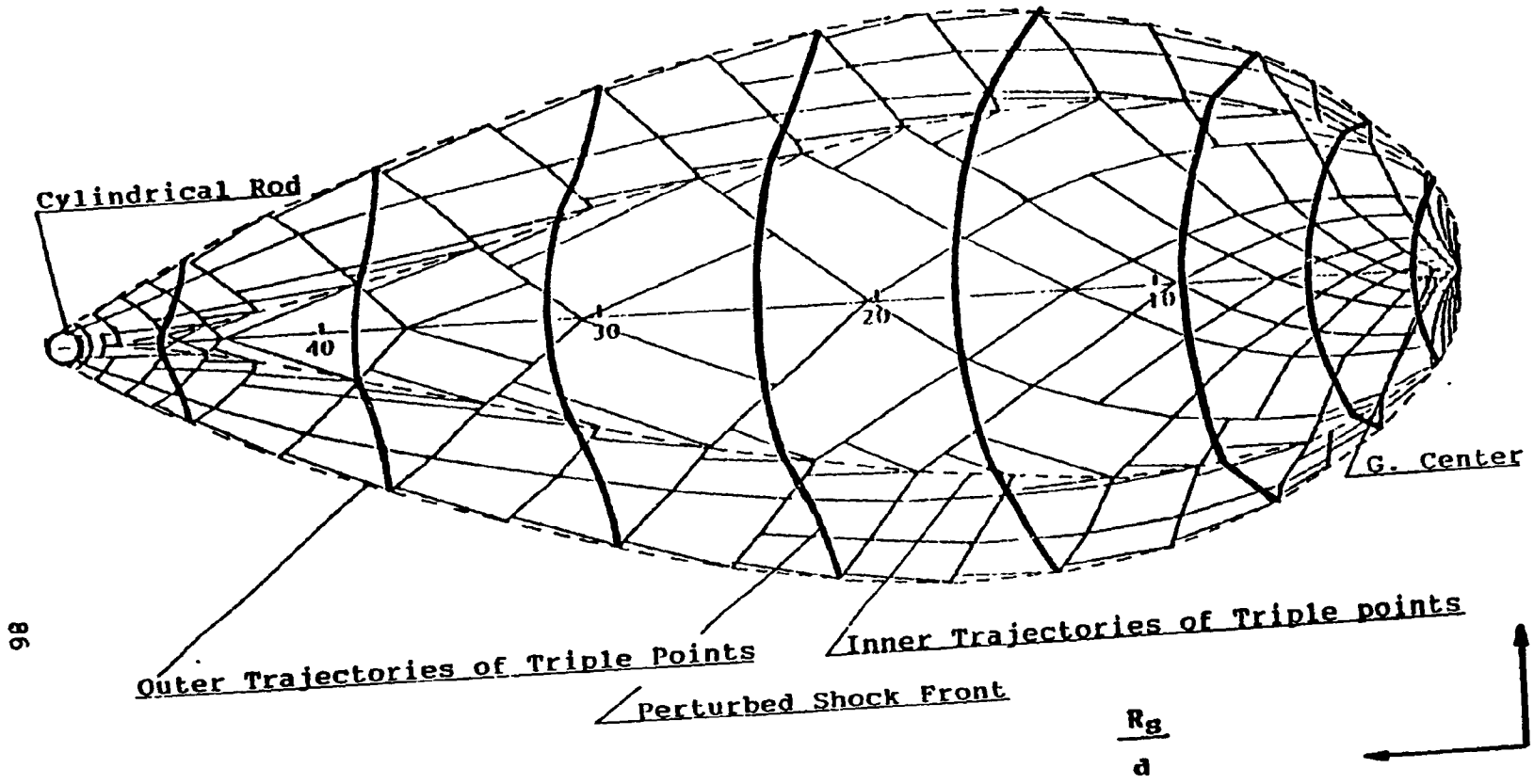

Fig. 4.8 Wave Diagram Illustrating the Successive Positions of a Weak Shock Perturbed by a Cylindrical Rod of Diameter 0.8 mm.

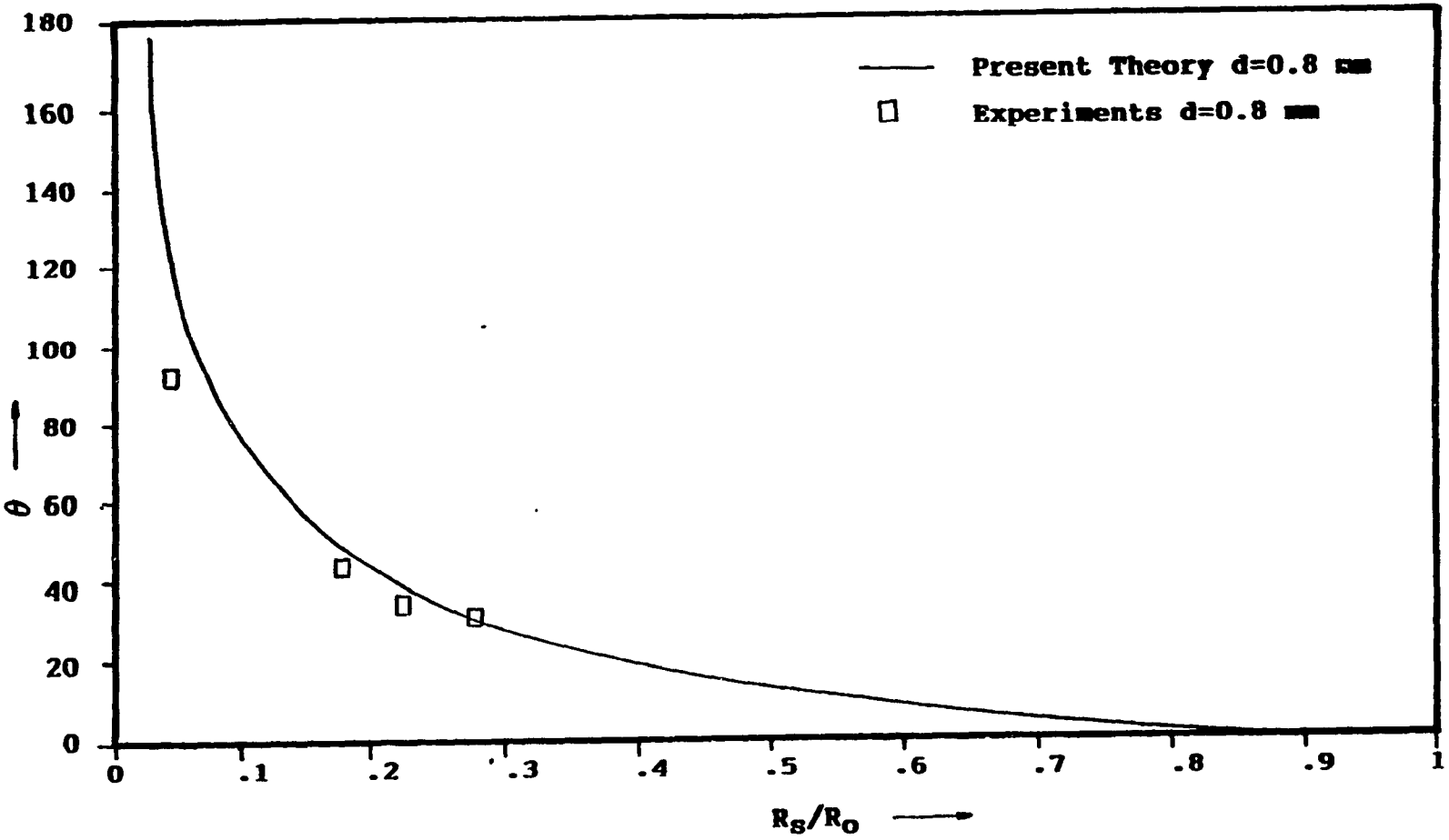

Fig. 4.9 Outer Shock-Shock Angle Versus Shock Radius, Rod Diameter = 0.8 mm

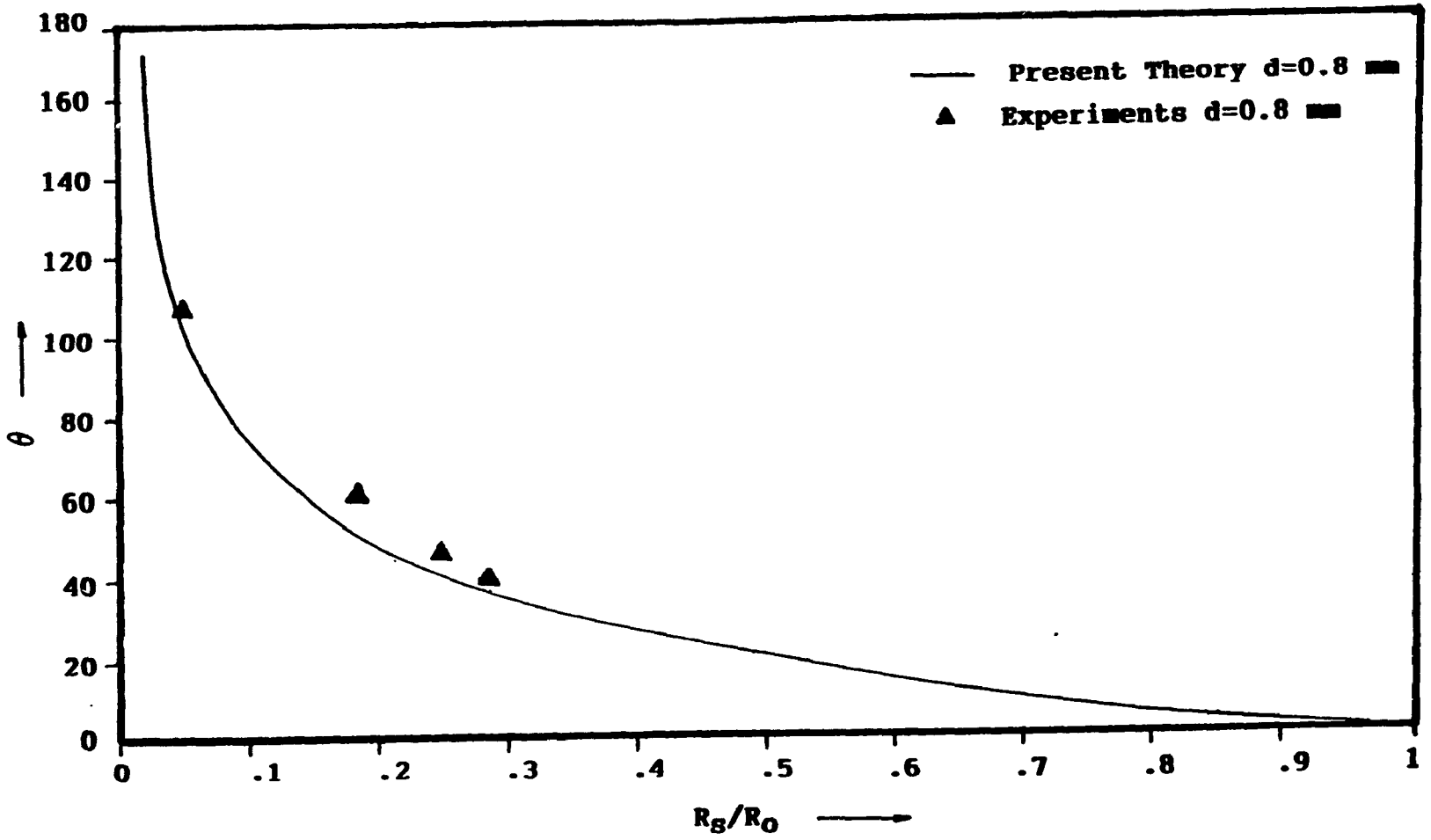

Fig. 4.10 Inner Shock-Shock Angle Versus Shock Radius, Rod Diameter = 0.8 mm

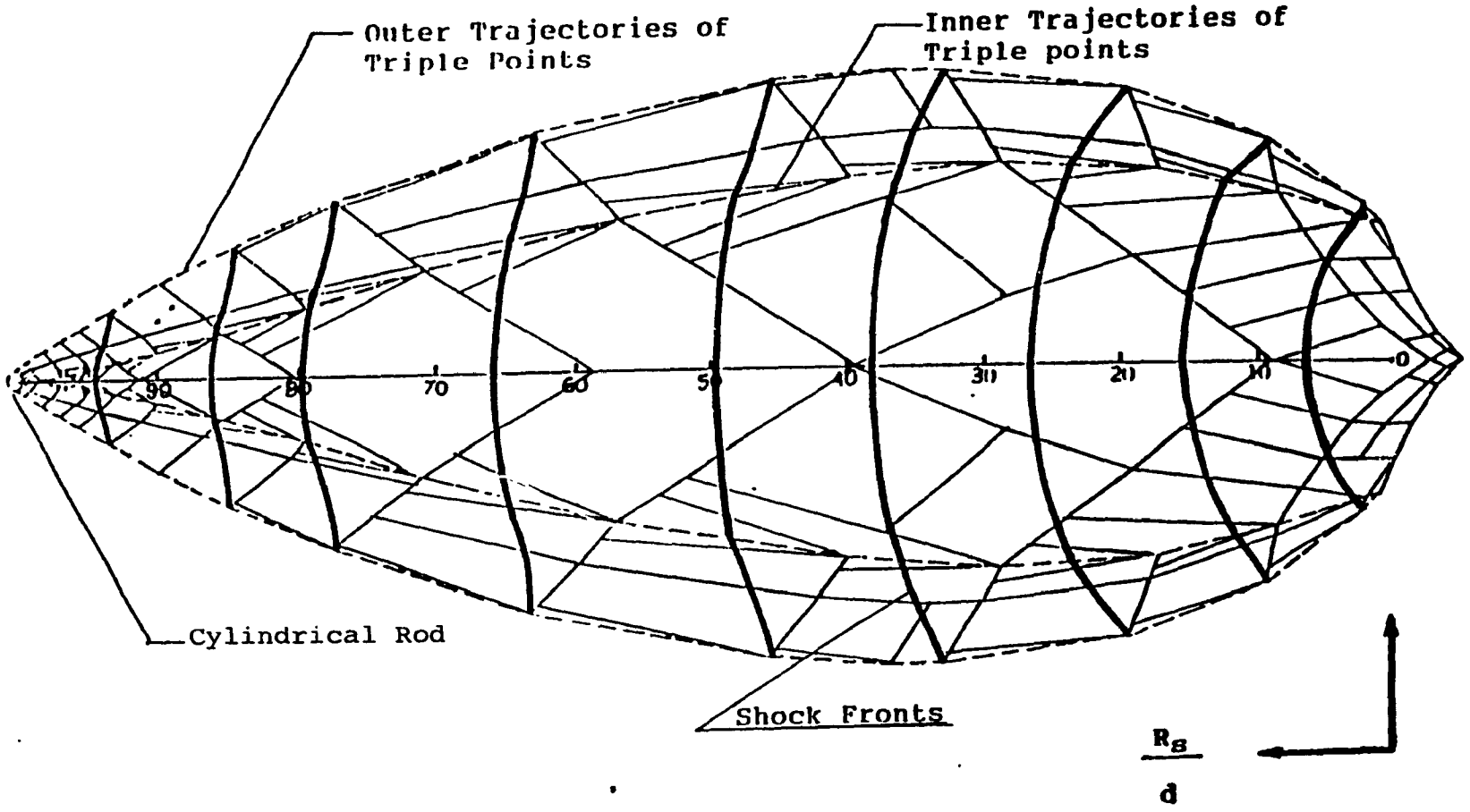

Fig. 4.11 Wave Diagram for the Initially Weak Cylindrical Shock, Perturbed by a Rod of Diameter 0.4 mm.

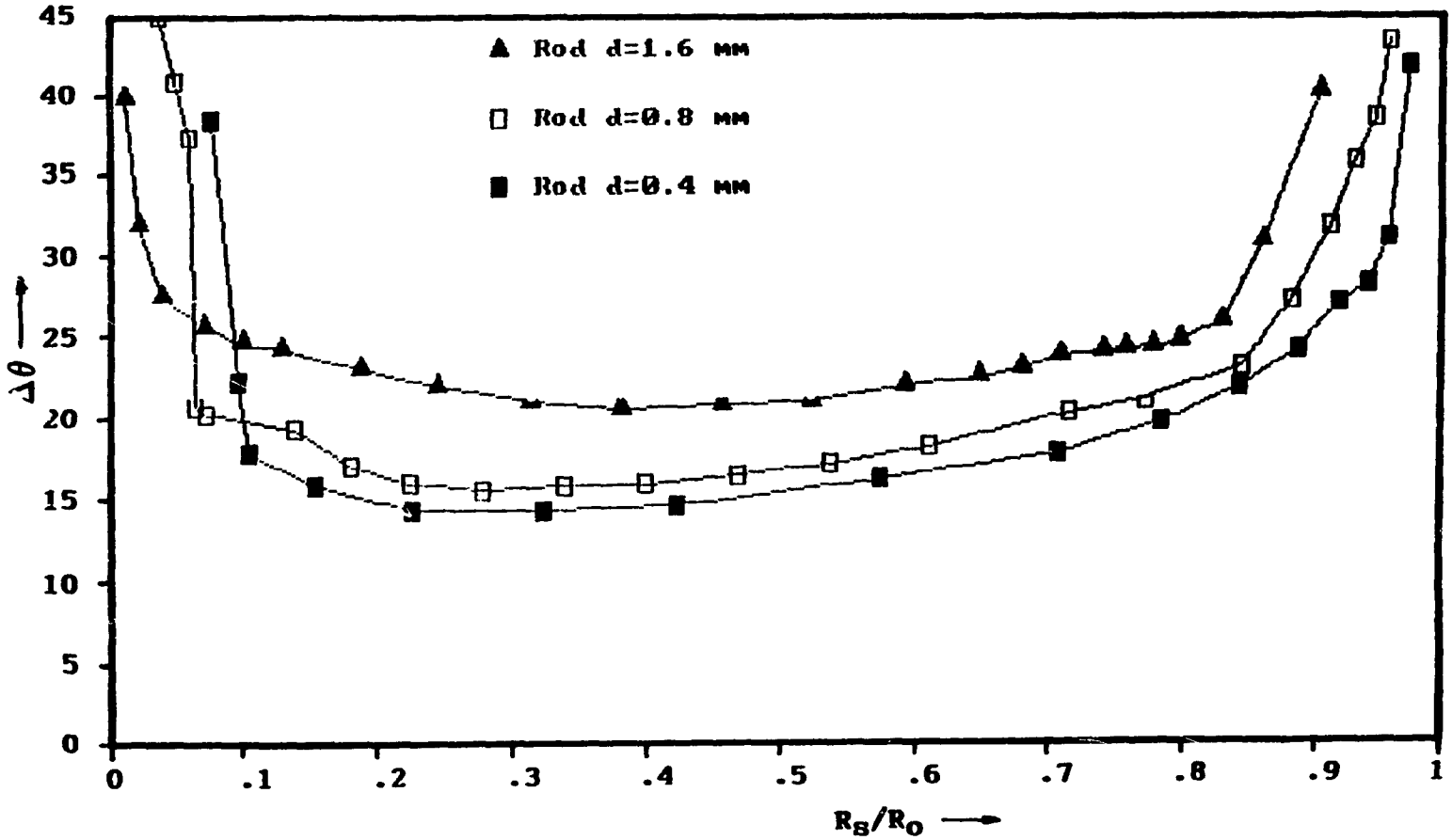

Fig. 4.12 Flow Deflection at the Inner Triple Point Versus Shock Radius. Cases of R_O/d= 25,50,100

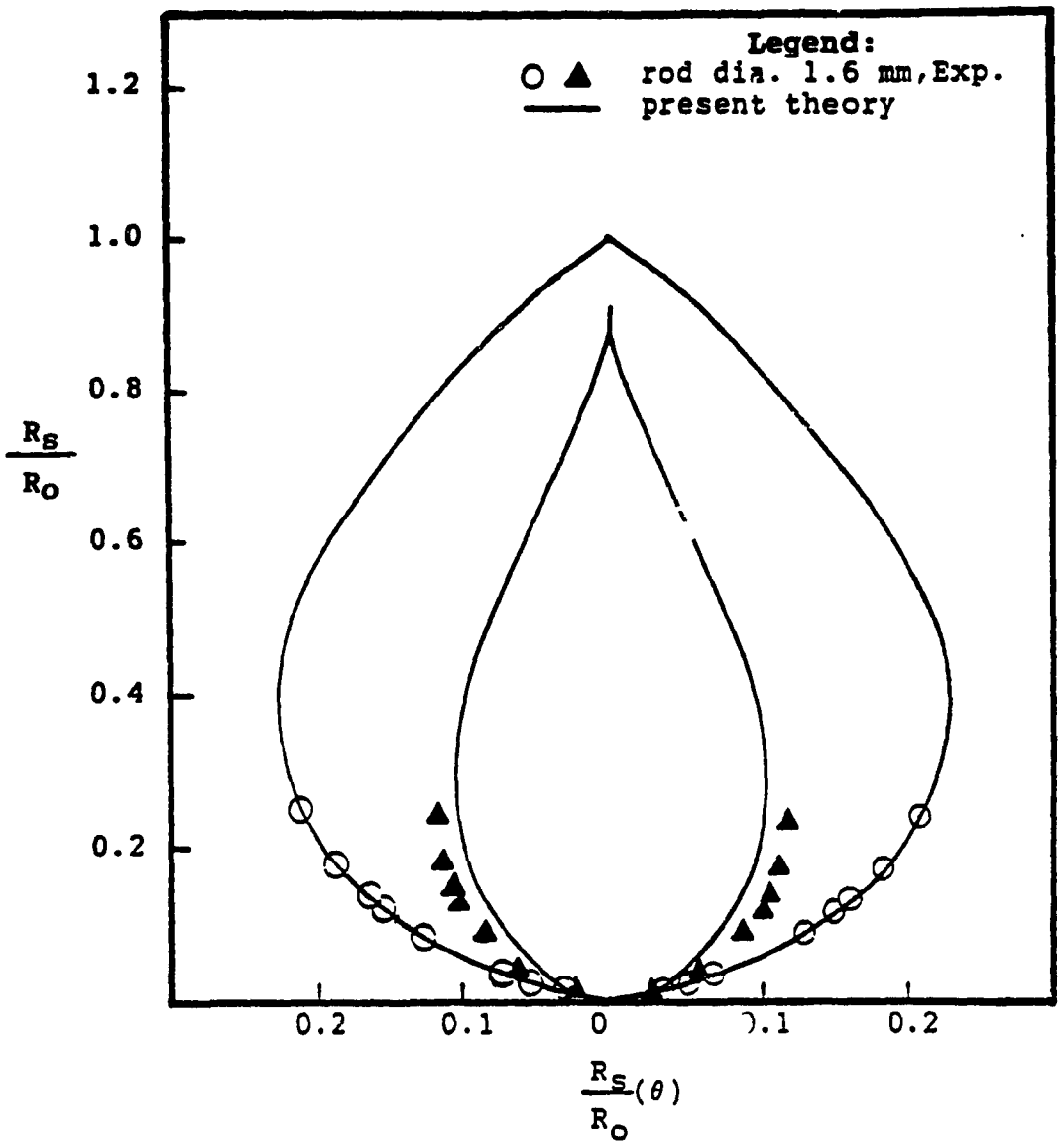

Fig. 4.13 Outer and Inner Trajectories, Rod of Diameter 1.6 mm

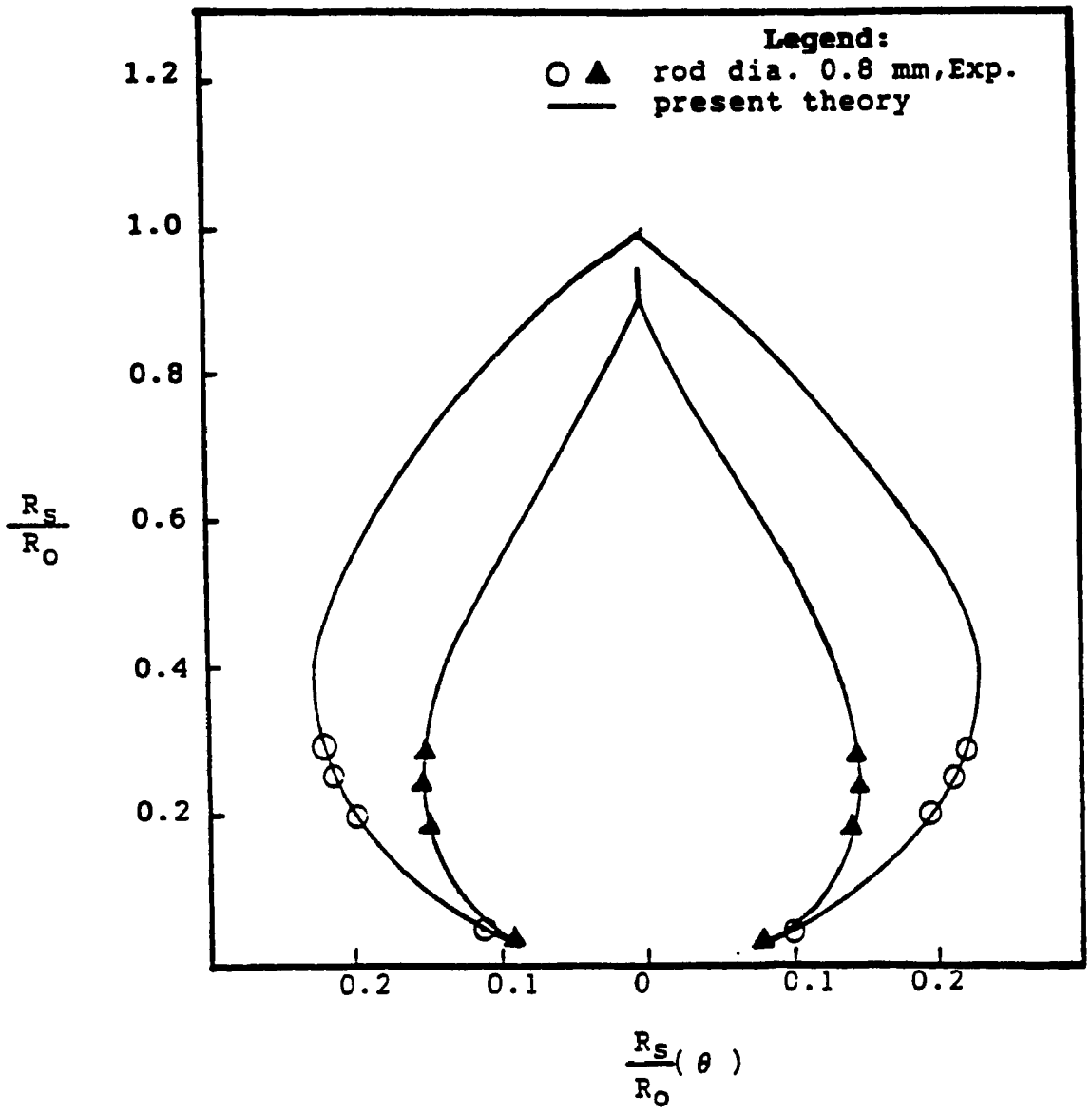

Fig. 4.14 Outer and Inner Trajectories, Rod of Diameter 0.8 mm

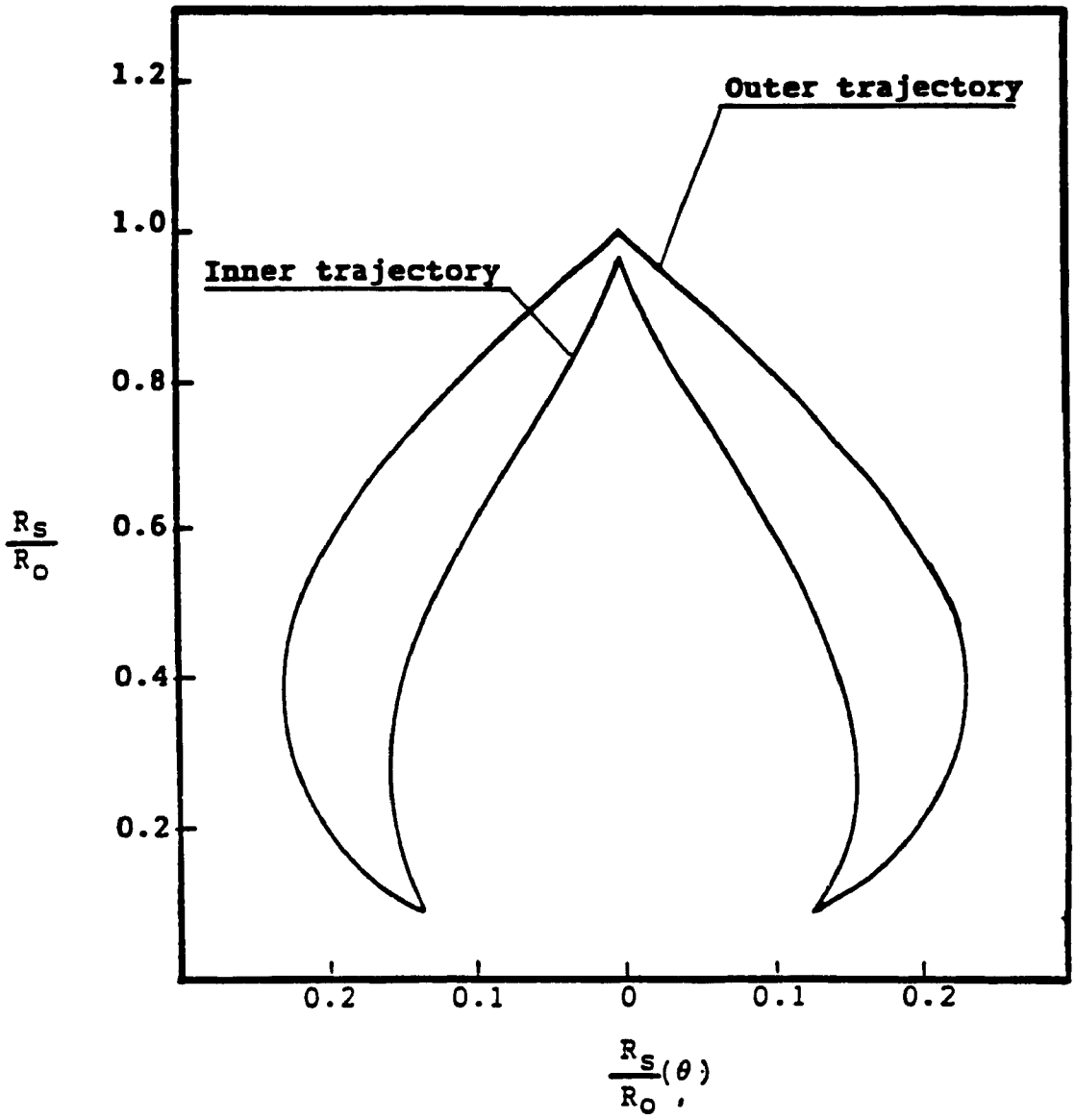

Fig. 4.15 Outer and Inner Trajectories, Rod of Diameter 0.4 mm

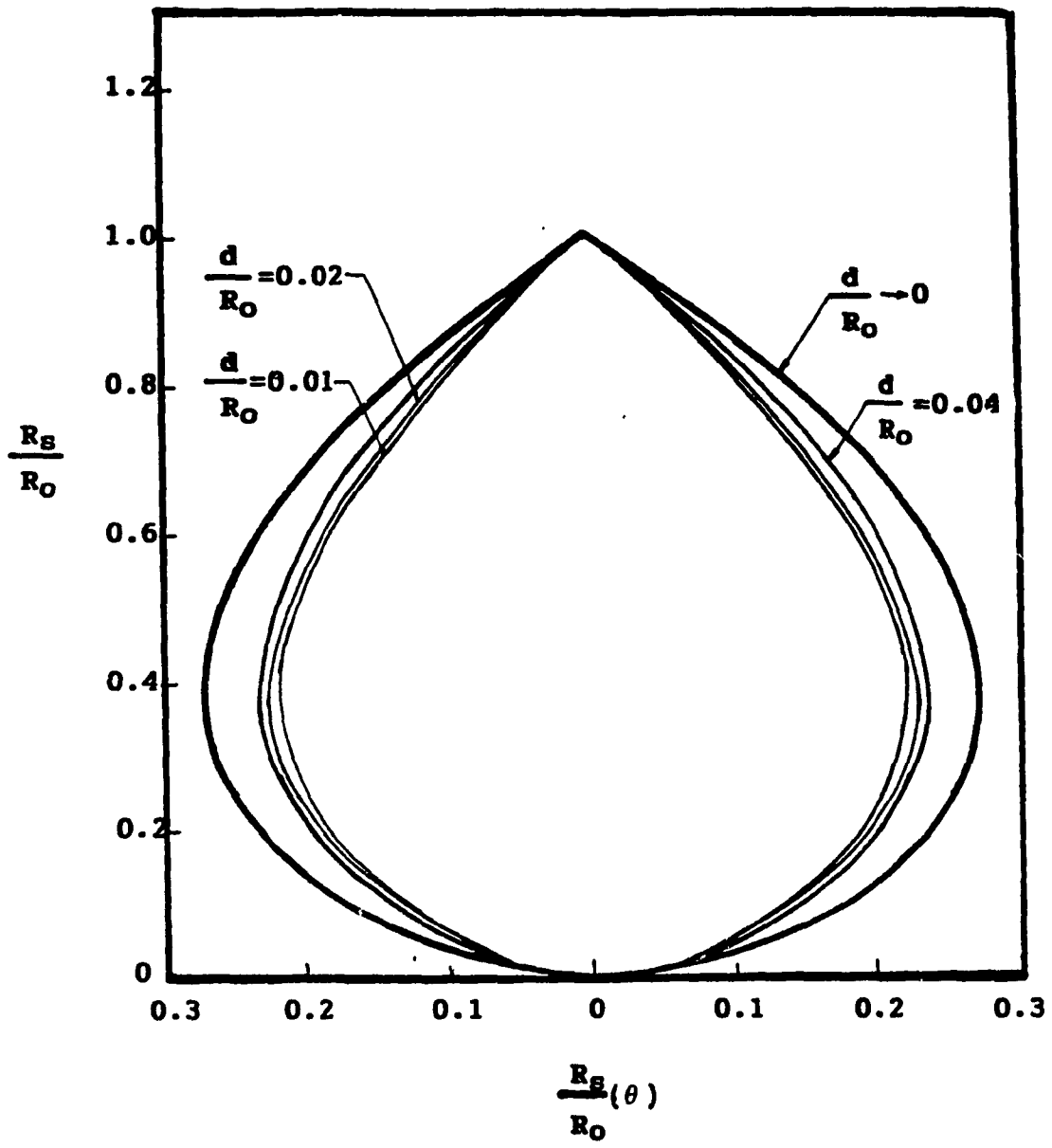

Fig. 4.16 Theoretical Shock-Shock Trajectories for Various Rod Diameters

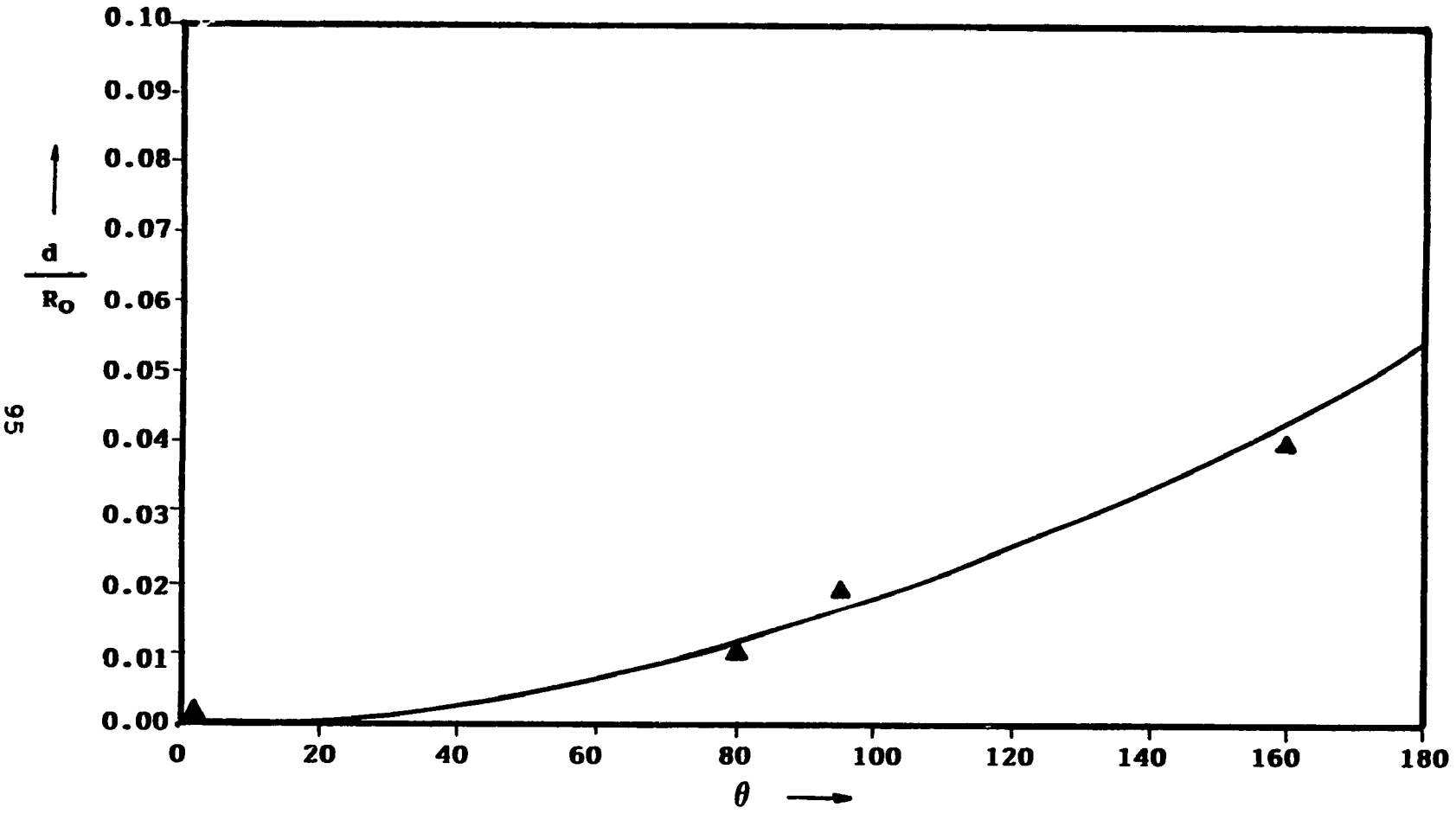

Fig. 4.17 Angles Where The Two Shock-Shock Merge

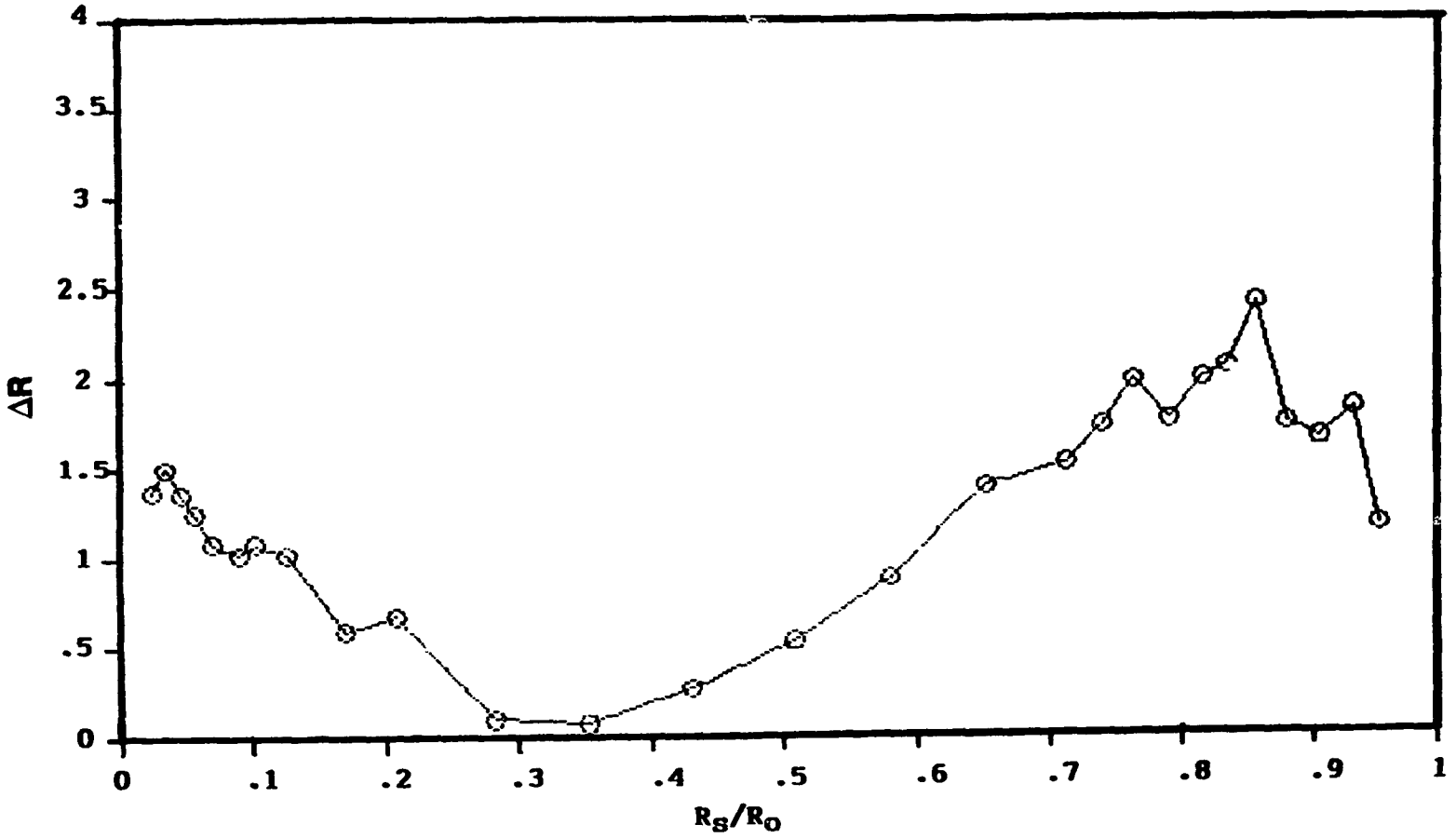

Fig. 4.18 Theoretical Values of the Displacement ΔR of the Perturbed Shock, $R_O/d=25$

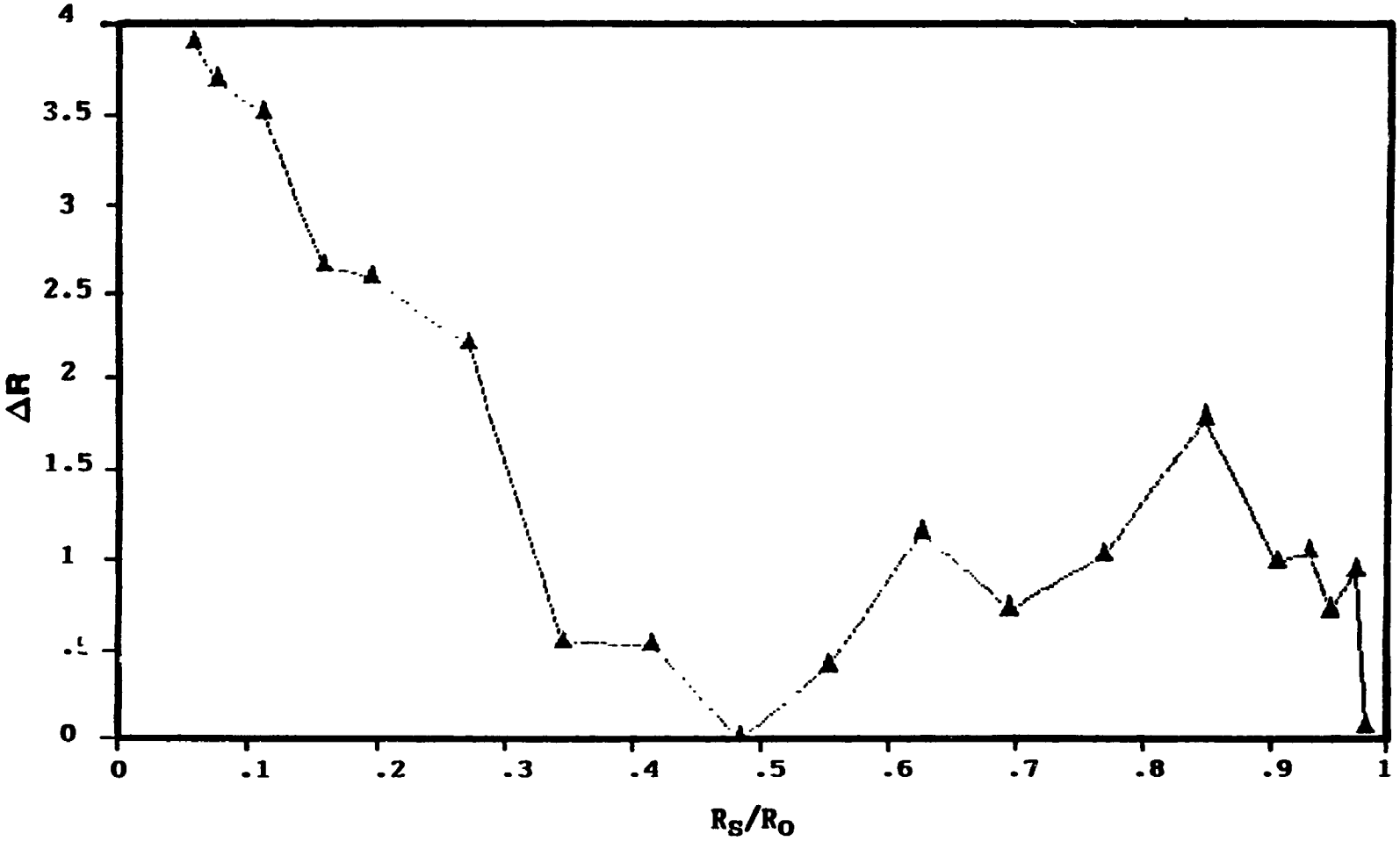

Fig. 4.19 Theoretical Values of the Displacement ΔR of the Perturbed Shock, $R_O/d=50$

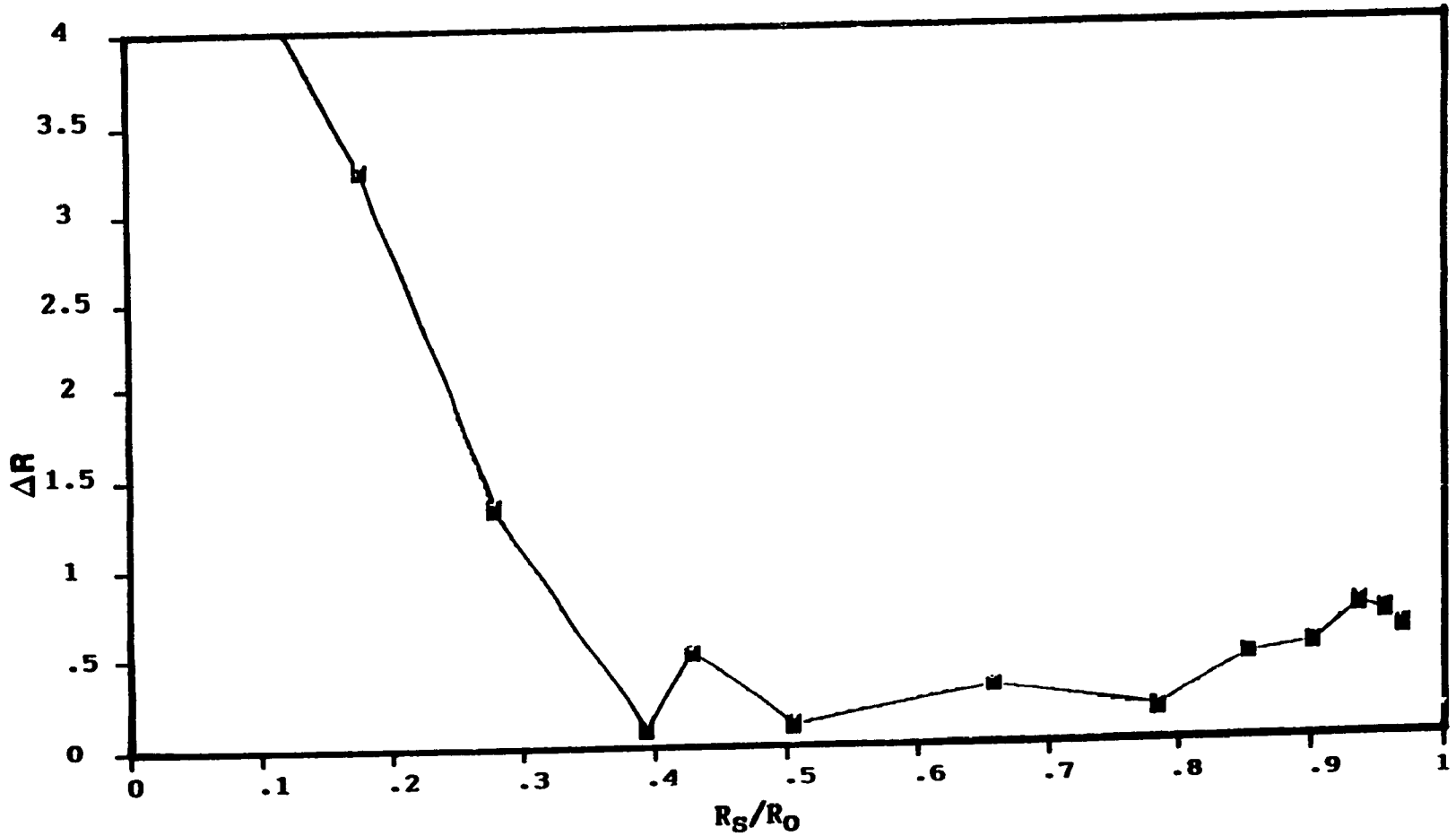

Fig. 4.20 Theoretical Values of the Displacement ΔR of the Perturbed Shock, $R_O/d=100$

Table 1. Characteristics Variables Versus Shock Mach Number

Mach No. M	Ray Area A x 10^n	ω Equation (2.63)	Characteristic Angle 'm' (Deg) Equation (2.70)
1.00		0	0.000
1.01	3.5846 + 2	0.283	7.925
1.05	1.3107 + 1	0.633	16.323
1.10	2.9462 + 0	0.806	21.071
1.15	1.1841 + 0	1.007	23.787
1.20	6.0536 - 1	1.266	25.512
1.25	3.5366 - 1	1.414	26.656
1.30	2.2507 - 1	1.547	27.429
1.35	1.5206 - 1	1.669	27.952
1.40	1.0740 - 1	1.728	28.298
1.45	7.8507 - 2	1.887	28.517
1.50	5.8981 - 2	1.984	28.644
1.55	4.5319 - 2	2.077	28.701
1.60	3.5481 - 2	2.165	28.707
1.65	2.8225 - 2	2.249	28.674
1.70	2.2764 - 2	2.330	28.612
1.75	1.8580 - 2	2.406	28.528
1.80	1.5326 - 2	2.480	28.428
1.85	1.2760 - 2	2.551	28.316
1.90	1.0713 - 2	2.619	28.195
1.95	9.0632 - 3	2.685	28.068
2.00	7.7194 - 3	2.749	27.938

Mach No. M	Ray Area A x 10^n	ω Equation (2.63)	Characteristic Angle 'm'(Deg) Equation(2.70)
2.05	6.6158 - 3	2.811	27.805
2.10	5.7023 - 3	2.871	27.672
2.15	4.9407 - 3	2.920	27.538
2.20	4.3015 - 3	2.985	27.406
2.25	3.7617 - 3	3.010	27.275
2.30	3.3034 - 3	3.094	27.146
2.40	2.5765 - 3	3.203	26.895
2.50	2.0370 - 3	3.302	26.656
2.60	1.6300 - 3	3.388	26.429
2.70	1.3183 - 3	3.477	26.214
2.80	1.0765 - 3	3.563	26.012
2.90	8.8681 - 4	3.645	25.822
3.00	7.3630 - 4	3.724	25.643
3.20	5.1842 - 4	3.875	25.318
3.40	3.7409 - 4	4.015	25.033
3.60	2.7570 - 4	4.148	24.781
3.80	2.0696 - 4	4.272	24.559
4.00	1.5789 - 4	4.308	24.363
4.50	8.5195 - 5	4.660	23.963
5.00	4.9260 - 5	4.900	23.731
6.00	1.9213 - 5	5.314	23.704
7.00	8.7059 - 6	5.672	23.702

Mach No. M	Ray Area A x 10^n	ω Equation (2.63)	Characteristic Angle 'm'(Deg) Equation(2.70)
8.00	4.3952 - 6	5.966	23.702
9.00	2.4032 - 6	6.232	23.701
10.00	1.4070 - 6	6.470	23.700
15.00	1.7863 - 7	7.385	23.704
20.00	4.1414 - 8	8.033	23.708
100.00	1.1724 - 11	11.670	23.803
∞	0	∞	23.900

Table 2. Various Quantities Corresponding to the Wave Diagram of Figure 4.5

POINT	$(\theta+\omega)$	$(\theta-\omega)$	θ (deg)	ω (rad)	$(\theta+m)$	$(\theta-m)$	M	N
4	2.7837	-2.0856	19.999	2.4347	48.488	-8.490	1.7694	
5	2.7837	-2.0856	20.000	2.4347	48.489	-8.489	1.7694	
6							1.5036	34.483
7	2.7820	-2.1300	18.683	2.4560	47.143	-9.777	1.7838	
8	2.6092	-2.0856	15.000	2.3474	43.593	-13.593	1.7114	
9	2.6092	-2.1300	13.728	2.3696	42.296	-14.840	1.7206	
10							1.5046	32.968
11	2.6087	-2.1255	13.845	2.3671	42.416	-14.726	1.7244	
12	2.1126	-2.1300	-0.500	2.3671	28.204	-29.204	1.5751	
13	2.1126	-2.1255	-0.37	2.1191	28.334	-29.074	1.5751	
14	2.4561	-2.1255	9.469	2.2908	38.111	-19.172	1.6758	
15							1.5076	31.500
16	2.4552	-2.1274	9.3953	2.2913	38.037	-19.246	1.6761	
17	2.1126	-2.1274	-0.424	2.1200	28.280	-29.128	1.5745	
18	0.8515	-2.1255	-36.500	1.4885	-9.411	-46.331	1.2780	
19	0.8515	-2.1274	-36.552	1.4895	-9.457	-63.647	1.2784	

POINT	$(\theta+\omega)$	$(\theta-\omega)$	θ (deg)	ω (rad)	$(\theta+m)$	$(\theta-m)$	M	ν
20	0.8515	-2.1261	-36.512	1.4895	-9.421	-63.602	1.2781	
21	-0.0209	-2.1261	-61.500	1.0525	-37.409	-85.596	1.1588	
22	2.3410	-2.1274	6.119	2.2342	34.799	-22.560	1.6411	
23	1.8854	-2.1274	-6.933	2.0064	21.725	-35.590	1.5120	
24	0.6108	-2.1261	-43.409	1.3684	-17.170	-69.775	1.2346	
25	0.6108	-2.1274	-43.447	1.3691	-17.140	-69.755	1.2348	
26	0.2498	-2.1261	-53.755	1.1880	-28.764	-78.746	1.1849	
27	0.1746	-2.1274	-55.944	1.1510	-31.198	-80.890	1.1778	
28	0.0994	-2.1261	-58.060	1.1128	-33.569	-82.550	1.1704	
29							1.5116	30.001
30	2.3417	-2.1317	6.013	2.2367	34.692	-22.666	1.6427	
31	2.1126	-2.1317	-0.547	2.1222	28.157	-29.251	1.5757	
32	1.885	-2.1317	-7.056	2.0086	21.603	-35.715	1.5132	
33	0.8515	-2.1317	-36.675	1.4916	-9.567	-63.782	1.2792	
34	0.8515	-2.1284	-36.580	1.4899	-9.483	-63.677	1.2785	
35	0.4125	-2.1274	-49.127	1.2501	-23.722	-74.532	1.1968	

POINT	$(\theta+\omega)$	$(\theta-\omega)$	θ (deg)	')	$(\theta+m)$	$(\theta-m)$	M	N
36	0.4125	-2.1284	-49.160	1.2705	-23.613	-74.706	1.2015	
37	0.8515	-2.1304	-36.640	1.4910	-9.538	-63.743	1.2789	
38	0.6208	-2.1284	-43.188	1.3746	-16.837	-69.540	1.2367	
39	0.6208	-2.1304	-43.246	1.3756	-16.887	-69.604	1.2370	
40	0.8515	-2.1311	-36.658	1.4914	-9.555	-63.760	1.2791	
41	0.6647	-2.1304	-41.989	1.2444	-15.460	-68.515	1.2444	
42	0.6647	-2.1311	-42.026	1.3982	-15.492	-68.561	1.2447	
43	2.3000	-2.1317	4.821	2.2158	28.687	-23.866	1.6302	
44							1.5155	24.717
45	2.3000	-2.1457	4.416	2.2228	31.100	-24.268	1.6344	
46	2.1126	-2.1457	-0.948	2.1292	27.756	-29.652	1.5796	
47	1.8854	-2.1457	-7.457	2.0156	21.206	-36.120	1.5796	
48	1.3713	-2.1317	-21.784	1.7515	6.547	-50.114	1.4074	
49	1.3713	-2.1457	-22.185	1.7585	6.155	-50.525	1.7585	
50	0.7051	-2.1311	-40.850	1.4181	-14.185	-67.515	1.2515	
51	0.7051	-2.1317	-40.870	1.4184	-14.210	-67.530	1.2516	

POINT	$(\theta+\omega)$	$(\theta-\omega)$	θ (deg)	ω (rad)	$(\theta+m)$	$(\theta-m)$	M	ν
52	2.4289	-2.4491	- 0.580	2.4390	27.900	-29.060	1.7723	4.420
53	1.0074	-2.1317	-32.206	1.5695	- 4.711	-59.701	1.3092	
54	1.0074	-2.1457	-32.608	1.5765	- 5.052	-60.164	1.3121	
55	2.3038	-2.3598	- 1.608	2.3318	27.004	-30.220	1.7012	
56	2.2546	-2.1457	- 3.120	2.2001	31.813	-25.573	1.6209	
57							1.5213	27.869
58	2.2546	-2.1457	- 2.457	2.2114	31.145	-26.232	1.6278	
59	2.1126	-2.1685	- 1.604	2.1406	27.101	-30.310	1.5892	
60	1.8854	-2.1685	- 8.110	2.0270	20.560	-36.780	1.5231	
61	1.3713	-2.1685	-22.838	1.7699	5.517	-51.194	1.4132	
62	1.1830	-2.1457	-27.577	1.6643	0.184	-55.338	1.3480	
63	1.1830	-2.1658	-28.155	1.6744	- 0.182	-56.128	1.6744	
64	2.2697	-2.3449	- 2.155	2.3073	26.474	-30.784	1.6860	
65	2.3073	-2.3073	0.000	2.3073	26.474	-26.474	1.6860	
66	2.2373	-2.1685	1.980	2.2029	30.672	-26.712	1.6225	

POINT	$(\theta+\omega)$	$(\theta-\omega)$	θ (deg)	ω (rad)	$(\theta+m)$	$(\theta-m)$	M	ν
67							1.5272	26.444
68	2.2304	-2.1965	0.978	2.2136	29.666	-27.709	1.6289	
69	2.1126	-2.1965	- 2.406	2.1546	26.300	-31.113	1.5941	
70	1.8854	-2.1965	- 8.912	2.0410	19.767	-37.591	1.5307	
71	1.3713	-2.1965	-23.640	1.7839	4.735	-52.015	1.4176	
72	1.3713	-2.1768	-23.076	1.7741	5.286	-51.437	1.4145	
73	1.2482	-2.1658	-26.288	1.7070	1.886	-54.462	1.3822	
74	1.2482	-2.1710	-26.436	1.7096	1.754	-54.626	1.3844	
75	2.3071	-2.3641	- 1.636	2.3356	26.979	-30.245	1.7037	11.151
76	2.3641	-2.3641	0.000	2.3641	28.574	-28.574	1.7224	
77	1.2755	-2.1710	-25.652	1.7232	2.638	-53.942	1.3959	
78	1.2755	-2.2112	-26.806	1.7433	1.524	-55.136	1.4048	
79	2.3216	-2.4056	- 2.406	2.3636	26.143	-30.955	1.7221	10.537
80	2.3126	-2.3641	- 1.475	2.2868	27.150	-30.300	1.6733	
81	2.2192	-2.1965	0.653	2.2078	29.343	-28.037	1.6255	

POINT	$(\theta+\omega)$	$(\theta-\omega)$	θ (deg)	ω (rad)	$(\theta+m)$	$(\theta-m)$	M	ν
82							1.5304	25.922
83	2.2192	-2.2112	0.230	2.2152	28.917	-28.460	1.6299	
84	2.1126	-2.2112	2.825	2.1619	25.822	-31.531	1.5982	
85	1.8854	-2.2112	- 9.334	2.0483	19.350	-38.017	1.5345	
86	1.3713	-2.2112	-24.064	1.7913	4.321	-52.450	1.4199	
87	2.2090	-2.2112	- 0.062	2.2101	28.630	-28.751	1.6268	
88							1.5330	25.415
89	2.2090	-2.2225	- 0.391	2.2157	28.296	-29.078	1.6302	
90	2.1126	-2.2225	- 3.324	2.1690	25.466	-31.934	1.6057	
91	1.8854	-2.2225	- 9.743	2.0554	19.026	-38.340	1.5340	
92	1.6284	-2.2225	-17.020	1.9254	11.538	-45.578	1.4663	
93	1.3713	-2.2225	-24.385	1.7969	3.998	-52.943	1.4195	
94	1.0325	-2.2112	-26.032	1.7568	2.293	-54.357	1.4090	
95	1.0325	-2.2225	-26.356	1.7625	1.980	-54.692	1.4097	
96	2.3341	-2.4025	- 1.961	2.3683	26.608	-29.464	1.7252	11.089

POINT	$(\theta+\omega)$	$(\theta-\omega)$	θ (deg)	ω (rad)	$(\theta+m)$	$(\theta-m)$	M	ν
97	2.3341	-2.3641	-0.859	2.3491	27.746	-29.464	1.7125	
98	2.4056	-2.4056	0.000	2.4056	28.528	-28.528	1.7500	
99	1.3262	-2.2157	-25.481	1.7709	2.876	-53.838	1.4135	
100	2.1998	-2.2089	- 0.260	2.4596	28.195	-28.715	1.7865	
101							1.5358	24.817
102	2.1998	-2.2364	- 1.050	2.2181	27.636	-29.736	1.6316	
103	2.1126	-2.2364	- 3.547	2.1745	25.157	-32.250	1.6056	
104	1.8854	-2.2364	-10.055	2.0609	18.636	-38.746	1.5413	
105	1.6284	-2.2364	-17.420	1.9324	11.160	-45.994	1.4734	
106	1.3713	-2.2364	-24.783	1.8039	3.619	-53.186	1.4239	
107	2.3435	-2.4056	- 1.977	2.3780	26.583	-30.537	1.7315	
108	1.3262	-2.2364	-26.075	1.7813	2.296	-54.446	1.4167	
109	2.3435	-2.4125	- 1.975	2.3780	26.585	-30.535	1.7316	11.083
110	2.1709	-2.2364	- 1.643	2.2077	27.047	-30.333	1.6254	
111							1.5409	23.806

POINT	$(\theta+\omega)$	$(\theta-\omega)$	θ (deg)	ω (rad)	$(\theta+m)$	$(\theta-m)$	M	χ
112	2.1790	-2.2588	- 2.841	2.2189	26.402	-30.970	1.6321	
113	2.1126	-2.2588	- 4.188	2.1857	24.510	-32.887	1.6123	
114	1.8854	-2.2588	-10.697	2.0721	18.000	-39.395	1.5473	
115	1.6284	-2.2588	-18.060	1.9436	10.532	-46.651	1.4792	
116	2.1690	-2.2588	- 2.571	2.2239	2.993	-53.843	1.4274	
117							1.5509	22.150
118	2.1690	-2.3063	- 3.927	2.2378	24.751	-33.186	1.6433	
119	2.1126	-2.3063	- 5.549	2.2095	23.140	-34.239	1.6265	
120	1.8854	-2.3063	-12.058	2.0959	16.646	-40.760	1.4348	
121	1.6284	-2.3063	-19.420	1.9674	9.202	-48.043	1.4914	
122	2.1507	-2.3063	- 4.457	2.2311	24.225	-28.682	1.6378	
123							1.5516	21.405
124	2.1507	-2.3158	- 4.748	2.2332	23.933	-33.423	1.6406	
125	2.1126	-2.3158	- 5.821	2.2142	22.866	-33.968	1.6293	
126	1.8854	-2.3158	-12.330	2.1006	16.373	-41.033	1.5635	

POINT	$(\theta+\omega)$	$(\theta-\omega)$	θ (deg)	ω (rad)	$(\theta+m)$	$(\theta-m)$	M	ν
127	1.6284	-2.3158	-19.693	1.9721	8.936	-48.321	1.4937	
128	1.3584	-2.2364	-25.152	1.7974	3.241	-53.545	1.4218	
129	1.3584	-2.2588	-25.794	1.8086	2.614	-54.202	1.4253	
130	2.3544	-2.4241	- 1.944	2.3893	26.352	-30.540	1.7390	11.302
131	2.3544	-2.4125	- 1.664	2.3834	26.894	-30.222	1.7351	
132	2.4125	-2.4125	0.000	2.4125	28.519	-28.519	1.7544	
133	1.4321	-2.2588	-23.683	1.8454	4.749	-52.115	1.4369	
134	1.4321	-2.3063	-25.043	1.8692	3.449	-53.535	1.4444	
135	2.3752	-2.4464	- 2.043	2.4108	26.477	-30.563	1.7533	11.857
136	2.4241	-2.4241	0.000	2.4241	28.400	-28.400	1.8122	
137	2.3572	-2.4241	- 1.917	2.3902	26.708	-30.540	1.7396	
138	1.4657	-2.3063	-24.081	1.8860	28.517	-52.598	1.4500	
139	1.4657	-2.3158	-24.353	1.8907	4.165	-52.871	1.4519	
140	2.3818	-2.4464	- 1.853	2.4141	26.675	-30.381	1.7555	12.350
141	2.4464	-2.4464	0.000	2.4464	28.473	-28.473	1.7773	

POINT	$(\theta+\omega)$	$(\theta-\omega)$	θ (deg)	ω (rad)	$(\theta+m)$	$(\theta-m)$	M	N
142	2.3818	-2.4146	- 1.850	2.4141	26.675	-30.381	1.7555	
143	2.1349	-2.3158	- 5.181	2.2253	23.502	-33.864	1.6358	
144							1.5598	19.972
145	2.1348	-2.3504	- 6.179	2.2426	22.497	-34.855	1.6462	
146	2.1126	-2.3504	- 6.813	2.2315	21.868	-35.493	1.6396	
147	1.8854	-2.3504	-13.321	2.1179	15.382	-42.025	1.5732	
148	1.6284	-2.3504	-20.684	1.9894	7.964	-49.331	1.5029	
149	2.1227	-2.3504	- 6.522	2.2365	22.157	-35.201	1.6425	
150							1.5691	18.650
151	2.1227	-2.3881	- 7.635	2.2548	21.034	-36.305	1.6536	
152	2.1126	-2.3881	- 7.893	2.2504	20.781	-36.560	1.6508	
153	1.8854	-2.3881	-14.401	2.1368	14.304	-43.106	1.5841	
154	1.6284	-2.3881	-21.764	2.0083	6.895	-50.422	1.5130	
155	1.5380	-2.3158	-22.282	1.9268	6.268	-50.832	1.4705	
156	1.5380	-2.3881	-24.353	1.9630	4.244	-52.950	1.4892	

POINT	$(\theta+\omega)$	$(\theta-\omega)$	θ (deg)	ω (rad)	$(\theta+m)$	$(\theta-m)$	M	ν
157	2.4304	-2.5126	- 2.353	2.4715	26.114	-30.820	1.7943	12.201
158	2.4304	-2.4464	- 0.458	2.8887	27.173	-28.089	2.1152	
159	2.1054	-2.3881	- 8.098	2.2468	20.576	-36.774	1.6487	
160							1.5861	15.710
161	2.0948	-2.4582	-10.156	2.2765	18.240	-39.069	2.2765	
162	1.8854	-2.4582	-16.409	2.1718	12.295	-45.114	1.6040	
163	1.6284	-2.4582	-23.772	2.0433	4.908	-52.452	1.5319	
164	1.5887	-2.3881	-22.899	1.9883	5.745	-51.543	1.5023	
165	1.5887	-2.4582	-24.909	2.0234	3.771	-53.589	1.5211	
166	2.4416	-2.5711	- 3.709	2.5064	24.709	-32.127	1.8186	11.146
167	2.5126	-2.5126	0.000	2.5126	28.300	-28.300	1.8463	
168	2.4416	-2.5126	- 2.034	2.4771	26.416	-30.484	1.7980	
169	2.0797	-2.4582	-10.715	2.2667	17.945	-39.375	1.6609	
170							1.6105	11.223
171	2.0797	-2.4582	-14.523	2.3333	14.085	-43.131	1.7022	

POINT	$(\theta+\omega)$	$(\theta-\omega)$	θ (deg)	ω (rad)	$(\theta+m)$	$(\theta-m)$	M	ν
172	1.8854	-2.5867	-20.091	2.2361	8.588	-48.770	1.6423	
173	1.6284	-2.5967	-27.453	2.1075	1.250	-56.156	1.5673	
174	1.6149	-2.4582	-24.158	2.0365	4.515	-52.831	1.5264	
175	1.6149	-2.5867	-27.840	2.1008	0.863	-56.543	1.5635	
176	2.4431	-2.6819	- 6.840	2.5625	21.455	-35.135	1.8585	7.606
177	2.5711	-2.5711	0.000	2.5711	28.280	-28.280	1.8647	
178	2.4431	-2.5711	- 3.667	2.5071	24.716	-32.054	1.8191	
179	2.0638	-2.5867	-14.980	2.3252	13.636	-43.595	1.6970	
180							1.6384	6.397
181	2.0642	-2.7184	-18.741	2.3911	9.804	-47.285	1.7403	
182	1.8854	-2.7184	-23.864	2.3019	4.770	-52.497	1.6826	
183	1.6441	-2.7184	-30.777	2.1812	-2.070	-59.484	1.6096	
184	2.4631	-2.8114	- 9.977	2.6373	18.730	-38.136	1.9139	4.830
185	2.6819	-2.6819	0.000	2.6819	28.700	-28.700	1.9476	
186	2.4631	-2.6819	- 6.268	2.5725	22.032	-34.568	1.8658	

POINT	$(\theta+\omega)$	$(\theta-\omega)$	θ (deg)	ω (rad)	$(\theta+m)$	$(\theta-m)$	M	χ
187	2.0484	-2.7184	-19.191	2.3833	9.362	-47.744	1.7350	
188							1.6757	0.596
189	2.0484	-2.8816	-23.872	2.4650	4.577	-52.321	1.7895	
190	1.4929	-2.4048	-26.123	1.9488	2.475	-53.122	1.4818	
191	1.6712	-2.8816	-34.674	2.2764	- 6.024	-63.324	1.6669	
192	2.4881	-2.9583	-13.474	2.7232	14.503	-41.451	1.9847	0.865
193	2.8114	-2.8114	0.000	2.8114	27.805	-27.805	2.0500	
194	2.4881	-2.8114	- 9.262	2.6497	18.874	-37.398	1.9232	
195	2.5449	-2.6819	- 3.925	2.6134	24.279	-32.128	1.8959	
196	2.5449	-2.8114	- 7.635	2.6781	20.433	-35.702	1.9448	
197	2.6326	-2.6819	- 1.412	2.6572	26.708	-29.533	1.9289	
198	2.6326	-2.8114	- 5.122	2.7220	22.871	-33.115	1.9789	
199	2.0257	-2.8816	-24.518	2.4536	3.946	-52.982	1.7821	
200							1.7230	-6.217
201	2.0254	-3.0690	-29.895	2.5473	- 1.573	-58.217	1.8473	

POINT	$(\theta+\omega)$	$(\theta-\omega)$	θ (deg)	ω (rad)	$(\theta+m)$	$(\theta-m)$	M	ν
202	1.8854	-3.0690	-29.895	2.4772	-33.908	- 5.476	1.7981	
203	1.7070	-3.0690	-39.018	2.3880	-10.454	-67.582	1.7381	
204	2.5448	-3.1388	-17.018	2.8418	10.718	-44.754	2.0757	- 3.352
205	2.6326	-3.1388	-14.500	2.8857	13.172	-42.172	2.1150	
206	2.8114	-3.1388	- 9.379	2.9751	18.031	-36.789	2.1911	
207	3.1388	-3.1388	0.000	3.1388	27.042	-27.042	2.3411	
208	2.0042	-3.0690	-30.504	2.5366	- 2.166	-58.843	1.8400	
209							1.7771	-13.885
210	2.0040	-3.3130	-36.471	2.6765	- 8.611	-64.616	1.9200	
211	1.8854	-3.3130	-40.898	2.5992	-12.667	-66.872	1.8854	
212	1.7186	-3.3130	-45.676	2.5158	-17.713	-74.179	1.8252	
213	2.5792	-3.3707	-22.676	2.9750	4.734	-50.086	2.1911	-10.051
214	2.5792	-3.1388	-16.031	2.8590	12.306	-44.368	2.0900	
215	1.9795	-3.3130	-38.202	2.6463	-10.060	-66.344	1.9270	
216							1.8574	-23.994

POINT	$(\theta+\omega)$	$(\theta-\omega)$	θ (deg)	ω (rad)	$(\theta+m)$	$(\theta-m)$	M	ν
217	1.9794	-3.5706	-45.584	2.7750	-17.702	-73.466	2.0210	
218	1.8854	-3.5706	-48.277	2.7280	-20.297	-76.258	1.9836	
219	1.7411	-3.5706	-52.409	2.6558	-24.285	-80.533	1.9278	
220	2.6326	-3.6173	-28.209	3.1250	- 1.126	-55.292	2.3285	-16.603
221	2.8114	-3.6173	-23.087	3.2143	2.231	-48.405	3.8850	
222	3.1388	-3.6173	-13.708	3.3780	12.747	-40.163	2.5883	
223	3.6173	-3.6173	0.000	3.6173	26.052	-26.052	2.7801	
224	1.9642	-3.5706	-46.020	2.7674	-18.121	-73.918	2.0148	
225							1.9170	-30.947
226	1.9636	-3.7719	-51.804	2.8678	-24.124	-75.928	2.0973	
227	1.8854	-3.7719	-54.044	2.8287	-26.278	-81.810	2.0646	
228	1.7649	-3.7719	-54.496	2.7684	-26.558	-54.336	2.0156	
229	2.6644	-3.7638	-31.496	3.2141	- 2.629	-58.363	2.4113	-19.276
230	2.6644	-3.6173	-27.298	3.1408	- 0.260	-54.336	2.3429	
231	1.8854	-3.7719	-52.317	2.8588	-24.617	-52.316	2.0898	

POINT	$(\theta+\omega)$	$(\theta-\omega)$	θ (deg)	ω (rad)	$(\theta+m)$	$(\theta-m)$	M	χ
232							2.0000	.483
233	1.9457	-4.0371	-59.923	2.9914	-32.540	-92.426	2.2127	
234	1.8854	-4.0371	-61.642	2.9613	-43.161	-89.123	2.1788	
235	1.7880	-4.0371	-64.432	2.9125	-36.757	-92.107	2.1357	
236	2.7091	-4.0646	-38.832	3.3869	-12.403	-65.261	2.5988	-28.337
237	2.7901	-3.6173	-23.697	3.2037	2.198	-50.592	2.4000	
238	2.8114	-4.0646	-35.901	3.4380	- 9.593	-62.209	2.6561	
239	3.3138	-4.0646	-26.522	3.6017	- 0.600	-52.444	2.8471	
240	4.0646	-4.0646	0.000	4.0646	24.939	-24.939	3.4746	
241	1.9316	-4.0371	-60.317	2.9843	-32.909	-93.725	2.1994	
242							2.0715	-47.606
243	1.9316	-4.2534	-66.514	3.0925	-39.365	-93.664	2.2986	
244	1.8854	-4.2534	-67.838	3.0694	-40.633	-95.043	3.0694	
245	1.8211	-4.0371	-63.483	2.9291	-36.265	-90.700	2.2723	
246	1.8211	-4.2534	-69.680	3.0373	-42.409	-96.962	2.2475	

POINT	$(\theta+\omega)$	$(\theta-\omega)$	θ (deg)	ω (rad)	$(\theta+m)$	$(\theta-m)$	M	γ
247	1.9151	-4.2534	-66.985	3.0842	-39.816	-94.155	2.2909	
248							2.1766	-65.267
249	1.9167	-4.5641	-75.900	3.2394	-49.093	-102.707	2.4368	
250	1.8854	-4.5641	-76.740	3.2274	-49.896	-103.582	2.4218	
251	1.8211	-4.5641	-78.581	3.1926	-51.662	-105.500	2.3904	
252	1.8120	-4.5641	-78.840	3.1880	-51.911	-105.769	2.3862	
253	2.7804	-4.5725	-51.340	3.6765	-25.546	- 77.134	2.9399	-42.073
254	2.7804	-4.0646	-36.789	3.4225	-10.438	- 63.140	2.6387	
255	2.8114	-4.5725	-50.451	3.6919	-24.736	- 76.166	2.9593	
256	3.1388	-4.5725	-41.072	3.8556	-15.713	- 66.431	3.1743	
257	1.9091	-4.5641	-76.061	3.2366	-49.247	-102.875	2.4340	
258							2.2461	-65.267
259	1.9096	-4.7588	-81.625	3.3342	-55.054	-108.196	2.5347	
260	1.8854	-4.7588	-82.317	3.3221	-82.137	-108.920	2.5234	
261	1.8211	-4.7588	-84.159	3.2899	-55.632	-110.844	2.4878	

POINT	$(\theta+\omega)$	$(\theta-\omega)$	θ (deg)	ω (rad)	$(\theta+m)$	$(\theta-m)$	M	N
262	1.8868	-4.7588	-82.276	3.3228	-55.540	-109.009	2.5242	
263							2.3214	-71.209
264	1.8858	-4.9330	-81.295	3.4094	-54.917	-107.672	2.6240	
265	1.8854	-4.9330	-87.307	3.4092	-60.930	-113.685	3.4092	
266	1.8533	-4.9330	-88.228	3.3932	-61.812	-114.645	3.3932	
267	1.8211	-4.9330	-89.149	3.3771	-62.691	-115.607	2.5872	
268	1.8804	-4.9330	-87.450	3.4067	-61.066	-113.843	2.6210	
269							2.4066	-79.460
270	1.8800	-5.1681	-94.200	3.5240	-68.096	-120.304	2.7547	
271	1.8533	-5.1681	-94.962	3.5107	-68.827	-121.097	2.7392	
272	1.8235	-5.1681	-95.813	3.4957	-69.613	-121.813	2.7217	
273	2.9595	-5.1869	-63.813	4.0732	-38.692	- 88.664	3.4875	-56.539
274	2.9595	-4.5725	-46.209	3.7660	-20.657	- 71.761	3.0556	
275	1.8713	-5.1681	-94.446	3.5197	-68.332	-120.560	2.7496	
276							2.5254	-88.788

POINT	$(\theta+\omega)$	$(\theta-\omega)$	θ (deg)	ω (rad)	$(\theta+m)$	$(\theta-m)$	M	χ
277	1.8715	-5.4463	-102.412	3.6589	-76.621	-128.202	2.9176	
278	1.8533	-5.4463	-102.932	3.6498	-77.121	-128.743	2.9061	
279	1.8663	-5.7177	-102.559	3.6563	-76.763	-128.356	2.9143	
280							2.6286	-97.183
281	1.8665	-5.7177	-110.330	3.7921	-84.830	-135.830	3.0468	
282	1.8533	-5.7177	-110.707	3.7855	-85.193	-136.221	3.0422	
283	1.8211	-5.7177	-111.629	3.7694	-86.082	-137.177	3.0312	
284	1.8599	-5.7177	-110.518	3.7888	-85.001	-136.035	3.0858	
285							2.7728	-107.60
286	1.8596	-6.0086	-118.860	3.9341	-93.644	-144.074	3.2845	
287	1.8533	-6.0086	-119.040	3.9310	-93.817	-144.263	3.2800	
288							3.0320	-124.72
289	1.8538	-6.5399	-134.246	4.1969	-109.54	-158.94	3.6788	
290	3.3309	-6.6203	- 94.240	4.9756	-68.509	-119.971	5.1828	-89.000
291	6.6203	-6.6203	0.000	6.6203	23.704	- 23.704	9.7977	

Table 3. Various Quantities Corresponding to the Wave Diagram of Figure 4.8

POINT	$(\theta+\omega)$	$(\theta-\omega)$	θ (deg)	ω (rad)	$(\theta+m)$	$(\theta-m)$	M	N
1	2.6559	-1.3120	38.500	1.9840	67.144	9.856	1.5000	
2							1.5000	39.200
3	2.5076	-1.4604	30.000	0.5236	58.644	1.356	1.9245	35.500
4							1.5000	35.500
5	2.8114	-2.1133	20.000	2.4623	48.452	-8.452	1.7881	
6							1.5017	35.150
7	2.7907	-2.1135	19.350	2.4530	47.815	-9.1148	1.7816	
8	2.6047	-2.0985	14.500	2.3516	43.088	-14.088	1.7142	
9	2.6047	-2.1153	14.020	2.3600	42.599	-14.599	1.7197	
10							1.5025	34.150
11	2.6631	-2.1133	15.750	2.3882	44.321	-12.821	1.7383	
12	2.6631	-2.1153	15.690	2.3892	44.236	-12.856	1.7389	
13	1.8186	-2.1153	-8.497	1.9669	20.122	-30.720	1.4912	
14	1.8186	-2.1133	-8.442	1.9659	20.178	-30.062	1.4906	
15							1.5036	32.880
16	2.5051	-2.1073	11.400	2.3062	40.000	-17.220	1.6853	

POINT	$(\theta+\omega)$	$(\theta-\omega)$	θ (deg)	ω (rad)	$(\theta+m)$	$(\theta-m)$	M	N
17	2.5051	-2.1133	11.224	2.3092	39.852	-17.404	1.6871	
18	1.8186	-2.1073	-8.270	1.9630	20.346	-36.886	1.4892	
19							1.5064	31.384
20	2.3838	-2.1038	8.024	2.2438	36.674	-20.626	1.6469	
21	2.3838	-2.1073	7.921	2.2455	36.578	-20.736	1.6415	
22	1.8186	-2.1038	-8.170	1.9612	20.392	-36.732	1.4882	
23	1.8186	-2.1143	-8.470	1.9664	20.150	-37.090	1.4909	
24	1.1019	-2.1143	-29.000	1.6081	-1.310	-56.690	1.3250	
25	1.1019	-2.1073	-28.800	1.6046	-1.124	-56.476	1.3236	
26	1.1019	-2.1038	-28.700	1.6029	-1.031	-56.368	1.3229	
27	1.1019	-2.1132	-28.972	1.6075	-1.284	-56.660	1.3248	
28	0.1934	-2.1132	-55.000	1.1533	-30.240	-79.760	1.1782	
29	0.3069	-2.1132	-51.750	1.2100	-26.238	-77.266	1.1892	
30	0.3069	-2.1073	-51.577	1.2071	-26.077	-77.077	1.1866	
31							1.5106	30.130
32	2.2952	-2.1138	5.200	2.2045	33.891	-23.491	1.6235	

POINT	$(\theta+\omega)$	$(\theta-\omega)$	θ (deg)	ω (rad)	$(\theta+m)$	$(\theta-m)$	M	N
33	2.2952	-2.1038	5.483	2.1995	34.177	-23.210	1.6205	
34	1.8186	-2.1138	-8.457	1.9662	20.164	-37.077	1.4908	
35	1.1019	-2.1138	-28.998	1.6078	-1.309	-56.687	1.3249	
36							1.5148	29.339
37	2.2531	-2.1270	3.615	2.1900	32.312	-25.082	1.6149	
38	2.2531	-2.1138	3.991	2.1834	32.691	-24.709	1.6109	
39	0.5316	-2.1073	-45.143	1.3195	-19.743	-70.543	1.2181	
40	1.1019	-2.1062	-28.770	1.6041	-1.100	-56.440	1.3230	
41	0.5316	-2.1062	-45.100	1.3187	-19.700	-70.500	1.2178	
42	1.1019	-2.1059	-56.436	1.6039	-1.089	-56.436	1.3233	
43	0.5929	-2.1059	-43.344	1.3494	-17.186	-69.500	1.2282	
44	0.5929	-2.1059	-43.344	1.3494	-17.344	-69.344	1.2282	
45	0.7644	-2.1059	-38.430	1.4351	-11.730	-50.160	1.2579	
46	0.7644	-2.1038	-38.371	1.2575	-11.676	-65.606	1.2575	
47	1.6979	-1.6979	0	1.6979	28.000	-28.000	1.3745	5.800
48	1.6979	-1.6979	0	1.6979	28.000	-28.000	1.3745	

POINT	$(\theta+\omega)$	$(\theta-\omega)$	θ (deg)	ω (rad)	$(\theta+m)$	$(\theta-m)$	M	N
49	1.6979	-1.6979	0	1.6979	28.000	-28.000	1.3745	
50	1.1019	-2.1046	-28.730	1.6033	-1.060	-56.400	1.3231	
51	0.8071	-2.1038	-37.147	1.4554	-10.252	-64.042	1.2655	
52	0.8071	-2.1046	-37.170	1.4558	-10.280	-64.060	1.2657	6.730
53	2.4164	-2.3874	0.830	1.4558	29.246	-27.702	1.7473	
54	2.3874	-2.3874	0	2.3874	28.549	-28.549	1.7377	
55	1.1019	-2.1057	-28.760	1.6038	-1.090	-56.430	1.3233	
56	0.8497	-2.1046	-35.950	1.4771	-8.910	-62.990	1.2737	
57	0.8497	-2.1057	-35.980	1.4777	-8.980	-62.980	1.2740	
58	2.3964	-2.3678	0.820	2.3821	29.570	-27.730	1.7343	6.920
59	2.3964	-2.3874	0.257	2.1385	28.957	-28.443	1.5849	
60	2.3678	-2.3678	0.	2.3678	28.600	-28.600	1.7248	
61	1.1019	-2.1080	-28.810	1.6049	-29.965	-56.499	1.3237	
62	0.9338	-2.1057	-33.570	1.5197	-6.370	-60.770	1.2898	
63	0.9338	-2.1080	-33.640	1.5209	-6.240	-61.040	1.2902	
64	2.4375	-2.3551	2.360	2.3963	30.899	-26.179	1.7436	

POINT	$(\theta+\omega)$	$(\theta-\omega)$	θ (deg)	ω (rad)	$(\theta+m)$	$(\theta-m)$	M	ν
65	2.3551	-2.3551	0.000	2.3551	28.584	-28.584	1.7165	
66	1.0720	-2.1080	-29.676	1.5900	-2.063	-57.589	1.3176	
67	1.0720	-2.1138	-29.845	1.5929	-2.220	-57.011	1.3188	
68	2.4080	-2.3328	2.155	2.3704	30.723	-26.413	1.7259	11.155
69	2.3328	-2.3328	0.000	2.3328	28.608	-28.608	1.7018	
70	1.8186	-2.1270	-8.835	1.9728	19.795	-37.465	1.4943	
71	1.4063	-2.1138	-18.721	1.7871	9.658	-47.100	1.4186	
72	1.4603	-2.1270	-19.099	1.7937	9.289	-47.487	1.4207	
73							1.5211	27.971
74	2.1959	-2.1459	1.433	2.1709	30.133	-27.267	1.6053	
75	2.1959	-2.1270	1.974	2.1614	30.684	-26.736	1.5979	
76	1.8186	-2.1459	-9.376	1.9822	19.265	-38.017	1.4990	
77	1.4603	-2.1459	-19.641	1.8031	8.760	-48.042	1.4236	
78							1.5477	25.237
79	2.1627	-2.2257	-1.804	2.1942	26.891	-30.499	1.6174	
80	2.1627	-2.1459	0.481	2.1543	28.187	-27.539	1.5939	

POINT	$(\theta+\omega)$	$(\theta-\omega)$	θ (deg)	ω (rad)	$(\theta+m)$	$(\theta-m)$	M	N
81	1.8186	-2.2257	-11.663	2.0221	17.017	-40.343	1.5205	
82	1.4603	-2.2257	-21.927	1.8430	6.529	-50.383	1.4362	
83							1.5495	22.165
84	2.1335	-2.2875	-4.413	2.2105	24.273	-33.092	2.1335	
85	2.1161	-2.2257	-3.140	2.1709	25.564	-31.844	1.6035	
86	1.8186	-2.2875	-13.433	2.0530	15.253	-42.119	1.5371	
87	1.4063	-2.2875	-23.697	1.8739	4.802	-52.196	1.4459	
88	1.1962	-2.1138	-26.287	1.3443	1.605	-54.179	1.3443	
89	1.1962	-2.1270	-26.665	1.6616	1.255	-54.585	1.3470	
90	2.3379	-2.3129	0.735	2.3257	29.350	-27.880	1.6970	12.335
91	2.3129	-2.3129	0.000	2.3129	28.625	-28.625	1.6894	
92	1.3104	-2.1270	-23.394	1.7187	4.849	-51.637	1.3921	
93	1.3104	-2.1459	-23.935	1.7281	4.363	-52.233	1.4000	
94	2.3250	-2.3490	-0.685	2.3370	27.915	-29.285	1.7046	13.190
95	2.3250	-2.3129	0.346	2.3189	28.966	-28.273	1.6932	
96	2.3490	-2.3490	0.000	2.3490	28.615	-28.615	1.6969	

POINT	$(\theta+\omega)$	$(\theta-\omega)$	θ (deg)	ω (rad)	$(\theta+m)$	$(\theta-m)$	M	N
97	1.4385	-2.1459	-8.060	1.7922	8.122	-48.650	1.4202	
98	1.4385	-2.2257	-22.551	1.8321	5.890	-50.992	1.4327	
99	2.3383	-2.3825	-1.251	2.3601	27.327	-29.829	1.7198	13.945
100	2.3383	-2.3490	-0.306	2.3436	28.291	-28.903	1.7089	
101							1.5710	18.713
102	2.0991	-2.3804	-8.060	2.2398	20.617	-36.737	1.6445	
103	2.0991	-2.2875	-5.300	2.1916	23.396	-33.996	1.6158	
104	1.8186	-2.3804	-16.094	2.0995	12.608	-44.796	1.5628	
105	1.6394	-2.3804	-21.226	2.0099	7.434	-49.886	1.5139	
106	1.6394	-2.2875	-18.566	1.9634	10.049	-47.181	1.4894	
107							1.5927	14.887
108	2.0784	-2.4840	-11.620	2.2812	17.029	-40.269	1.6699	
109	2.0784	-2.3804	-8.651	2.2294	20.030	-37.332	1.6383	
110	1.8186	-2.4840	-19.062	2.1513	9.644	-47.768	1.5922	
111	1.6394	-2.4840	-24.196	2.0617	4.495	-52.887	1.5418	
112							1.6176	10.555

POINT	$(\theta+\omega)$	$(\theta-\omega)$	θ (deg)	ω (rad)	$(\theta+m)$	$(\theta-m)$	M	V
113	2.0656	-2.6047	-15.445	2.3352	13.161	-44.051	1.7034	
114	2.0656	-2.4840	-11.986	2.2748	16.668	-40.640	1.6659	
115	1.8186	-2.6047	-22.520	2.2116	6.168	-51.208	1.6278	
116	1.6394	-2.6047	-27.654	2.1220	1.050	-56.358	1.5756	
117	1.8186	-2.2650	-12.790	2.0418	15.889	-41.469	1.5311	
118	1.5000	-2.2257	-20.786	1.8628	7.684	-49.256	1.4392	
119	1.5000	-2.2650	-21.916	1.8825	6.595	-50.427	1.4487	
120	2.3483	-2.3977	-1.416	2.3730	27.148	-29.710	1.7283	14.290
121	2.3977	-2.3977	0.000	2.3977	28.537	-28.537	1.7445	
122	1.6032	-2.2875	-19.603	1.9453	8.990	-48.196	1.4800	
123	1.6032	-2.3804	-22.265	1.9918	6.383	-50.913	1.5042	
124	2.3601	-2.4950	-3.865	2.4276	24.633	-32.363	1.7646	13.127
125	2.3601	-2.3977	-1.077	2.3789	27.468	-29.623	1.7391	
126	1.6505	-2.3804	-20.910	2.0154	7.753	-49.573	1.5169	
127	1.6505	-2.4840	-23.878	2.0673	4.817	-52.573	1.5448	
128	2.3691	-2.5879	-6.266	2.4785	22.164	-34.696	1.7990	11.266

POINT	$(\theta+\omega)$	$(\theta-\omega)$	θ (deg)	ω (rad)	$(\theta+m)$	$(\theta-m)$	M	N
129	2.3691	-2.3977	-0.819	2.3834	27.734	-29.372	1.7351	
130	1.6993	-2.4840	-22.481	2.0916	6.221	-51.027	1.5583	
131	1.6993	-2.6047	-25.938	2.1520	2.768	-54.644	1.5926	
132	2.3745	-2.6969	-9.238	2.5357	19.102	-37.578	1.8392	8.498
133	2.3745	-2.3977	-0.664	2.3861	27.886	-29.214	1.7368	
134	2.6969	-2.6969	0.000	2.6969	28.034	-28.034	1.9593	
135							1.6456	5.737
136	2.0571	-2.7387	-19.525	2.3979	9.011	-48.061	1.7447	
137	2.0571	-2.6047	-15.687	2.3309	12.924	-44.298	1.7006	
138	1.9421	-2.6047	-18.982	2.2734	9.673	-47.637	1.6651	
139	1.9421	-2.7387	-22.821	2.3404	5.779	-57.421	1.7069	
140	1.8186	-2.7387	-26.359	2.2786	2.292	-55.070	1.6683	
141							1.6806	0.050
142	2.0516	-2.8973	-24.229	2.4745	4.211	-52.669	1.7963	
143	2.0516	-2.7387	-19.684	2.3952	8.856	-48.224	1.7429	
144	1.9421	-2.8973	-27.364	2.4197	1.145	-55.873	1.7592	

POINT	(θ+ω)	(θ−ω)	θ (deg)	ω (rad)	(θ+m)	(θ−m)	M	N
145	1.8186	-2.8973	-30.902	2.3579	-2.321	-59.483	1.7184	
146							1.7227	-6.277
147	2.0328	-3.0712	-29.747	2.5520	-1.438	-58.056	1.8507	
148	2.0328	-2.8973	-24.766	2.4650	3.682	-53.214	1.7898	
149	1.9421	-3.0712	-32.346	2.5066	-3.960	-60.732	1.8187	
150	1.8186	-3.0712	-35.884	2.4449	-7.409	-64.359	1.7763	
151	1.7466	-2.6047	-24.581	2.1756	4.121	-53.283	1.6070	
152	1.7466	-2.7387	-28.421	2.2426	0.255	-57.097	1.6462	
153	2.3935	-2.8201	-12.221	2.6068	15.995	-40.437	1.8910	5.614
154	2.3935	-2.6969	-8.692	2.5452	19.633	-37.017	1.8460	
155	1.7820	-2.7387	-27.405	2.2969	1.232	-56.042	1.6795	
156	1.7820	-2.8973	-31.951	2.3396	-3.350	-60.552	1.7063	
157	2.4118	-2.9686	-15.957	2.6902	12.106	-44.014	1.9541	1.770
158	2.4118	-2.6969	-8.167	2.5543	20.143	-36.477	1.8524	
159	2.5543	-2.6969	-4.083	2.6255	24.099	-32.265	1.9049	
160	2.4118	-2.8327	-12.059	2.6227	16.128	-40.246	1.9029	

POINT	$(\theta+\omega)$	$(\theta-\omega)$	θ (deg)	ω (rad)	$(\theta+m)$	$(\theta-m)$	M	N
161	2.5543	-2.8327	-7.975	2.7807	20.075	-36.025	1.9566	
162	2.5543	-2.9686	-11.869	2.7614	16.042	-39.780	2.0100	
163	2.6969	-2.8327	-3.890	2.7648	24.014	-31.794	2.0127	
164	1.8136	-2.8973	-31.044	2.3554	-2.461	-59.627	1.7167	
165	1.8136	-3.0712	-36.027	2.4424	-7.549	-64.505	1.7746	
166	2.4277	-3.1337	-20.227	2.7807	7.713	-47.627	2.0256	-2.670
167	2.4277	-2.9686	-15.495	2.9682	12.546	-43.563	1.9603	
168							1.7785	-13.811
169	2.0113	-3.2834	-36.443	2.6474	-8.303	-64.583	1.9215	
170	2.0113	-3.5604	-30.364	2.5412	-2.033	-58.695	1.8431	
171	1.9421	-3.2834	-38.425	2.6127	-10.219	-66.631	1.8954	
172							1.8643	-23.107
173	1.9792	-3.5604	-45.300	2.7698	-17.500	-73.100	2.0168	
174	1.9792	-3.2834	-37.363	1.9087	-9.193	-65.533	1.9087	
175	1.9421	-3.5604	-46.361	2.7513	-18.428	-74.294	2.0018	
176	2.5543	-3.1337	-16.598	2.8440	11.134	-44.330	2.0075	

POINT	$(\theta+\omega)$	$(\theta-\omega)$	θ (deg)	ω (rad)	$(\theta+m)$	$(\theta-m)$	M	N
177	2.6969	-2.9686	-6.924	2.8177	20.866	-34.714	2.8177	
178	2.6969	3.1337	-12.513	2.9153	15.091	-40.117	2.1382	
179	2.8327	-2.8327	0.000	2.8327	27.756	-27.756	2.0681	
180	2.8327	-2.9686	-3.893	2.9006	23.732	-31.519	2.1255	
181	2.9686	-2.9686	0.000	2.9686	27.457	-27.457	2.1854	
182	2.8327	-3.1337	-8.623	2.9832	18.788	-36.034	2.1984	
183	2.9686	-3.1337	-4.729	3.0512	22.518	-31.977	2.2604	
184	1.8332	-3.0712	-35.466	2.4522	-7.001	-63.931	1.7812	
185	1.8332	-3.2834	-41.545	2.5583	-13.243	-69.847	1.8554	
186	2.4545	-3.3392	-25.345	2.8969	2.298	-52.988	2.1223	-8.411
187	2.4545	-3.1337	-19.457	2.7941	8.473	-47.387	2.0363	
188	2.5543	-3.3392	-22.486	2.9467	5.041	-50.013	2.1658	
189	2.6969	-3.3392	-18.400	3.0180	8.927	-45.727	2.2300	
190	2.8327	-3.3392	-14.510	3.0860	12.655	-41.675	2.2926	
191	2.9686	-3.3392	-10.617	3.1539	16.383	-37.617	2.3550	
192	3.1337	-3.1337	0.000	3.1337	27.054	-27.054	2.3364	

POINT	$(\theta+\omega)$	$(\theta-\omega)$	θ (deg)	ω (rad)	$(\theta+m)$	$(\theta-m)$	M	N
193	3.1337	-3.3392	-5.887	3.2364	20.927	-32.701	2.4338	
194	1.8515	-3.2834	-41.021	2.5675	-12.735	-69.307	2.5675	
195	1.8515	-3.5604	-48.956	2.7059	-20.931	-76.981	1.9664	
196	2.4968	-3.6053	-31.756	3.0511	-4.506	-59.006	2.2603	
197	2.4968	-3.3392	-24.133	2.9180	3.467	-51.733	2.1405	
198	2.5543	-3.6053	-30.109	3.0798	-2.929	-57.289	3.0798	
199	2.6969	-3.6053	-26.024	3.1511	0.990	-53.038	2.3524	
200	2.8327	-3.6053	-22.133	3.2190	4.372	-48.989	2.4162	
201	2.9686	-3.6053	-18.240	3.2869	8.453	-44.933	2.4848	
202	3.3392	-3.3392	0.000	3.3392	26.558	-26.558	2.5432	
203	3.1337	-3.6053	-13.510	3.3695	12.968	-39.988	2.5784	
204							1.9115	-31.085
205	1.9707	-3.7701	-51.550	2.8704	-23.880	-79.220	2.0995	
206	1.9707	-3.5604	-45.550	2.7657	-17.648	-20.764	2.0135	
207	1.8968	-3.5604	-47.658	2.7286	-19.679	-75.637	1.9841	
208	1.8968	-3.7701	-53.666	2.8334	-25.928	-81.404	2.0686	

POINT	$(\theta+\omega)$	$(\theta-\omega)$	θ (deg)	ω (rad)	$(\theta+m)$	$(\theta-m)$	M	χ
209							1.9972	-40.690
210	1.9462	-4.0451	-60.128	2.9957	-32.748	-87.508	2.2097	
211	1.9462	-3.7701	-52.250	2.8582	-24.379	-80.121	2.0393	
212	1.8631	-3.5604	-48.462	2.7117	-20.611	-76.637	1.9708	
213	1.8631	-3.7701	-54.631	2.8166	-26.681	-82.581	2.0046	
214	2.5229	-3.7526	-35.231	3.1378	-8.186	-62.276	2.3402	-20.431
215	2.5229	-3.6053	-31.008	3.0641	-3.791	-58.225	2.2722	
216	1.8968	-4.0451	-61.544	2.9709	-34.094	-88.994	2.1874	
217	2.5543	-3.7526	-34.328	3.1534	-7.328	-61.328	2.3544	
218	2.6969	-3.7526	-30.243	3.2247	-3.401	-57.085	2.4218	
219	2.8327	-3.7526	-26.353	3.2926	0.325	-53.031	2.4904	
220	2.9686	-3.7526	-22.460	3.3606	4.041	-48.961	2.5680	
221	3.1337	-3.7526	-17.730	3.4431	8.566	-44.026	2.6618	
222	3.3392	-3.6053	- 7.623	3.4722	18.602	-33.848	2.6946	
223	3.3392	-3.7526	-11.843	3.5459	14.209	-37.895	2.7806	
224	1.8750	-3.7701	-54.288	2.8225	-26.348	-82.228	2.0090	
225	1.8750	-4.0451	-62.168	2.9600	-34.684	-89.652	2.1777	

POINT	$(\theta+\omega)$	$(\theta-\omega)$	θ (deg)	ω (rad)	$(\theta+m)$	$(\theta-m)$	M	X
226	2.5555	-4.0798	-43.668	3.3177	-17.053	-70.283	2.5181	-28.924
227	2.5555	-3.7526	-34.294	3.1540	- 7.293	-61.295	2.3550	
228	2.6969	-4.0798	-39.617	3.3883	-13.189	-66.045	2.3550	
229	2.8327	-4.0798	-35.726	3.4563	- 9.462	-61.990	2.6766	
230	2.9686	-4.0798	-31.833	3.5242	- 5.730	-57.936	2.7548	
231	3.1037	-4.0798	-27.103	3.6067	- 1.193	-53.013	2.8533	
232	3.3392	-4.0798	-21 216	3.7095	4.459	-46.891	2.9817	
233	3.6053	-3.6053	0.000	3.6053	25.913	-25.913	2.8516	
234	3.6053	-3.7526	- 4.220	3.6789	21.525	-29.964	2.9429	
235	3.6053	-4.7098	-13.593	3.8425	11.819	-39.005	3.1570	
236							2.1673	-58.412
237	1.9079	-4.5538	-75.800	3.2309	-48.973	-102.627	2.4283	
238	1.9079	-4.0457	-61.226	2.9765	-33.794	-88.658	2.1924	
239	1.8933	-4.0457	-61.643	2.9692	-34.188	-89.098	2.1859	
240	1.8933	-4.5538	-76.217	3.2235	-49.372	-103.062	2.4206	
241	2.6104	-4.5587	-55.817	3.5846	-29.855	- 81.779	2.8263	

POINT	$(\theta+\omega)$	$(\theta-\omega)$	θ (deg)	ω (rad)	$(\theta+m)$	$(\theta-m)$	M	χ
242	2.6104	-4.0451	-41.101	3.3277	-14.513	-67.689	2.5298	
243	2.6969	-4.5587	-53.336	3.6278	-27.475	-79.197	2.8970	
244	2.8327	-4.5587	-49.446	3.6957	-23.739	-75.153	2.9642	
245	2.9686	-4.5587	-45.553	3.7636	-19.987	-71.119	3.0524	
246	3.1337	-4.5587	-40.823	3.8462	15.418	-66.228	3.1618	
247	3.3392	-4.5587	-34.936	3.9489	- 9.754	-60.118	3.3056	
248	3.7526	-3.5726	0.000	3.7526	25.587	-25.587	3.3078	
249	3.7526	-4.0798	-9.373	3.9162	15.883	-34.629	3.2588	
250	3.6053	-4.5587	-27.313	4.0820	-2.407	-52.219	3.5008	
251	3.7526	-4.5587	-23.093	4.1556	1.674	-56.638	3.6122	
252							2.2255	-63.441
253	1.9032	-4.7032	-80.242	3.3032	-53.590	-106.894	2.5014	
254	1.9032	-4.5538	-75.934	3.2285	-49.101	-102.767	2.4258	
255							2.2465	-65.218
256	1.8923	-4.7597	-82.125	3.3257	-35.508	-109.166	2.5277	
257	1.8923	-4.5583	-76.375	3.2253	-49.738	-103.012	2.5225	
258							2.5277	-48.612

POINT	$(\theta+\omega)$	$(\theta-\omega)$	θ (deg)	ω (rad)	$(\theta+m)$	$(\theta-m)$	M	X
259	2.6226	-4.7597	-61.225	3.7283	-35.508	-86.942	2.9585	-48.612
260	2.6226	-4.5587	-55.465	3.5906	-29.517	-81.413	2.8336	
261	2.6969	-4.7597	-59.095	3.7283	-33.461	-84.729	3.0056	
262	2.8327	-4.7597	-55.205	3.7962	-29.703	-80.707	3.0956	
263	2.9686	-4.7597	-51.311	3.8641	-25.941	-76.681	3.1856	
264	3.1337	-4.7597	-46.581	3.9467	-21.394	-71.768	3.3024	
265	3.3392	-4.7597	-40.694	4.0494	-15.727	-65.661	3.4518	
266	3.6053	-4.7597	-33.071	4.1825	- 8.352	-57.790	3.6556	
267	3.7526	-4.7597	-28.951	4.2561	- 4.264	-53.438	3.7744	
268	4.7597	-4.7597	0.000	4.7597	23.866	-23.866	4.7075	
269							2.2863	-59.210
270	2.6805	-4.9428	-64.810	3.8117	-39.338	-90.282	3.1162	
271	2.6805	-4.7597	-59.564	3.7201	-33.913	-85.215	2.9951	
272	2.6969	-4.9428	-64.340	3.8198	-38.884	-89.796	3.1268	
273	2.8327	-4.9428	-60.450	3.3877	-35.130	-85.770	3.2180	
274	2.9686	-4.9428	-56.556	3.9557	-31.390	-81.722	3.3152	